DYSTONIA

April

Motor Circuits and Motor Symptoms in Dystonia: Translational Approaches from Animal Models to Patients

Issue Editors

Daniela Popa
Institut de biologie de l'Ecole Normale Supérieure, France

Cecile Gallea
Institut du Cerveau et de la Moelle épinière (ICM), France

frontiers | Publishing Partnerships

DYSTONIA

Motor Circuits and Motor Symptoms in Dystonia: Translational Approaches from Animal Models to Patients

ISSN 2813-2106
ISBN 978-2-8325-4672-7
DOI 10.3389/978-2-8325-4672-7

Dystonia is a motor disorder characterized by muscle contractions causing abnormal postures and/or movements, which are very disabling and painful in severe forms. Dystonia is sometimes the only symptom of the disease, but it is also present in combination with other motor dysfunctions in many neurological diseases, including Parkinson's disease and dyskinetic disorders. The possibilities of medical treatment still remain quite limited with side effects. The pathophysiologic mechanisms of dystonia concern aberrant communication within brain networks, particularly involving the basal ganglia, the sensorimotor cortex, and the cerebellum. Aberrant communication involves a combination of physiological and structural abnormalities, involving nodes that relay information between these three main actors (thalamus, brainstem nuclei, cortical nodes). However, the ways the different loops and nodes embedded in this interconnected complex system participate in explaining the symptoms are unclear, which leads to the fact that the etiology of dystonia remains poorly understood.

This Special Issue aims to publish studies in mammalian and non-mammalian phenotypic and genotypic animal models, as well as in patients. The focus is a better understanding of the pathophysiological mechanisms of dystonia, by deciphering how the functional/structural abnormalities in motor system can generate or amplify dystonic movements and postures. A better understanding of the dysfunction of each region in the network, their interactions and their link with the symptoms are important topics to address. We welcome researchers and clinicians working on animal models and/or patients (ideally translational work involving both) to participate to this issue and to shed light on novel pathophysiological processes to contribute to a deeper understanding of dystonia as a circuit disorder in relationship with motor symptoms.

Together, this Special Issue will present complementary studies in the human (including different dystonia subtypes) and animal models (including worms, fruit flies, rodents, and others) that will allow for the characterization of common physiological processes implicated in dystonia. We believe this is an important step to advance in the development of new treatments acting on motor circuits with less adverse side effects than observed with medications.

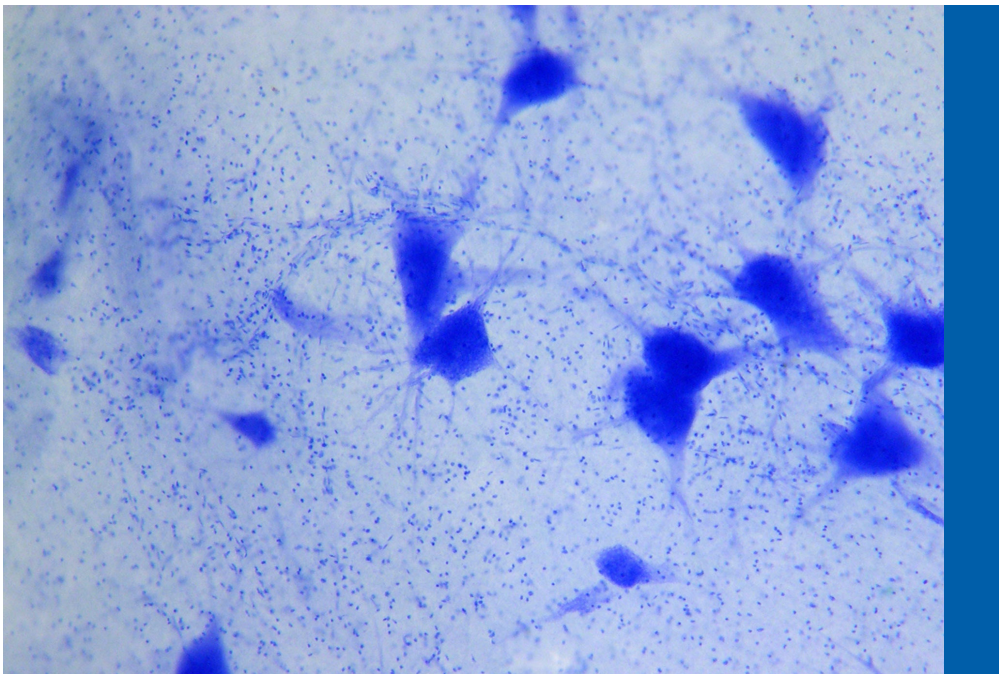

Table of contents

DYSTONIA

TYPE Editorial
PUBLISHED 01 February 2024
DOI 10.3389/dyst.2023.12554

OPEN ACCESS

EDITED BY
Roy Sillitoe,
Baylor College of Medicine,
United States

*CORRESPONDENCE
Cécile Gallea,
cecile.gallea.icm@gmail.com
Daniela Popa,
dpopa@biologie.ens.fr

RECEIVED 12 December 2023
ACCEPTED 18 December 2023
PUBLISHED 01 February 2024

CITATION
Gallea C and Popa D (2024), Editorial: Exploring dystonia symptoms through animal models and patient studies. *Dystonia* 2:12554.
doi: 10.3389/dyst.2023.12554

Editorial: Exploring dystonia symptoms through animal models and patient studies

Cécile Gallea[1]* and Daniela Popa[2]*

[1]Institut National de la Santé et de la Recherche Médicale U1127 Institut du Cerveau et de la Moelle Épinière (ICM), Paris, France, [2]Institut National de la Santé et de la Recherche Médicale U1024 Institut de Biologie de l'Ecole Normale Supérieure, Paris, France

KEYWORDS

dystonia, pathophysiology, therapeutic approaches, animal models, patient studies

Editorial on the Special Issue
Motor circuits and motor symptoms in dystonia: translational approaches from animal models to patients

Fine control of postural tone and complex limb coordination are generated at multiple levels in the brain, primarily through the integration of information from the basal ganglia (BG) and cerebellum (CB) in conjunction with the cerebral cortex. In dystonia, these motor abilities are lost due to impaired integration of information between and within these brain nodes, leading to abnormal postures and/or movements. Symptom expression can be isolated, or in combination with other motor disorders or neurological diseases, including Parkinson's disease. Importantly, the penetrance of genetic forms of dystonia is variable and the symptoms vary in severity, age of onset, focal or generalized localization and progression, even in patients carrying identical mutations [1]. This intrinsic variability in dystonia suggests the involvement of interacting mechanisms that either synergize or counteract at different levels of central motor centers, ultimately influencing the onset of symptoms.

The present Special Issue brings together researchers working on animal models and patients, as well as experts in physiology of the cerebral cortex, basal ganglia and cerebellum. Some consider a global view on different nodes of this network (Gray et al., Kasiri et al., Zeuner et al.), while others focus on single nodes to understand the functional underpinning of this particular structure in dystonia (Gray et al., Huber et al., Salazar-Leon and Sillitoe). These complementary approaches are crucial for understanding the pathophysiological processes of this complex disease.

The primary sensorimotor area has refined somatotopic representation of body parts, particularly those involved in precise movements (hands, lips, tongue). Dystonia is associated with a loss of inhibition, increased excitability, and somatotopic disorganization (see Zeuner et al.). Investigating cortical activity in patients with writer's cramp, Huber et al. take advantage of advanced MRI to improve our knowledge of cortical organization in focal hand dystonia. Their findings reveal that disorganization of cortical activity of the hand representation occurs at different levels of

cortical layers, i.e., at the level of interneurons receiving cortico-cortical interactions and at the level of cortico-spinal neurons controlling the motor output. Being the main origin of the cortico-spinal connections, the primary motor cortex also represents the main output pathway of the voluntary motor command [2], and possibly involuntary dystonic signals. Gray and collaborators investigate the cortical mechanisms underlying dystonic attack using multimodal electrophysiological and calcium imaging approaches in mice model of episodic ataxia type 2. They demonstrate that M1 activity is not at the origin of the dystonic attacks. Combining results from both human and mouse studies, it appears that the primary sensorimotor cortex exhibits abnormal integration of information coming from multiple sources and seem to propagate (rather than initiate) certain dystonic features into the motor command.

The BG are a hierarchically organized set of interconnected subcortical nuclei, including the striatum, the globus pallidum (GP), subthalamic nucleus (STN) and the thalamus (TH). Classical models of dystonia suggest that involuntary muscle contractions result from reduced activity in GP internus (GPi) leading to inadequate inhibition of thalamic inputs to cortex during the movement. Here, Kasiri et al. perform deep electrophysiological recordings of multiple BG nodes in three children with genetic dystonia. In contrast with the classical model of opposite activity patterns of GPi and TH, activity was elevated in both GPi and TH during movement. In a refinement of the classical model, the authors propose that the cerebral cortex primarily excites the thalamus. The role of the GPi would be to selectively inhibit the cortical excitatory afferent at the thalamic level, effectively shaping the thalamo-cortical loop. This precise mechanism would be impaired in dystonia.

Within the BG, the striatum contributes to learning. Zeuner et al. review striatal dysfunction during learning of finger sequences in focal hand dystonia. In particular, striatal dysfunction could be associated with alteration in the subcortical dopaminergic network important for learning. For instance, dystonia symptoms occur in Parkinson's disease, which primarily affects dopaminergic pathways. In this Special Issue, Norris et al. investigate common mechanisms and the temporal interplay between dystonia and Parkinson symptoms by combining behavioral scoring, post-mortem counting of striatal and nigral dopaminergic neurons in MPTP monkeys. Their findings indicate that the severity of dystonic symptoms predicted the severity of Parkinsonism, but the relationship between striatal dopamine and dystonic symptom was complex and depended on the severity of nigral dopaminergic cell loss. This suggests that the sequential order of node dysfunction is significant. It gives additional evidence that dopaminergic system is a vulnerable point of network dysfunction in dystonia [3, 4].

Traditionally, the CB was considered a crucial node for motor execution and learning. However, in patients with focal dystonia, cerebellar activity and connectivity are altered during both the execution and imagination of movements in absence of motor output (see Zeuner et al. in the present Special Issue). Recent work suggest that the cerebellum can contribute to sleep regulation [5, 6]. In the present issue, Salazar-Leon and Sillitoe use two different mice lines with disrupted afferents to the CB, each with different coverage over climbing fibers only or over both climbing and mossy fibers, inducing different motor severities. Despite the differences in dystonia-related motor severities, the mutant mice exhibited similarly impaired sleep physiology and disrupted circadian rhythms, mirroring patterns observed in human pathology [7, 8]. This work indicates that aberrant cerebellar activity not only disrupts motor function but also impacts sleep.

By considering results in both human patients and animal models, we progress in our understanding of dystonia pathophysiology. Collectively, the findings in this Special Issue indicate that dystonia is a circuit disorder in which abnormalities in one system may well lead to dysfunction of the other because of their reciprocal connections in the brain. Data obtained from dystonic patients and animal models allows identifying common pathophysiological mechanisms on a robust foundation, that inhibiting the thalamic region could potentially block dystonia. Animal models can recreate the circuit-wide defects through different connections. This Special Issue also introduces innovative therapeutic approaches focused on retraining to achieve enduring improvements in motor symptoms. The ongoing research involving animal models and patients is paving the way for improved future therapeutics that have the potential to simultaneously address both motor and non-motor dysfunctions in the context of motor diseases.

Author contributions

All authors listed have made a substantial, direct, and intellectual contribution to the work and approved it for publication.

Conflict of interest

The authors declare that the research was conducted in the absence of any commercial or financial relationships that could be construed as a potential conflict of interest.

References

1. Fuchs T, Saunders-Pullman R, Masuho I, Luciano MS, Raymond D, Factor S, et al. Mutations in GNAL cause primary torsion dystonia. *Nat Genet* (2013) 45(1): 88–92. doi:10.1038/ng.2496

2. Lemon RN. The cortical "upper motoneuron" in health and disease. *Brain Sci* (2021) 11(5):619. doi:10.3390/brainsci11050619

3. Ribot B, Aupy J, Vidailhet M, Mazère J, Pisani A, Bezard E, et al. Dystonia and dopamine: from phenomenology to pathophysiology. *Prog Neurobiol* (2019) 182:101678. doi:10.1016/j.pneurobio.2019.101678

4. Berman BD, Hallett M, Herscovitch P, Simonyan K. Striatal dopaminergic dysfunction at rest and during task performance in writer's cramp. *Brain* (2013) 136(12):3645–58. doi:10.1093/brain/awt282

5. Zhang LB, Zhang J, Sun MJ, Chen H, Yan J, Luo FL, et al. Neuronal activity in the cerebellum during the sleep-wakefulness transition in mice. *Neurosci Bull* (2020) 36(8):919–31. doi:10.1007/s12264-020-00511-9

6. Dang-Vu TT, Schabus M, Desseilles M, Albouy G, Boly M, Darsaud A, et al. Spontaneous neural activity during human slow wave sleep. *Proc Natl Acad Sci U S A* (2008) 105(39):15160–5. doi:10.1073/pnas.0801819105

7. Antelmi E, Ferri R, Provini F, Scaglione CML, Mignani F, Rundo F, et al. Modulation of the muscle activity during sleep in cervical dystonia. *Sleep* (2017) 40(7). doi:10.1093/sleep/zsx088

8. Silvestri R, De Domenico P, Di Rosa AE, Bramanti P, Serra S, Di Perri R. The effect of nocturnal physiological sleep on various movement disorders. *Mov Disord Off J Mov Disord Soc* (1990) 5(1):8–14. doi:10.1002/mds.870050104

DYSTONIA

TYPE Brief Research Report
PUBLISHED 01 February 2023
DOI 10.3389/dyst.2023.10806

OPEN ACCESS

EDITED BY
Daniela Popa,
INSERM U1024 Institut de Biologie de l'Ecole Normale Supérieure, France

*CORRESPONDENCE
Silvina G. Horovitz,
silvina.horovitz@nih.gov

RECEIVED 28 July 2022
ACCEPTED 09 January 2023
PUBLISHED 01 February 2023

CITATION
Huber L, Kassavetis P, Gulban OF, Hallett M and Horovitz SG (2023), Laminar VASO fMRI in focal hand dystonia patients.
Dystonia 2:10806.
doi: 10.3389/dyst.2023.10806

Laminar VASO fMRI in focal hand dystonia patients

Laurentius Huber[1], Panagiotis Kassavetis[2,3], Omer Faruk Gulban[1,4], Mark Hallett[3] and Silvina G. Horovitz[3]*

[1]Department of Cognitive Neuroscience, Faculty of Psychology and Neuroscience, Maastricht University, Maastricht, Netherlands, [2]Department of Neurology, University of Utah, Salt Lake City, UT, United States, [3]Human Motor Control Section, NINDS, NIH, Bethesda, MD, United States, [4]Brain Innovation, Maastricht, Netherlands

Focal Hand Dystonia (FHD) is a disabling movement disorder characterized by involuntary movements, cramps and spasms. It is associated with pathological neural microcircuits in the cortical somatosensory system. While invasive preclinical modalities allow researchers to probe specific neural microcircuits of cortical layers and columns, conventional functional magnetic resonance imaging (fMRI) cannot resolve such small neural computational units. In this study, we take advantage of recent developments in ultra-high-field MRI hardware and MR-sequences to capture altered digit representations and laminar processing in FHD patients. We aim to characterize the capability and challenges of layer-specific imaging and analysis tools in resolving laminar and columnar structures in clinical research setups. We scanned N = 4 affected and N = 5 unaffected hemispheres at 7T and found consistent results of altered neural microcircuitry in FHD patients: 1) In affected hemispheres of FHD patients, we found a breakdown of ordered finger representation in the primary somatosensory cortex, as suggested from previous low-resolution fMRI. 2) In affected primary motor cortices of FHD patients, we furthermore found increased fMRI activity in superficial cortico-cortical neural input layers (II/III), compared to relatively weaker activity in the cortico-spinal output layers (Vb/VI). Overall, we show that layer-fMRI acquisition and analysis tools have the potential to address clinically-driven neuroscience research questions about altered computational mechanisms at the spatial scales that were previously only accessible in animal models. We believe that this study paves the way for easier translation of preclinical work into clinical research in focal hand dystonia and beyond.

KEYWORDS

layer-fMRI, VASO, focal hand dystonia, 7 Tesla, cerebral blood volume fMRI

Introduction

Focal Hand Dystonia (FHD) is a disabling movement disorder characterized by involuntary movements, cramps and spasms. Common sub-forms are known as writer's cramp and musician's cramp (Karp 2017) with epidemiological prevalence up to 1 in 2,500 people (1). FHD is associated with pathological neural microcircuits in the

cortical somatosensory system. FHD is expected to have closer (1–2 mm) and more overlapping finger representation in the somatosensory system (2–7). While invasive preclinical neuroimaging modalities in animal models allow researchers to probe specific neural microcircuits at the mesoscopic scale of cortical layers and columns (8), conventional non-invasive functional magnetic resonance imaging (fMRI) in humans cannot resolve such small neural computational units. Thus, until now, non-invasive research tools that are routinely applicable in patients, could not yet reach their full potential in translating pre-clinical findings of mesoscopic neural circuitry to patients. Recent developments in ultra-high field MRI hardware and functional contrast generation allows researchers for the first time to capture layer-specific fMRI responses at the spatial scale of sub-millimeter voxels. Specifically, mesoscale fMRI with blood volume sensitive VASO (9, 10) methods can map functional activation changes in the laminar microcircuitry and columnar finger representations without unwanted large draining vein effects of conventional BOLD fMRI (11). For example, previous high-resolution VASO imaging could capture the fine scale finger movement representations across layers and columns in healthy volunteers (HV) (11, 12). These proof-of-principle studies exploited highly optimized experimental environments that might not be fulfilled with patients (Figure 1). Specifically, submillimeter fMRI in clinical populations as opposed to healthy volunteers might be challenged by the following constraints.

- **Scan duration:** Previous studies could collect up to 18 h of fMRI data per participant. This was achieved by inviting the participants for up to 10 two-hour scan sessions (12). Such large numbers of data collection sessions are not practical for FHD patients.
- **Head motion:** Access to patients is limited. Thus, the experimenter does not have the luxury to solely invite those individuals that have the ability to lie perfectly still for long periods of time (approx. 2 h). As exemplified in Figure 1A), this is not always the case for MRI-naive participants, such as FHD patients.
- **Noise in task compliance:** FHD patients can have a hard time following the task instructions. For example, when instructed to move the ring finger only, the middle finger and fifth finger are often moved too. This reduces the finger functional contrast-to-noise ratio.
- **EPI Artifact level:** Sub-millimeter fMRI is limited by low bandwidths and small coverages. In previous applications in healthy volunteers, this had been accounted for with iterative online fine tuning of acquisition parameters during the data acquisition phase (iterative B0-shimming, GRAPPA regularization, alignment, readout bandwidth). Within the limited scan time of patients, such fine tuning is not feasible. Thus, the raw functional images can be challenged by EPI phase-inconsistency artifacts as exemplified in Figure 1C.

Due to these challenges, the applicability of laminar and columnar functional imaging with fMRI in patient populations remains unclear. The aim of this study is to characterize and mitigate these challenges. We used the altered digit representation in FHD patients as a testbed to explore the capability of applying layer-fMRI VASO to investigate mesoscopic neural representations in patients. Specifically, we sought to investigate the quantifiability of pathological alterations of the mesoscopic finger representations in FHD patients across cortical depth as well as across topographical arrangements along the cortical sheet.

Methods

Patient procedure

Study participants were recruited under the NIH Institutional Review Board protocol 17-N-0126 (ClinicalTrials.gov identifier: NCT03223623). Four FHD patients (2M/2F; 50 ± 4.6 years, disease duration 3 to 20 years) receiving regular botulinum toxin injections were scanned at least 3 months after their last injection. Additionally, data from a prior study (12) were analyzed to control for task speed (N = 2).

MRI scanner

The functional imaging sequence was implemented on a 'classic' MAGNETOM 7T scanner (Siemens Healthineers, Erlangen, Germany) using the vendor-provided IDEA environment (VB17A-UHF). For RF transmission and reception, a single-channel-transmit and 32-channel receive head coil (Nova Medical, Wilmington, MA, United States) was used. The scanner was equipped with a SC72 body gradient coil (maximum effective gradient strength used here: 49 mT/m; maximum slew rate used: 199 T/m/s).

MRI sequence

Slice-selective slab-inversion (SS-SI) VASO sequence (Huber 2014) was used in combination with a 3D-EPI readout, as previously implemented (13). VASO is a non-invasive fMRI sequence approach that is sensitive to changes in CBV by means of an inversion-recovery contrast generation (10). In VASO fMRI, an inversion-recovery pulse sequence is used to selectively null out blood water magnetization at the time of the image acquisition, while leaving extra-vascular signals for detection. An increase in CBV during task-evoked neural

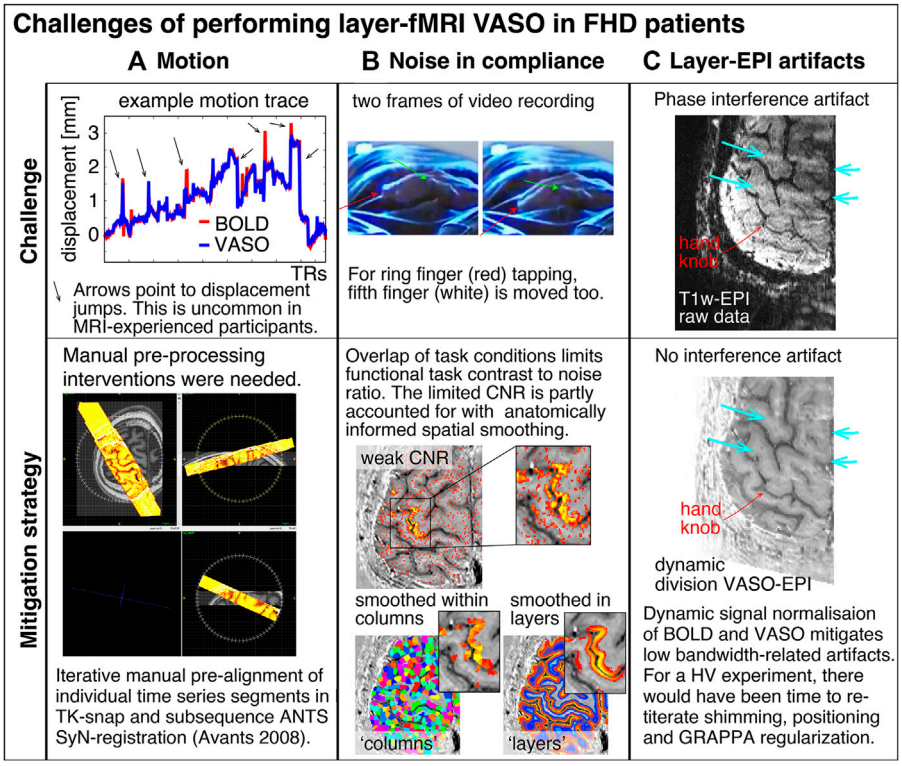

FIGURE 1
Selected examples of challenging aspects in the acquisition and processing of sub-millimeter VASO fMRI in FHD patients. **(A)** In this study, head motion was mitigated with time consuming manual corrections. **(B)** Limited finger specific functional contrast-to-noise-ratio (CNR) was mitigated with anatomically informed signal pooling within layers and columns, respectively. **(C)** Time constant EPI phase interference artifacts were mitigated by means of dynamic division of odd and even time points with identical artifacts in SS-SI VASO. The purpose of this figure is to exemplify challenges of performing mesoscopic fMRI experiments, which we had not encountered in previous studies. Different from this study, for data collection in previous studies, the sequence-developer had operated the scanner themselves and they had solely scanned experienced healthy volunteers with extraordinary skills to lie perfectly still.

activation is then associated with an overall MR-signal decrease, which in-turn is believed to be proportional to the volume increase of nulled blood. In the specific SS-SI VASO variant, CBV sensitive images are concomitantly acquired with conventional BOLD signals in an interleaved fashion. This means that every other TR (here 2.2s) we acquired CBV-sensitive and BOLD-sensitive images, respectively (this results in a pair TR of 4.4s). More practical information, including sequence diagrams and its specific implementation for classical MAGNETOM 7T SIEMENS scanners is provided in form of a manual here: https://layerfmri.com/ss-si-vaso-sequence-manual/. The optimal sequence parameters were tested and optimized in previous studies (12). In short: No slab-oversampling, slab-excitation profile with a bandwidth-time-product of 25, T1-related blurring mitigation with variable flip angles, FLASH GRAPPA 3, vendor's GRAPPA reconstruction algorithms (Siemens software identifier: IcePAT WIP 571), partial Fourier (6/8) reconstruction with POCS 8, in-plane resolution 0.75 mm, slice-thickness: 0.89 mm, TE = 24 ms, TR/TI = 2.2/1.1s. The 3D-EPI readout consisted of 24 shots for 24 k_z-partitions. This refers to 24 slices in image space. The two outermost slices were disregarded in the form of 9.1% oversampling in order to mitigate fold-over artifacts in the second phase encoding direction. This results in 22 slices for further processing and a usable slab thickness of 19.2 mm. The overall field of view after oversampling in both phase encoding directions was 122 mm × 162.6 mm x 19.8 mm. A full list of protocol parameters is available on Github: https://github.com/layerfMRI/Sequence_Github/blob/master/FocalHandDystonia/FHD.pdf. The sequence binaries are freely available *via* the SIEMENS sequence 'Appstore' in Teamplay (https://teamplay.siemens.com/).

Scanning

The VASO imaging slab was positioned to be approximately perpendicularly oriented to the main surface of the central sulcus

of one hemisphere. This was achieved by tilting it in two directions. Scanning was conducted using preset parameters for layer-fMRI VASO experiments, without individualized settings to optimize the time of the patients in the scanner. This scanning setup can be used to exemplify the usability and scalability of the experimental procedures beyond specialized MRI-development research groups. No specific custom hardware was necessary during the scanning, beyond the common 7T MRI configuration that is available at >100 centers worldwide. We scanned N = 4 patients and N = 2 healthy volunteers. Together, we collected data from N = 5 healthy hemispheres and N = 4 affected hemispheres.

Task

For the sake of consistency and comparability with previous studies, we used the same tapping tasks as previously used (Huber 2020). Briefly, before each run, subjects were instructed on what hand to tap with. Participants were instructed to tap one finger by extension-flexion at the metacarpophalangeal joint. The same tapping task was repeated for each finger. The tapping frequency was self-paced at a frequency of approximately every 1–2 s. During the scan, a video prompted which finger to move and when to rest. The tapping timing was locked to scanner triggers in units of 16 TRs (2.2 s each) and contains visual cues when to tap which finger and for how long. The task was controlled *via* Psychopy 2 with publicly available scripts (https://github.com/layerfMRI/Phychopy_git/tree/master/Tapping_withTR_all_fingers). The same task was repeated for each hand. Each run lasted approximately 33 min.

Processing

Concomitantly acquired time series consisting of blood-nulled and BOLD contrasts were separately corrected for motion using SPM12 (Functional Imaging Laboratory, University College London, United Kingdom). Motion-corrected time series were corrected for BOLD contaminations, by means of dynamically dividing blood-nulled signals with not-nulled BOLD signals using LayNii's v2.2.1 (14) LN_BOCO. In order to mitigate non-steady state effects (transients of hemodynamic response), the division was performed on a two-fold temporally upsampled time series. This form of BOLD correction in SS-SI VASO has been originally been developed, described, and validated for 7T imaging (15) and is based on the assumption that the VASO T_1-contrast (in the M_z-direction) is completely orthogonal to the BOLD T_2^*-contrast (in the M_{xy}-direction). Block design activation z-scores and beta estimates were extracted with FSL-FEAT (16). Layerification and columnification were done with the `LN2_LAYERS` program in LayNii. The motivation and the working principle of the underlying algorithms are explained here https://layerfmri.com/equivol/ and here https://thingsonthings.org/ln2_layers/, respectively.

Hands-on tutorials (with maintained QnA sections), analysis manuals, and "click-along" video instruction of the entire pre-processing and layerification analysis that is performed here can be found at https://layerfmri.com/analysispipeline/.

Cortical patch flattening was performed with the LN2_MULTILATERATE and LN2_PATCH_FLATTEN programs in LayNii (17). The algorithms and how we practically applied them is illustrated here https://thingsonthings.org/ln2_multilaterate/ and here https://youtube.com/playlist?list=PLs_umVHtShfadNm8brOweXHUSmqVDTk4q, respectively. Layer-extraction was manually constrained to the Brodmann area BA4a. This is the evolutionary older part of the primary motor cortex (as opposed to BA4p). In order to pinpoint it, we followed previously described landmarks (11). In short: we located the lateral part of the hand knob as the location on the precentral gyrus with the shortest curvature radius and selected the cortical patch medial to it. Further information of the landmarks with a collection of anatomical examples and instructions of the placement of the fMRI slab and area selection is available here: https://layerfmri.com/finding-roi-of-the-double-layers-in-m1/. The specific ROIs of all patients and hemispheres as used in this study are shown in Figure 4C.

Re-analysis from previously published studies

We collected short video recordings of the FHD patients while they were performing the tapping task (example screenshots in Figure 1B). This video material suggested a qualitative trend that FHD patients might have performed the tapping at a slower pace than what we were used to from previous studies with the same task. In order to quantify the effect of the tapping frequency on the interpretability of the results of this study, we obtained previously acquired layer-fMRI VASO data that were recorded with varying tapping frequencies. As described in (13), the resolution was 0.75 mm × 0.75 mm × 1.2 mm, with VASO, at 7T in healthy participants. The tapping frequencies were 2 and 0.25 Hz, which covers the range of tapping frequencies that we saw in FHD patients.

Results

Across all data sets, we find tapping induced activation both in M1 and in S1. This means that five out of five patient hemispheres show clear CBV changes in M1 and also four out of four patient hemispheres show clear CBV changes in S1. This is a success rate of 100% for both brain areas. Activation

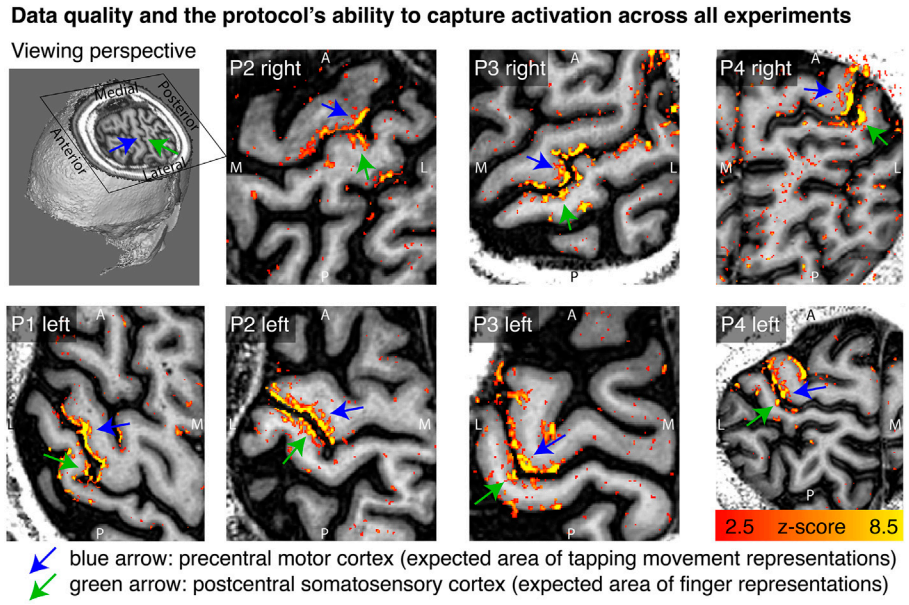

FIGURE 2
Tapping induced activation maps across patients. Within the 33 min functional experiments, enough data are obtained to extract significant VASO signal changes across all patients and hemispheres. The figures represent the signal without spatial smoothing in spatially upsampled in-plane resolution of 0.4 mm (nominal resolution 0.75 mm). The purpose of this figure is to show that the imaging protocol tested here is capable of capturing blood volume at sub-millimeter resolutions within 33 min functional experiments. We see significant activation in each and every patient and hemisphere.

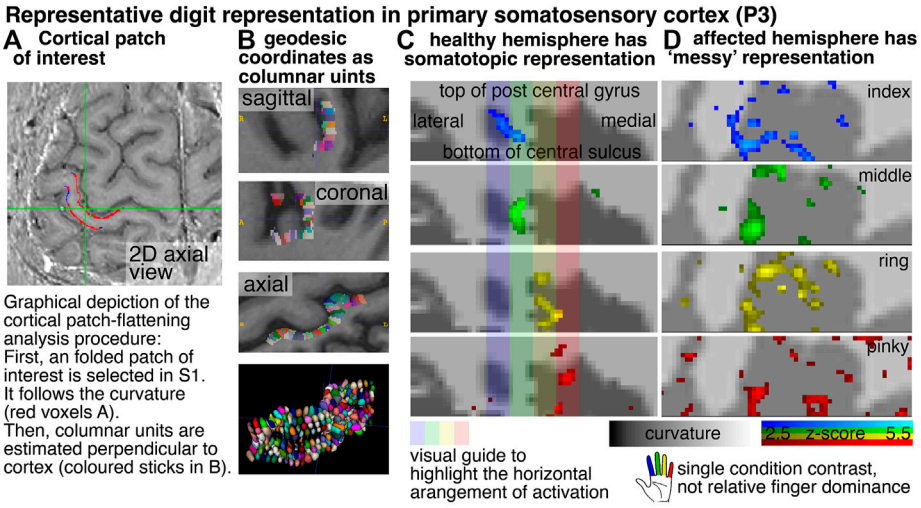

FIGURE 3
Cortical flattening of thin MRI slab Columns **(A,B)** exemplify the analysis procedure of the cortical flattening. With the methods developed here, the flattening is possible despite the fact that the thin slab does not fulfill common topology requirements that are necessary in mesh-based analyses. Here, we imposed a local coordinate system in the distorted EPI data with LN2_MULTILATERATE (17). More explanations of the underlying algorithms are explained here https://thingsonthings.org/ln2_multilaterate/. Representative VASO-fMRI finger responses in panel **(C,D)** show somatotopic alignment in the healthy hemisphere and less so in the affected hemisphere (smoothed across layers only, no smoothing in the lateral direction). The activation patterns in panel **(C,D)** refer to the average signal across all cortical depths. In this figure, laminar signal distributions are not resolved. The purpose of this figure is to exemplify that sub-millimeter fMRI methods have the potential to address research questions of topographical neural representations in the sub-millimeter spatial scale.

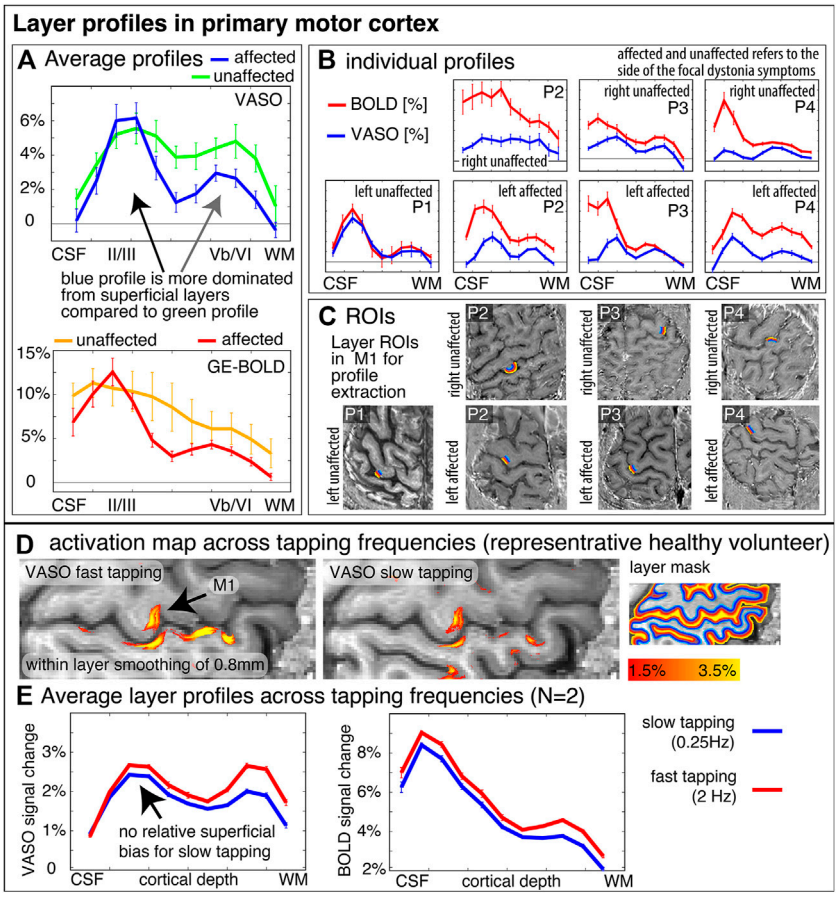

FIGURE 4
Layer-fMRI profiles in the primary motor cortex for BOLD and VASO in healthy and affected hemispheres. Panels **(A,B)** highlight how all layer profiles consistently show a larger superficial bias in GE-BOLD compared to VASO, while still showing clear indication of a secondary "bump" in the deeper output layers [gray in **(A)**]. Compared to the deeper layers, the superficial layers in the affected hemispheres seem to be relatively stronger activated compared to their healthy counterparts (see black arrow compared to gray arrow). Signal pooling of layers was done from unsmoothed data. The corresponding ROIs are depicted in Panel **(C)**. Note that the layer profiles depicted here are referring to data that are collapsed across the columnar direction. This means that the analysis procedure shown here does not represent topographical signal distributions along the cortical ribbon. Panels **(D,E)** show layer-dependent CBV responses across tapping frequencies in healthy participants. It can be seen that slower tapping results in overall smaller fMRI signal changes. The relative reduction of fMRI signal changes is stronger in the deeper "output" layers compared to the superficial "input" layers. This suggests that the layer-specific signal modulation between healthy and affected hemispheres in Panel **(A)** cannot be explained by different tapping frequencies. The purpose of this figure is to exemplify the potential of sub-millimeter methodology to address questions of alterations in laminar processing. Furthermore, it is shown how consistent the results are across a small sample of patients.

maps of all hemispheres in Figure 2 shows that the experimental sub-millimeter VASO imaging setup can reliably capture neurally-induced functional cerebral blood volume (CBV) changes in patients across hemispheres and individuals. It can be seen how the activity is confined to gray matter (GM) without the sensitivity of large drain pial veins above the GM surface.

In order to explore the spatial structure of finger representation in the primary somatosensory cortex on the posterior bank of the central sulcus, we imposed a local coordinate system within the GM cortical sheet. Exemplary data of one representative participant show exemplary how the finger representation follows the somatotopic alignment for the healthy hemisphere (Figure 3). The spatial structure of the representations in the FHD-affected hemisphere are less clear. This is not for the lack of detection sensitivity. In fact, large patches of the primary somatosensory cortex are clearly engaged during finger tapping tasks. It's just that the spatial arrangement of the finger-specific activation patches does not follow as clear arrangements as for the healthy hemisphere.

Aside from topographical finger-representations in the sensory cortex, we also explored the laminar blood volume responses in the primary motor cortex. Figure 4 depicts M1 layer-profiles of all patients. As expected, GE-BOLD signals show an increased bias towards the superficial layers compared to CBV-sensitive VASO. This is manifested in steeper slopes of the BOLD profiles compared to the VASO profiles in all hemispheres,

in all patients, and in all functional tasks (100% of a total of N = 14), without exceptions. The affected hemispheres seem to be more dominated by superficial cortico-cortical input-layers compared to the healthy hemispheres, in all participants (100% of N = 4).

Video material of the FHD patients performing the task inside the scanner bore suggested a qualitative trend that FHD patients might have performed the tapping at a slower pace compared to typical tapping frequencies in healthy participants. To quantify the effect of tapping frequency on the interpretation of the layer profiles shown in Figure 4A, we also show the tapping frequency dependence of the layer profile as collected in previous studies. These results are shown in Figure 4E and suggest that a potentially different tapping frequency cannot explain the layer-dependent fMRI signal modulations that we find in healthy vs. affected hemispheres.

Discussion

In this study, we explored the capabilities and challenges of high-resolution layer-fMRI to inform research questions of affected cortical microcircuitry in patients. We scanned N = 4 focal hand dystonia patients and found consistently altered somatotopic and laminar activation patterns in affected and unaffected hemispheres. The results presented here suggest that the high-resolution acquisition and analysis protocols developed here allow clinical neuroscientists to investigate pathological laminar pathologies in patients. Specifically, we found that cortical hemispheres that were affected by FHD appear to have a less structured somatotopic alignment of finger representation in the primary somatosensory homunculus of the postcentral gyrus. These results are consistent with the parallel ongoing imaging efforts of high-resolution functional mapping of finger representations at 7T (18). This study had already overcome some challenges and mapped the finger representation in FHD patients with 1.5 mm GE-BOLD (18). At lower spatial resolutions of 2.4 mm, no alterations of finger representations in the primary somatosensory cortex could be detected (19). Here, we pushed the imaging protocols further and used sub-millimeter vein-bias-free VASO to capture laminar fMRI modulations. Aside from the altered somatotopic topographical digit representations in the primary sensory cortex, we also explored layer-dependent fMRI response in the primary motor cortex. Across all participants, we found that the superficial cortico-cortical input layers seem to have an increased activation during finger tapping tasks compared to unaffected hemispheres while the opposite is true for deeper layers. The increased activation may be due to decreased inhibition, and, in this way, these findings would be consistent with the notion that FHD is associated with a lack of neural surround-inhibition mechanisms (6, 20–22). However, the relative dominance of fMRI signal changes in input layers could also be partly related to increased mental load (attention, motor planning, incorporating sensory feedback) and corresponding cortico-cortical input that is expected in the superficial layers (23–25). While the tapping frequency might have been slower for affected and unaffected hemispheres, we do not think that this can influence the interpretability of the layer-dependent activity modulation. In fact, slower tapping frequencies are expected to result in weaker superficial activation (Figure 4E), which we do not see in the results of FHD affected hemispheres.

Relevance of this work

Looking beyond FHD, the tools developed and tested in this study provide a starting point for mapping layer-specific connections in patient populations in the general context of clinical neuroscience. Many influential theories of brain function of disorders posit hypotheses of neural deficits in distinct cortical layers and their role of feedforward and feedback processing. For example: mental disorders, such as autism and schizophrenia, and neurodegenerative diseases such as Parkinson's or Huntington's disease. Specifically.

- Layer-fMRI VASO has been discussed to be the key future technology to probe predictions of axonal loss and microcircuit dysfunction to provide insights for neurodegenerative motor disease (26, 27). The results shown there suggest that the imaging and analysis methodology is now ready to be applied for such proposed studies.
- Layer-fMRI has been discussed to be a key future technology to act as Occam's razor for multiple competing hypotheses of hierarchical microcircuit disruptions in psychosis (28, 29). Namely in the context of predictive coding, one theory about psychosis discusses delusion symptoms in terms of deficits in learning. This is associated with respective predicted pathological neural computations in feedback dominated superficial and deeper layers. Another theory of psychosis discusses the same hallucination symptoms in terms of deficits in perceptual inference with respective predicted pathological neural computations in feedforward dominated middle layers. Until now, the methodological ability to constrain the models with empirical data has been limited. The usability of the layer-fMRI VASO protocols developed here allows future clinical neuroscientists to test and thus constrain these models.

These examples show that layer-fMRI applications in patients open the door to investigating computational mechanisms at the spatial scales that were previously only accessible in animal models. We believe that this study paves the way for easier translation of preclinical work into clinical research in focal hand dystonia and beyond.

In conclusion

While there are plentiful review articles about the value of layer-fMRI for clinical neuroscience research (26–29) experimental layer-fMRI data are scarce (30). Here, we present fMRI results of laminar and columnar CBV changes in FHD patients. We could not confirm previous findings of closer finger representations (2, 4, 5) because the finger representations in our maps did not show clear locations from which the distances could be calculated. We find that FHD affected hemispheres had a relatively stronger activity in motor input-layers (II/III) compared to the activity in motor output-layers (Vb/VI). This might be due to reduced surround inhibition in the superficial layers of the affected hemispheres. It could also be related to increased mental load (attention, motor planning, incorporating sensory feedback) that is related to neural input terminating in superficial layers. More data are needed to ultimately determine the stability of this finding. This study has built the methodological groundwork that future clinically-focused neuroscience application studies of layer-fMRI can be based on.

Data availability statement

The datasets generated for this study are deposited in the NIH.BOX / data.ninds.gov repository https://layerfmri.page.link/FHD_data. Access is granted individually without conditions and should be requested from the corresponding author silvina.horovitz@nih.gov.

Ethics statement

The studies involving human participants were reviewed and approved by NIH Institutional Review Board protocol 17-N-0126 (ClinicalTrials.gov identifier: NCT03223623). The patients/participants provided their written informed consent to participate in this study.

Author contributions

All authors listed have made a substantial, direct, and intellectual contribution to the work and approved it for publication.

Funding

LH was funded by the NWO VENI project 016.Veni.198.032. The project was supported by the NINDS Intramural Research Program. OG is financially supported by Brain Innovation.

Conflict of interest

Author OG was employed by the company Brain Innovation B.V.

The remaining authors declare that the research was conducted in the absence of any commercial or financial relationships that could be construed as a potential conflict of interest.

Acknowledgments

We thank Sean Marrett for bringing together members from HMCS, NINDS and from SFIM, NIMH. Being introduced by him was the starting point of this cross-institute, cross-discipline collaboration project. We thank David Linden for discussions on how to address potential differences of tapping frequency which resulted in additional validation experiments shown in Figures 4D, E. Help with scanning: These data were acquired with the kind support of the FMRIF core facility, specifically with the friendly help from Sean Marrett to test the acquisition protocols used here. We thank Kenny Chung for scan support. We thank Benedikt Poser for kindly providing the 3D-EPI sequence code used here. Ethics: We thank Avanti Iyer for help with the IRB protocol 17-N-0126.

References

1. Torres-Russotto D, Perlmutter JS. Focal dystonias of the hand and upper extremity. *J Hand Surg Am* (2008) 33(9):1657–8. doi:10.1016/j.jhsa.2008.09.001

2. Bara-Jimenez W, Catalan MJ, Hallett M, Gerloff C. Abnormal somatosensory homunculus in dystonia of the hand. *Ann Neurol* (1998) 44(5):828–31. doi:10.1002/ana.410440520

3. Butterworth S, Francis S, Kelly E, McGlone F, Bowtell R, Sawle GV. Abnormal cortical sensory activation in dystonia: An fMRI study. *Mov Disord* (2003) 18(6):673–82. doi:10.1002/mds.10416

4. Catalan MJ, Ishii K, Bara-Jimenez W, Hallett M. Reorganization of the human somatosensory cortex in hand dystonia. *J Movement Disord* (2012) 5(1):5–8. doi:10.14802/jmd.12002

5. Elbert T, Candia CAV, Altenmüller E, Rau H, Sterr A, Rockstroh B, et al. Alteration of digital representations in somatosensory cortex in focal hand dystonia. *NeuroReport* (1998) 9(16):3571–5. doi:10.1097/00001756-199811160-00006

6. Hallett M. Neurophysiology of dystonia: The role of inhibition. *Neurobiol Dis* (2011) 42(2):177–84. doi:10.1016/j.nbd.2010.08.025

7. Nelson AJ, Blake DT, Chen R. Digit-specific aberrations in the primary somatosensory cortex in writer's cramp. *Ann Neurol* (2009) 66(2):146–54. doi:10.1002/ana.21626

8. Goense J, Bohraus Y, Logothetis NK. fMRI at high spatial resolution: Implications for BOLD-models. *Front Comput Neurosci* (2016) 10():66–14. doi:10.3389/fncom.2016.00066

9. Hua J, Jones CK, Qin Q, Van Zijl PC. Implementation of vascular-space-occupancy MRI at 7T. *Magn Reson Med* (2013) 69(4):1003–13. doi:10.1002/mrm.24334

10. Lu H, Golay X, Pekar JJ, Van Zijl PCM. Functional magnetic resonance imaging based on changes in vascular space occupancy. *Magn Reson Med* (2003) 50(2):263–74. doi:10.1002/mrm.10519

11. Huber L, Handwerker DA, Jangraw DC, Chen G, Hall A, Stüber C, et al. High-resolution CBV-fMRI allows mapping of laminar activity and connectivity of cortical input and output in human M1. *Neuron* (2017) 96(6):1253–63. doi:10.1016/j.neuron.2017.11.005

12. Huber L, Finn ES, Handwerker DA, Bönstrup M, Glen DR, Kashyap S, et al. Sub-millimeter fMRI reveals multiple topographical digit representations that form action maps in human motor cortex. *NeuroImage* (2020) 208:116463. doi:10.1016/j.neuroimage.2019.116463

13. Poser BA, Koopmans PJ, Witzel T, Wald LL, Barth M. Three dimensional echo-planar imaging at 7 tesla. *NeuroImage* (2010) 51(1):261–6. doi:10.1016/j.neuroimage.2010.01.108

14. Huber LRR, Poser BA, Bandettini PA, Arora K, Wagstyl K, Cho S, et al. LayNii: A software suite for layer-fMRI. *NeuroImage* (2021) 237:118091. doi:10.1016/j.neuroimage.2021.118091

15. Huber L, Ivanov D, Krieger SN, Streicher MN, Mildner T, Poser BA, et al. Slab-selective, BOLD-corrected VASO at 7 tesla provides measures of cerebral blood volume reactivity with high signal-to-noise ratio. *Magn Reson Med* (2014) 72(1):137–48. doi:10.1002/mrm.24916

16. Jenkinson M, Beckmann CF, Behrens TEJ, Woolrich MW, Smith SM. Fsl. *NeuroImage* (2012) 62:782–90. doi:10.1016/j.neuroimage.2011.09.015

17. Gulban OF, Bollmann S, Huber R, Wagstyl K, Goebel R, Poser BA, et al. Mesoscopic quantification of cortical architecture in the living human brain. *Neuroimage* (2022).

18. Pakenham D, Asghar M, Glover P, O'Neill G, Sengupta A, Schluppeck D, et al. Assessing somatotopic and mototopic organisation in Focal Hand Dystonia using high-resolution 7T fMRI. In: Proc. Joint Annual Meeting ISMRM (2019). p. 0361.

19. Sadnicka A, Wiestler T, Butler K, Altenm¨uller E, Edwards M, Ejaz N, et al. Intact finger representation within primary sensorimotor cortex of musician's dystonia. *Brain* (2022) awac356. page awac356. doi:10.1093/brain/awac356

20. Brüggemann N. Contemporary functional neuroanatomy and pathophysiology of dystonia. *J Neural Transm* (2021) 128:499–508. doi:10.1007/s00702-021-02299-y

21. Gallea C, Herath P, Voon V, Lerner A, Ostuni J, Saad Z, et al. Loss of inhibition in sensorimotor networks in focal hand dystonia. *NeuroImage: Clin* (2018) 17:90–7. doi:10.1016/j.nicl.2017.10.011

22. Kassavetis P, Sadnicka A, Saifee TA, Pareés I, Kojovic M, Bhatia KP, et al. Reappraising the role of motor surround inhibition in dystonia. *J Neurol Sci* (2018) 390:178–83. doi:10.1016/j.jns.2018.04.015

23. Persichetti AS, Avery JA, Huber L, Merriam EP, Martin A. Layer-specific contributions to imagined and executed hand movements in human primary motor cortex. *Curr Biol* (2020) 30(9):1721–5. doi:10.1016/j.cub.2020.02.046

24. Trampel R, Bazin P-L, Schäfer A, Heidemann RM, Ivanov D, Lohmann G, et al. Laminar-specific fingerprints of different sensorimotor areas obtained during imagined and actual finger tapping. *Proc Intl Soc Mag Reson Med* (2012) 20:663.

25. Turner R. Uses, misuses, new uses and fundamental limitations of magnetic resonance imaging in cognitive science. *Philosophical Trans R Soc B: Biol Sci* (2016) 371:20150349. doi:10.1098/rstb.2015.0349

26. McColgan P, Joubert J, Tabrizi SJ, Rees G. The human motor cortex microcircuit: Insights for neurodegenerative disease. *Nat Rev Neurosci* (2020) 21(8):401–15. doi:10.1038/s41583-020-0315-1

27. Schreiber S, Northall A, Weber M, Vielhaber S, Kuehn E, McColgan P, et al. Reply to 'Topographical layer imaging as a tool to track neurodegenerative disease spread in M1'. *Nat Rev Neurosci* (2021) 22(1):69. doi:10.1038/s41583-020-00405-9

28. Haarsma J, Kok P, Browning M. The promise of layer-specific neuroimaging for testing predictive coding theories of psychosis. *Schizophrenia Res* (2020) 245:68–76. doi:10.1016/j.schres.2020.10.009

29. Stephan KE, Petzschner F, Kasper L, Bayer J, Wellstein K, Stefanics G, et al. Laminar fMRI and computational theories of brain function. *NeuroImage* (2019) 197:699–706. doi:10.1016/j.neuroimage.2017.11.001

30. Wan Y, Qian C, Wen W, Zhang P. (2021). Layer-dependent amblyopic deficits in feedforward and lateral processing in human early visual cortex. In OHBM, page 2632.

DYSTONIA

TYPE Review
PUBLISHED 09 February 2023
DOI 10.3389/dyst.2023.11067

OPEN ACCESS

EDITED BY
Aasef Shaikh,
Case Western Reserve University,
United States

*CORRESPONDENCE
Kirsten E. Zeuner,
k.zeuner@neurologie.uni-kiel.de

RECEIVED 18 November 2022
ACCEPTED 23 January 2023
PUBLISHED 09 February 2023

CITATION
Zeuner KE, Baumann A and Witt K (2023), Treatment of writer's cramp based on current pathophysiological concepts.
Dystonia 2:11067.
doi: 10.3389/dyst.2023.11067

Treatment of writer's cramp based on current pathophysiological concepts

Kirsten E. Zeuner[1]*, Alexander Baumann[1] and Karsten Witt[2]

[1]Department of Neurology, Kiel University, Kiel, Germany, [2]Department of Neurology, Research Center Neurosensory Science, School of Medicine and Health Sciences, University of Oldenburg, Oldenburg, Germany

Task specific dystonia belongs to the group of focal dystonias. They are debilitating movement disorders that present with co-contraction of antagonist muscles during a specific task. The most common one is writer's cramp. Botulinum toxin is the symptomatic standard treatment. Its response rate is 50% after 1 year, and the overall efficacy limited due to unwanted weakness in not injected muscles. The pathophysiology of writer's cramp remains unclear, but genetic and additional environmental causes have been proposed. A possible underlying mechanism may be maladaptive reorganization in the sensorimotor cortex. Based on this background alternative treatment strategies were developed such as several different sensory and motor training programs that have been applied to reverse these brain abnormalities. In some studies, sensory and motor training were combined and adjunct with fitness exercises. They were conducted either as an outpatient setting or were established home based. Clinical outcome was measured with different clinical scales such as the writer's cramp rating scale, the arm dystonia rating scale or the Burke, Fahn Marsden Scale. For objective assessment, kinematic handwriting parameters were analyzed. Functional or structural changes of the sensorimotor cortex were estimated using functional magnetic tomography, magnetencephalography and voxel-based morphometry. The results of these training programs were promising; however, one drawback is that the number of patients studied were small and the programs were not controlled since it is difficult to establish a control training to conduct a randomized controlled study.

KEYWORDS

writer's cramp, treatment, pathophysiology, sensorimotor disorganization, structural and functional imaging

Introduction

Writer's cramp (WC) is the most common task specific form of dystonia. With a prevalence of 3.8–80/1,000,000 people it ranks among the orphan diseases (1). The mean age of onset is 38 years. Clinically, patients present with co-contraction of antagonist muscles during writing. In some cases, involuntary flexion of one or several fingers and/or the wrist are the main complaints. Others show extension of their fingers and/or the wrist

during writing or the abnormal posture may be accompanied by tremor (2) (see Figure 1). Mirror dystonia may occur in up to 44.6% of patients in the affected, resting hand, when they are asked to write with their contralateral, non - affected hand (3). In simple writer's cramp co-contraction presents mainly during writing, while in more complex forms other fine motor tasks are also affected (4). In the literature, the complex forms of writer's cramp have also been referred to as dystonic writer's cramp because of the occurrence of dystonia during other activities (5). Patients with writer's cramp often use a high pen pressure and increased axial pressure during writing (6–8). The writing speed and frequency are often reduced and the writing movement is irregular (9). Moreover, with high sensitivity and specificity abnormal word legibility and peak accelerations have been discovered when using a handwriting recognition software to record word legibility in an automated manner (10).

Task specific dystonia may also affect other professions such as musician's, golfer's, typists or hairdressers. In musician's dystonia the fingers are most commonly affected, rather than the hand. Task specific dystonia impacts patient's livelihood and has substantial socio-economic impact, causing many patients to give up their profession (11). The standard treatment includes botulinum toxin (BoNT) injections into affected muscles. However, BoNT injections are not always helpful and may cause a number of side effects (12). As alternative treatment approaches training programs have been developed (13). In this review we will focus on these treatment strategies that are based on the current neurophysiological findings and discuss their methodology and outcome. We will also discuss future perspectives.

Pathophysiology of writer's cramp

The pathophysiology is multifactorial and has been linked to environmental and genetic factors (14–17). It is considered a motor network disorder including the sensorimotor cortex, basal ganglia, thalamus and cerebellum and provides a model for other forms of task specific dystonia areas (18–21). Several studies demonstrated impaired sensory function (13, 22–27), abnormal reorganization of the somatosensory cortex (S1) (28, 29) and sensorimotor integration (30) as result of maladaptive neural plasticity (31), alterations in motor planning with a lack of neuronal inhibition (13, 17), and cerebellar dysfunction (19, 32, 33). These areas are also involved during writing (34–36). Probably, not only the planning of a writing movement is affected (37), but it seems like the parieto-premotor-M1 network, which codes well-trained and skillful tasks, is deficient (38, 39).

The sensory system is deficient in writer's cramp

Several structural and functional imaging as well as neurophysiological methodologies have been implemented to understand the deficient sensory system in writer's cramp. The general view is that maladaptive reorganization of the somatotopic finger representations within the primary somatosensory cortex is a pathogenic feature in task specific dystonia.

For example functional connectivity was strengthened between the somatosensory cortical-putamen loop during a visuo-motor control task (40). The putamen seems to play a major role as its grey matter volume is elevated (39, 41). The thalamus, another area that contributes to sensory processing, is considered as a central dysfunctional hub integrating basal ganglia and cerebellar output and gating sensory streams (26). Here, grey matter decreases were found bilaterally in affected patients (42).

Beside imaging studies there are a number of neurophysiological studies that demonstrated abnormalities of the sensory system in writer's cramp. First, proprioceptive processing was defective as shown in a tonic vibration task (43, 44). Second, contact heat-evoked potentials and pain rating were reduced using quantitative sensory testing (45). Third, tactile information processing was impaired (26). Specifically, temporal (26, 48) and spatial discrimination thresholds (SDT) (22, 48, 49) are increased. Fourth, fine force regulation was disturbed. Patients with writer's cramp had not only deficits in the coordination of grip and lift load (50), but also in scaling of the precision grip force in a drawer opening task (51). A grip force overshoot during the initial lifts of an

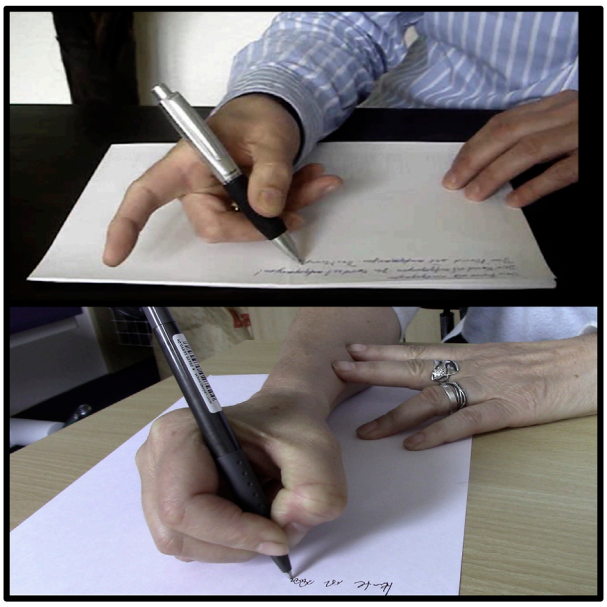

FIGURE 1
Figure shows two different types of writer's cramp. The upper patient presents with extension of the index finger during writing. In the bottom part of the figure the patient has flexion of the thumb with contraction of flexor pollicis longus muscle.

unfamiliar object has been described (52). Fifth, patients with writer's cramp showed increased error, greater variability, and longer release in a force tracking task indicating a generalized deficit in sensorimotor integration (53). Finally, they presented with an abnormal rate of force production and relaxation during wrist movements when measuring peak torque output at the elbow joint and in multiple flexor and extensor muscle groups (54). They had difficulties in adjusting the pressure of their index finger to rather low force plateaus given by visual cues (55). In a probabilistic cued fine motor task writer's cramp patients were capable of anticipatory adaptation of forces, but could not utilize the decision range in motor planning and adjust their force (23).

Writer's cramp is a sensorimotor network disorder

Functional and structural imaging studies have advanced our understanding of the pathophysiology in WC (21). Studies examining the morphometric changes in focal dystonia detected either increased or decreased grey matter volume, in some studies bilaterally, in the putamen or globus pallidus (41, 56–59). In patients with writer's cramp, voxel-based analysis showed larger grey matter volume bilateral in the posterior part of the putamen and globus pallidus (39). Conversely, decreased grey matter density was found in the hand area of the left primary sensorimotor cortex, bilaterally in the cerebellum, and subcortically in the thalamus in the same patient group (42). Diffusion tensor imaging (60) identified lower fractional anisotropy in the tracts between the middle frontal gyrus and putamen (61). In contrast, higher fractional anisotropy has been reported bilaterally between the posterior internal capsule and the ventroposteriolateral thalamic nucleus. Tractography demonstrated that changes involved fiber tracts connecting the primary sensorimotor or the brainstem (62). Finally, more recent work included diffusion-weighted imaging (DWI) and graph theoretical analysis to examine the structural connectome. The structural regional networks in dystonic patients showed a reduction in the number of nodes mainly in the bilateral putamen. In writer's cramp, the abnormalities occurred bilateral in the insula and the anterior and middle cingulate cortex. The cerebellar vermis, the left cerebellar lobule VIII and the inferior temporal gyrus were also affected. Thus, structural changes in areas that are involved in dystonia represented nodes of a large structural network disruption that were related to areas responsible for sensorimotor planning and processing during writing (18).

Using functional imaging, patients with WC exhibited abnormal blood oxygenation level dependent (BOLD) activity in the sensorimotor cortex, cerebellum and possibly thalamus during writing in an fMRI study (63). The BOLD response was decreased in cortical and subcortical areas during a finger tapping tasks in patients with in simple and/or complex WC compared to controls (39, 64), the hippocampus (65) and the hippocampal-striatal functional connectivity reduced, while the activity was increased in the putamen (65). After practice, premotor-striatal areas, which connectivity correlated with motor performance, were overactive (65). Dynamic causal modelling techniques revealed that patients with WC used the same neural network as healthy individuals during finger tapping, but the effective connectivity patterns differed between both groups. Specifically, the effective connectivity between the globus pallidus' inhibitory influence on the motor cortex (M1) was weakened while M1 inhibited the putamen stronger in WC. Furthermore, connectivity between M1 and the cerebellum and the cerebellum and the putamen was altered in WC (20). Functional network changes have further been explored using graph theoretical analysis approaches. Here, hub analysis revealed alterations in communication patterns of the primary motor cortex, the thalamus and the cerebellum. Especially the abnormal activity in the cerebellum had been attributed to compensatory rerouting at an early stage of the disease (33) (see Figure 2).

The influence of writing on the cortical and subcortical network

The premotor cortex is involved in planning and monitoring writing movements while the superior parietal cortex controls the somatosensory information and integration into a motor plan (34–36). In an executed writing compared to an imagined writing task the activated network was the same, although during writing the activation of the fronto–parieto-temporal network was clearly more pronounced during the execution of writing in a group of healthy individuals (Figure 3). In contrast, WC patients displayed reduced connectivity between the dorsal premotor and superior parietal cortex (66) that was positively correlated with the severity of dystonic symptoms. They demonstrated a more pronounced BOLD signal in the contralateral sensorimotor cortex, the supplementary- and dorsal premotor cortex as well as in the putamen and thalamus during motor imagery of writing (66). Motor imagery of grasping a pencil for writing lead to an elevated BOLD response in the supplementary-, dorsal pre- and motor cortex (BA 6) indicating alterations in planning a writing movement (37). In the task specific network of the dominant hand, WC patients showed a deficient parieto-premotor-M1 network, which codes well-trained and skillful tasks (38, 39). The cerebellum (vermis und lobulus VI) and the anterior, associative putamen showed decreased activation in writer's cramp patients that were unrelated to the specific task (38).

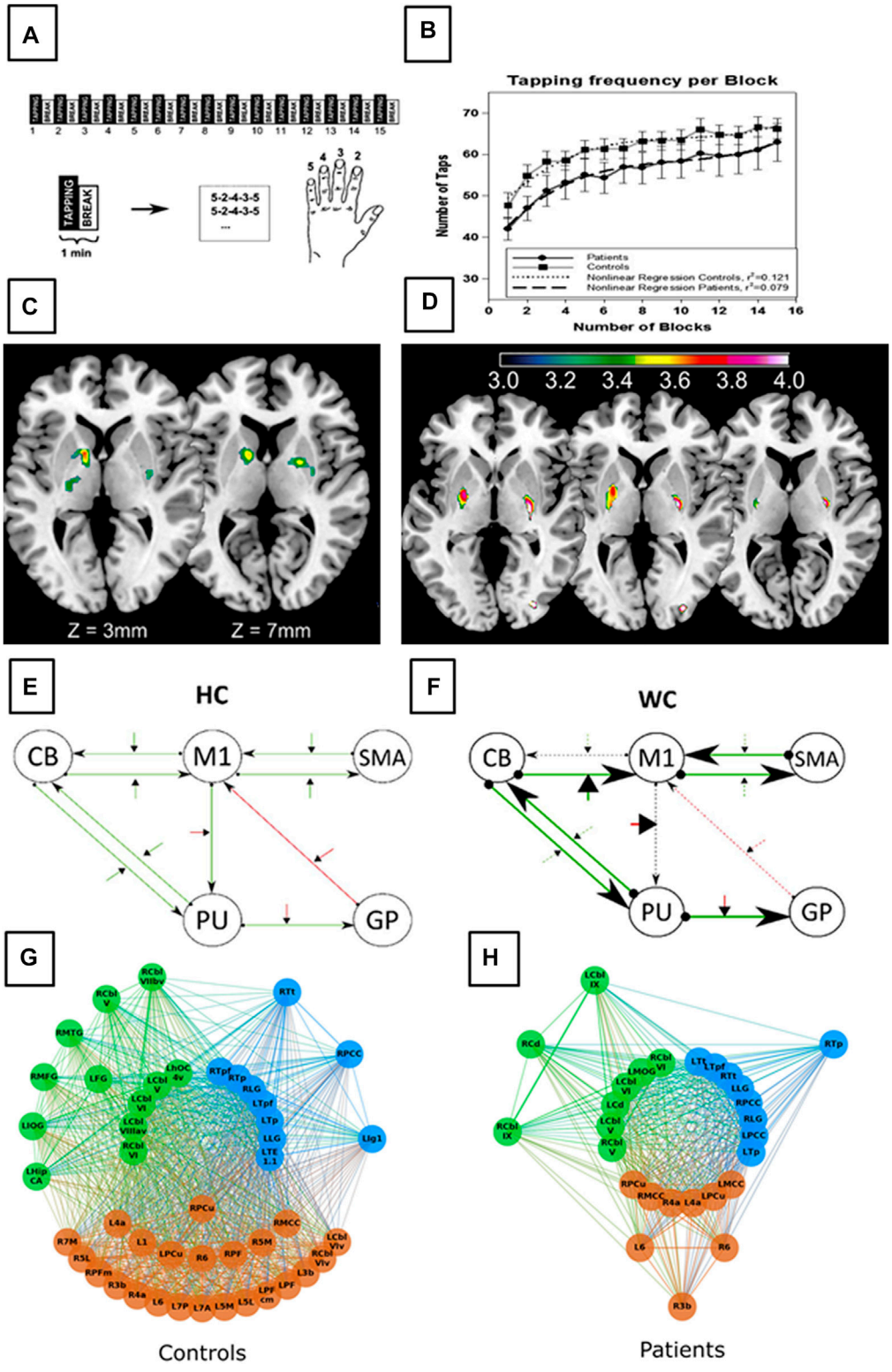

FIGURE 2
Figure displays morphometric alterations and functional disturbances in network communication in WC patients compared to healthy controls (HC). The task included a block-wise executed sequential finger-tapping task **(A)** of the non-dominate hand to avoid dystonic contraction during tapping. Behavioural results demonstrate comparable motor performance in HC and WC patients **(B)**. Voxel based morphometry demonstrate increase grey matter density within the basal ganglia in WC patients **(C)**. Functional magnetic resonance imaging revealed altered basal ganglia

(*Continued*)

FIGURE 2 (Continued)
activation **(D)** in WC patients (putamen and globus pallidus). In addition, altered network functions in WC patients can be demonstrated using dynamic causal modeling **(E,F)** with stronger task activated connectivity in both, the cortico-cerebellar and the cortico-basal ganglia loops. Graph theorem analysis revealed altered modular hub formation in WC patients. The order of the circles display different hierarchical hubs, starting with the connector hubs in the innermost circle, provincial hubs in the intermediate circle and high influence nodes on the outer circle. WC patients network architecture differs in terms of the number of hubs per network (blue the front-occipital module, green the parietal module and brown a subcortical module) and a reduction in high influence nodes, and provincial hubs. These results together identifie WC as a network disorder even detectable in the non-dystonic hand (Figures 1A–D adapted from Zeuner et al. (39); Figures 1E, F adapted from Rothkirch et al. (20); Figures 1 G, F adapted from Schill et al. (33).

Increased excitability and loss of inhibition in writer's cramp

Reduced inhibitory control over cortical motor areas might be responsible for sustained muscle contraction in patients with writer's cramp (31). For decades, not only loss of inhibition, but also increased excitability at multiple levels have been discussed as an underlying pathophysiological feature in patients with writer's cramp (67). This includes the motor cortex (M1), premotor cortex, somatosensory cortex (S1), and the cerebellum. Gamma-aminobutyric acid (GABA) is an inhibitory neurotransmitter in the brain. GABAergic deficits have been described in the sensorimotor cortex and in the cerebellum and might be an explanation for the loss of inhibitory control resulting from maladaptive plasticity and abnormal surround inhibition (68).

Treatment of writer's cramp

Standard treatment of writer's cramp

The standardized therapy, botulinum neurotoxin (BoNT) injections into affected muscles, has been shown to be effective in a number of uncontrolled (69) and one randomized, placebo controlled study (12, 70). Kruisdjik et al. (2007) included 40 patients writer's cramp (12). Their patients received either BoNT or placebo EMG guided in a randomized manner twice with 1 month apart in case they were unsatisfied with the treatment effect. The primary outcome measure was the patients' decision to either continue or stop the injections after 3 months. They were followed for a year. Fourteen from 20 patients reported a positive effect from BoNT and chose to continue the treatment, while in the placebo group 13 of 19 patients wished to stop with the injections. The positive results were supported by improvements in the visual analogue scale (writing), the writer's cramp rating scale, the writing speed and the symptom severity scale. Ideally, the application of the toxin should be performed with ultrasound or with stimulation through the EMG needle in order to target the correct muscle for injection (69, 71, 72). However, most patients display several ways to compensate their dystonic posture, so frequently it is difficult to identify the dystonic muscles (70). Hence, just 50% of patients, who were treated for 1 year (12) decided to continue with BoNT treatment. In a retrospective 10 years follow-up, only 20/214 patients continued this treatment. The reasons for discontinuation included a lack of treatment efficacy or involuntary paresis in not injected muscles probably caused by spreading of the toxin into neighboring muscles. Affected patients might then show a paresis in both, the injected and non-injected muscles, which can result in restraints in their daily activities that are more severe than the disability in writing (73).

Sensorimotor training based on pathophysiological concepts

Alternative treatment approaches based on the pathophysiology of writer's cramp have been developed. This includes re-training programs with different concepts. The purpose of these training programs was to achieve a long-term effect.

One of the first training programs that had been developed aimed at re-organizing the disturbed somatosensory maladaptation and disorganization in the sensory cortex by implementing a sensory training with Braille reading (74). As an objective parameter the grating orientation task was used. Patients improved their writing and their performance in the grating orientation task, but a long-term effect remained only as long as they trained (75).

In subsequent motor training programs with (76) or without precedent immobilization (77, 78) patients learned individualized finger movements. Immobilization was carried out continuously with a splint for the wrist and the finger joints. Patients with writer's cramp have difficulties in activating fingers individually, because they often present with co-contraction. Therefore, therapeutic putty has been used to teach patients moving each finger separately. Pathophysiologically the intention was to reverse cortical disorganization, enhance the training efficacy and normalize sensorimotor integration. Their efficacy on writing was measured with kinematic analyses of writing movements (6, 9, 76–78). The purpose of those motor training programs was to decrease the abnormally increased writing pressure (6), disturbed regularity of movement kinematics (9, 78) and dystonic symptoms (6, 76, 78). Training without

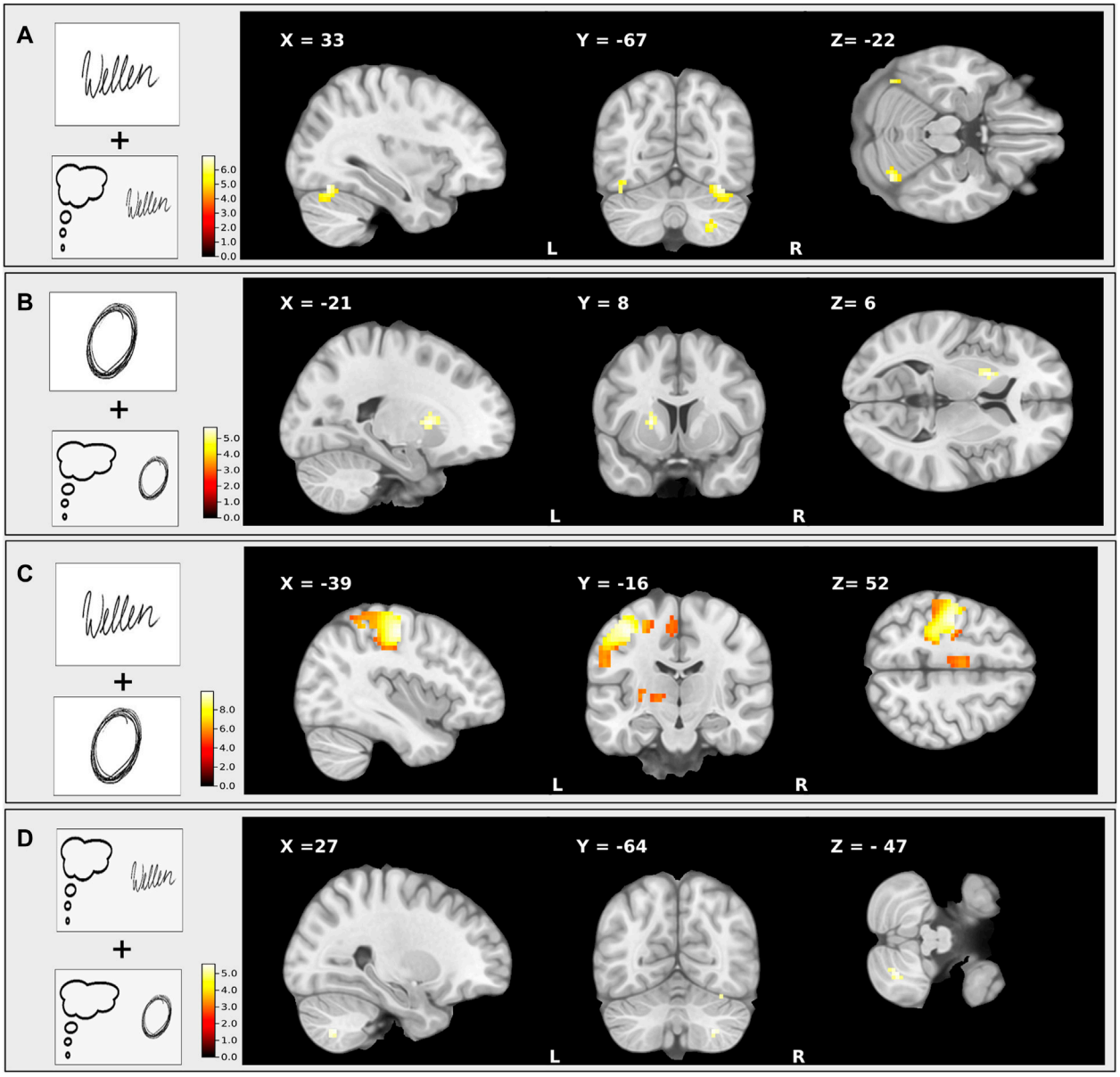

FIGURE 3
This figure shows the T-maps of four different conjunction contrasts: **(A)** executed writing and imagined writing were accompanied by an increased activity of the ipsilateral cerebellum and the contralateral sensorimotor cortex; **(B)** executed drawing and imagined drawing revealed elevated activity of a fronto–parieto-temporal network; **(C)** executed writing and executed drawing induced an enhanced activation of the left somatosensory and premotor area; **(D)** imagined writing and imagined drawing revealed a higher involvement of occipital activation during. The clusters were significant within the ROI analysis after FWE-correction on $p < 0.05$. This figure is adapted from Baumann et al. (36).

immobilization led to mild improvement in simple handwriting parameters (77), while the combination of a 4 weeks forearm immobilization with subsequent re-training over 8 weeks improved the writing fluency, and patients exerted less vertical force on the digitizing tablet (76). In addition, there was significantly clinical improvement as indexed by a decrease in the writer's cramp rating scale (79) and an increase in the arm dystonia rating scale (80). Transcranial magnetic stimulation (TMS) was implemented to test concurrent changes in regional excitability. Grey matter changes in the contralateral primary motor hand area (M1HAND) were evaluated utilizing voxel-based morphometry (VBM). Specifically, either suppression of regional excitability or grey matter decrease after immobilization or enhancement and grey matter increase after re-training of the right, dominant hand were analyzed in the contralateral left M1HAND area. While immobilization reduced corticomotor

excitability and caused relative grey matter decrease in the contralateral left M1HAND, subsequent training reversed the effects of immobilization, causing an increase in regional grey matter density and excitability (41).

Sensory discriminative and motor training has also been combined with fitness and resulted in clinical gains of motor control, motor accuracy, sensory discrimination and physical performance (81, 82). After 6 months, all 11 patients were contacted. Ten out of 11 patients returned to work, and the improvement was scored 84%–90% for the specific task that was impaired. Patients, whose training was supervised, showed a better outcome (81). Enlarged and disorganized hand representations were reversed after prolonged rehabilitation of 5.5 months investigated with magnetencephalography (MEG) and 3D-MRI 3D brain reconstructions that were paralleled with clinical recovery and improved writing performance (83). There was, however no long-term follow up, so it remains unclear, whether patients continued their training, and how long the positive training effect lasted. That program included several different training aspects including relaxation techniques, elementary movement and postures correction, pen control. Several studies started with simple movements and progressed to more complex movements during the course of the training (6, 76, 78, 83).

Biofeedback to reverse abnormally high muscle activity

Biofeedback is another technique that had been used to treat writer's cramp. This approach was based on faulty inhibition due to the abnormal reorganization in the sensorimotor cortex. Therefore, the training approach was to teach patients active inhibition of proximal muscles and thus reduce the overflow of motor areas pertaining to them. The authors implemented auditorial EMG feedback from affected muscles with abnormally high activity during writing. This feedback served as a control measure to teach patients writing in a relaxed manner (84). Patients received practice sessions once every 2 weeks and instructions for a home-based training program. On a visual analogue scale, nine of 10 patients reported an overall improvement ranging from 37.5% to 93.4% (84). To reverse decreased striatal D2 receptor-binding, as measured with single-photon emission computed tomography (SPECT) with [123I] iodobenzamide (IBZM), patients were instructed to visually maintain the EMG motor unit amplitude at the minimum possible level while writing exercises (85). The authors concluded from their data that with a biofeedback-based sensorimotor training it was possible to reorganize the activity in the nigrostriatal dopaminergic pathway (85).

A different biofeedback method that lead to a significant improvement in writing was auditory grip force feedback (86). In that study the authors used a pen wrapped with a force sensor matrix. Writer's cramp patients received 7 h training sessions that was distributed over several weeks. They performed the specialized training with a standard pen over 50 min, and for the last 10 minutes with the force sensor matrix wrapped writing stylus to measure grip force and to give auditory grip force feedback. Patients improved their handwriting performance, the writing pressure, and reported to have less pain (86).

Non-invasive brain stimulation techniques to reverse abnormal excitability

Furthermore, non-invasive stimulation techniques have been investigated using repetitive transcranial magnetic stimulation (rTMS) and transcranial direct current stimulation (tDCS) (67, 87–92). The purpose was to reduce deficient inhibition. Low-(<1 Hz) frequency TMS decreases cortical excitability and had been applied in patients with writer's cramp to improve handwriting. The area that had been stimulated included the premotor cortex, the primary motor cortex and the supplementary motor area with the intention to improve handwriting and pen pressure (69, 87–91). In most studies showed short-term positive effects after 15–30 min and in some studies 10–15 days post stimulation (67). More recent studies imply that repetitive sessions over consecutive days are necessary to achieve therapeutic effects (67). In a tDCS study that applied anodal, cathodal, or sham tDCS to the cerebellum the authors reported improved writing kinematics with reduced cerebellar inhibition with anodal tDCS (92). However, there are a number of tDCS studies with negative results according to clinical parameters that were investigated (67).

Discussion and future directions

Writer's cramp is a rare task specific form of dystonia. In their medical history, many affected patients report long daily writing hours and often they have professions, in which writing is required. Therefore, the impact on patients' everyday life is tremendous, especially when they are working. BoNT offers one treatment possibility. However, over the years, a high percentage of patients refrain from BoNT injections. The main reasons are that this treatment form is not efficient for the patient's daily life or the side effects are not tolerable. For example, severe paresis may occur in the injected muscles. Sometimes the toxin spreads to neighboring muscles causing involuntary paresis and can cause constraints in daily life, even if writing has improved.

Therefore, based on the pathophysiology, several rehabilitative treatment approaches have been suggested (69). Studies with re-training programs for several weeks were designed to reverse abnormal sensorimotor reorganization and to achieve long-lasting therapeutic effects. In a subsequent study

biofeedback was combined with a re-training program to improve muscle co-contraction. Low-frequency rTMS studies have to be considered as short -term projects. Positive effects were measured during the first 30 min post-stimulation or a maximum of 15 days. There is ongoing discussion, whether the stimulation has to be repeated after a certain time to achieve long-term results in rTMS (67).

Currently, writer's cramp is considered as a network disorder affecting the sensory system, the motor system, the basal ganglia and the cerebellum. Especially, maladaptive reorganization in the sensory cortex (30), increased excitation or faulty inhibition have been reported in a number of studies (13, 17, 31). However, this view has been challenged due to the development of new technologies for examining brain region reorganization and it is expected that further advances will be made leading to additional changes in our understanding. For example, normal digit representation maps between fingers in patients with musician's dystonia have been reported very recently using an optimized spatial metric multivariate pattern analysis (93). So, perhaps, as we get a deeper understanding of the pathophysiology, it is necessary to reconsider current treatment approaches. This may also apply to the way, how writing has been evaluated. Mostly, a kinematic writing analysis has been used, and parameters such as increased axial pressure, decreased writing frequency, and irregular writing movements have been found to be characteristic features in writer's camp (9, 86). On the other hand, a handwriting recognition software has been recently applied for writer's cramp patients to evaluate word legibility in an automated manner. In that study, patients with writer's cramp showed abnormal word legibility and peak accelerations (10) with high sensitivity and specificity, but mean axial pen pressure, average velocity, stroke length, or CV of peak vertical velocity were normal. Therefore, it is conceivable that re-training should focus on alternative aspects of writing.

One major problem that applies to all treatment studies is the small number of patients. It is not possible to compare any occupational treatment to normal controls, therefore a randomized controlled study is not feasible. Another challenge is to establish a control training. It is impossible to introduce a control motor training, because any motor training will always have an influence on the sensorimotor network, independently of its specificity. A control training that includes no motor aspects might unblind writer's cramp patients, who expect some way of motor intervention to treat this motor disorder.

Therefore, future studies with new technologies have to be performed with larger sample sizes to either confirm or reject the current view of the pathophysiology. Depending on the results, the rehabilitative treatment approaches have to be reassessed and adapted. Ideally, future treatment studies should be performed in a multicentre setting with a higher number of patients and a control training needs to established.

Author contributions

KEZ developed the concept and wrote the first draft of the manuscript. AB and KW reviewed and revised the manuscript for content. In addition, they provided the figures.

Conflict of interest

KEZ has received research support from the Christa and Hans-Peter Thomsen Foundation, the German Research Foundation (DFG 5919/4-1) and from Strathmann GmbH & Co. KG. She reports speaker's honoraria from Bayer Vital GmbH, BIAL, Alexion, AbbVie Allergan and Merz outside the submitted work. She has served as a consultant and received fees from Merz, Ipsen, Alexion and the German Federal Institute for Drugs and Medical Devices (BfArM). KW receives research support for the German Research Foundation (DFG GK 2783) and form STADAPHARM. He serves as a consultant for BIAL and receives speaker's honoraria form BIAL, STADAPHARM and Boston Scientific.

The remaining author declares that the research was conducted in the absence of any commercial or financial relationships that could be construed as a potential conflict of interest.

References

1. Defazio G, Berardelli A, Hallett M. Do primary adult-onset focal dystonias share aetiological factors? *Brain* (2007) 130(5):1183–93. doi:10.1093/brain/awl355

2. Goldman JG. Writer's cramp. *Toxicon* (2015) 107:98–104. doi:10.1016/j.toxicon.2015.09.024

3. Jedynak PC, Tranchant C, de Beyl DZ. Prospective clinical study of writer's cramp. *Mov Disord* (2001) 16(3):494–9. doi:10.1002/mds.1094

4. Stahl CM, Frucht SJ. Focal task specific dystonia: A review and update. *J Neurol* (2017) 264(7):1536–41. doi:10.1007/s00415-016-8373-z

5. Sheehy MP, Marsden CD. Writers' cramp-a focal dystonia. *Brain* (1982) 105(3):461–80. doi:10.1093/brain/105.3.461

6. Baur B, Furholzer W, Jasper I, Marquardt C, Hermsdorfer J. Effects of modified pen grip and handwriting training on writer's cramp. *Arch Phys Med Rehabil* (2009) 90(5):867–75. doi:10.1016/j.apmr.2008.10.015

7. Hermsdorfer J, Marquardt C, Schneider AS, Furholzer W, Baur B. Significance of finger forces and kinematics during handwriting in writer's cramp. *Hum Mov Sci* (2011) 30(4):807–17. doi:10.1016/j.humov.2010.04.004

8. Schneider AS, Furholzer W, Marquardt C, Hermsdorfer J. Task specific grip force control in writer's cramp. *Clin Neurophysiol* (2014) 125(4):786–97. doi:10.1016/j.clinph.2013.09.043

9. Zeuner KE, Peller M, Knutzen A, Holler I, Munchau A, Hallett M, et al. How to assess motor impairment in writer's cramp. *Mov Disord* (2007) 22(8):1102–9. doi:10.1002/mds.21294

10. Bukhari-Parlakturk N, Lutz MW, Al-Khalidi HR, Unnithan S, Wang JE, Scott B, et al. Suitability of automated writing measures for clinical trial outcome in writer's cramp. *Mov Disord* (2022). doi:10.1002/mds.29237

11. Amini D. Occupational therapy interventions for work-related injuries and conditions of the forearm, wrist, and hand: A systematic review. *Am J Occup Ther* (2011) 65(1):29–36. doi:10.5014/ajot.2011.09186

12. Kruisdijk JJ, Koelman JH, Ongerboer de Visser BW, de Haan RJ, Speelman JD. Botulinum toxin for writer's cramp: A randomised, placebo-controlled trial and 1-year follow-up. *J Neurol Neurosurg Psychiatry* (2007) 78(3):264–70. doi:10.1136/jnnp.2005.083170

13. Zeuner KE, Molloy FM. Abnormal reorganization in focal hand dystonia--sensory and motor training programs to retrain cortical function. *NeuroRehabilitation* (2008) 23(1):43–53. doi:10.3233/nre-2008-23105

14. Lohmann K, Schmidt A, Schillert A, Winkler S, Albanese A, Baas F, et al. Genome-wide association study in musician's dystonia: A risk variant at the arylsulfatase G locus? *Mov Disord* (2014) 29(7):921–7. doi:10.1002/mds.25791

15. Lange LM, Junker J, Loens S, Baumann H, Olschewski L, Schaake S, et al. Genotype-phenotype relations for isolated dystonia genes: Mdsgene systematic review. *Mov Disord* (2021) 36(5):1086–103. doi:10.1002/mds.28485

16. Zeuner KE, Acewicz A, Knutzen A, Dressler D, Lohmann K, Witt K. Dopamine Drd2 polymorphism (Drd2/Annk1-Taq1a) is not a significant risk factor in writer's cramp. *J Neurogenet* (2016) 30(3-4):276–9. doi:10.1080/01677063.2016.1238916

17. Hallett M. Pathophysiology of writer's cramp. *Hum Mov Sci* (2006) 25(4-5):454–63. doi:10.1016/j.humov.2006.05.004

18. Hanekamp S, Simonyan K. The large-scale structural connectome of task-specific focal dystonia. *Hum Brain Mapp* (2020) 41(12):3253–65. doi:10.1002/hbm.25012

19. Neychev VK, Fan X, Mitev VI, Hess EJ, Jinnah HA. The basal ganglia and cerebellum interact in the expression of dystonic movement. *Brain* (2008) 131(9):2499–509. doi:10.1093/brain/awn168

20. Rothkirch I, Granert O, Knutzen A, Wolff S, Govert F, Pedersen A, et al. Dynamic causal modeling revealed dysfunctional effective connectivity in both, the cortico-basal-ganglia and the cerebello-cortical motor network in writers' cramp. *Neuroimage Clin* (2018) 18:149–59. doi:10.1016/j.nicl.2018.01.015

21. Simonyan K. Neuroimaging applications in dystonia. *Int Rev Neurobiol* (2018) 143:1–30. doi:10.1016/bs.irn.2018.09.007

22. Molloy FM, Carr TD, Zeuner KE, Dambrosia JM, Hallett M. Abnormalities of spatial discrimination in focal and generalized dystonia. *Brain* (2003) 126(10):2175–82. doi:10.1093/brain/awg219

23. Zeuner KE, Knutzen A, Granert O, Trampenau L, Baumann A, Wolff S, et al. Never too little: Grip and lift forces following probabilistic weight cues in patients with writer's cramp. *Clin Neurophysiol* (2021) 132(12):2937–47. doi:10.1016/j.clinph.2021.09.010

24. Todt I, Baumann A, Knutzen A, Granert O, Tzvi E, Lindert J, et al. Abnormal effective connectivity in the sensory network in writer's cramp. *Neuroimage Clin* (2021) 31:102761. doi:10.1016/j.nicl.2021.102761

25. Merchant SHI, Frangos E, Parker J, Bradson M, Wu T, Vial-Undurraga F, et al. The role of the inferior parietal lobule in writer's cramp. *Brain* (2020) 143(6):1766–79. doi:10.1093/brain/awaa138

26. Conte A, Defazio G, Hallett M, Fabbrini G, Berardelli A. The role of sensory information in the pathophysiology of focal dystonias. *Nat Rev Neurol* (2019) 15(4):224–33. doi:10.1038/s41582-019-0137-9

27. Conte A, Ferrazzano G, Belvisi D, Manzo N, Suppa A, Fabbrini G, et al. Does the somatosensory temporal discrimination threshold change over time in focal dystonia? *Neural Plast* (2017) 2017:9848070. doi:10.1155/2017/9848070

28. Garraux G, Bauer A, Hanakawa T, Wu T, Kansaku K, Hallett M. Changes in brain anatomy in focal hand dystonia. *Ann Neurol* (2004) 55(5):736–9. doi:10.1002/ana.20113

29. Lerner A, Shill H, Hanakawa T, Bushara K, Goldfine A, Hallett M. Regional cerebral blood flow correlates of the severity of writer's cramp symptoms. *Neuroimage* (2004) 21(3):904–13. doi:10.1016/j.neuroimage.2003.10.019

30. Patel N, Jankovic J, Hallett M. Sensory aspects of movement disorders. *Lancet Neurol* (2014) 13(1):100–12. doi:10.1016/S1474-4422(13)70213-8

31. Quartarone A, Hallett M. Emerging concepts in the physiological basis of dystonia. *Mov Disord* (2013) 28(7):958–67. doi:10.1002/mds.25532

32. Shakkottai VG, Batla A, Bhatia K, Dauer WT, Dresel C, Niethammer M, et al. Current opinions and areas of consensus on the role of the cerebellum in dystonia. *Cerebellum* (2017) 16(2):577–94. doi:10.1007/s12311-016-0825-6

33. Schill J, Zeuner KE, Knutzen A, Todt I, Simonyan K, Witt K. Functional neural networks in writer's cramp as determined by graph-theoretical analysis. *Front Neurol* (2021) 12:744503. doi:10.3389/fneur.2021.744503

34. Planton S, Jucla M, Roux FE, Demonet JF. The "handwriting brain": A meta-analysis of neuroimaging studies of motor versus orthographic processes. *Cortex* (2013) 49(10):2772–87. doi:10.1016/j.cortex.2013.05.011

35. Planton S, Longcamp M, Peran P, Demonet JF, Jucla M. How specialized are writing-specific brain regions? An fmri study of writing, drawing and oral spelling. *Cortex* (2017) 88:66–80. doi:10.1016/j.cortex.2016.11.018

36. Baumann A, Todt I, Knutzen A, Gless CA, Granert O, Wolff S, et al. Neural correlates of executed compared to imagined writing and drawing movements: A functional magnetic resonance imaging study. *Front Hum Neurosci* (2022) 16:829576. doi:10.3389/fnhum.2022.829576

37. Delnooz CC, Helmich RC, Medendorp WP, Van de Warrenburg BP, Toni I. Writer's cramp: Increased dorsal premotor activity during intended writing. *Hum Brain Mapp* (2013) 34(3):613–25. doi:10.1002/hbm.21464

38. Gallea C, Horovitz SG, Najee-Ullah M, Hallett M. Impairment of a parieto-premotor network specialized for handwriting in writer's cramp. *Hum Brain Mapp* (2016) 37(12):4363–75. doi:10.1002/hbm.23315

39. Zeuner KE, Knutzen A, Granert O, Gotz J, Wolff S, Jansen O, et al. Increased volume and impaired function: The role of the basal ganglia in writer's cramp. *Brain Behav* (2015) 5(2):e00301. doi:10.1002/brb3.301

40. Moore RD, Gallea C, Horovitz SG, Hallett M. Individuated finger control in focal hand dystonia: An fmri study. *Neuroimage* (2012) 61(4):823–31. doi:10.1016/j.neuroimage.2012.03.066

41. Granert O, Peller M, Gaser C, Groppa S, Hallett M, Knutzen A, et al. Manual activity shapes structure and function in contralateral human motor hand area. *Neuroimage* (2011) 54(1):32–41. doi:10.1016/j.neuroimage.2010.08.013

42. Delmaire C, Vidailhet M, Elbaz A, Bourdain F, Bleton JP, Sangla S, et al. Structural abnormalities in the cerebellum and sensorimotor circuit in writer's cramp. *Neurology* (2007) 69(4):376–80. doi:10.1212/01.wnl.0000266591.49624.1a

43. Kaji R, Rothwell JC, Katayama M, Ikeda T, Kubori T, Kohara N, et al. Tonic vibration reflex and muscle afferent block in writer's cramp. *Ann Neurol* (1995) 38(2):155–62. doi:10.1002/ana.410380206

44. Trompetto C, Curra A, Buccolieri A, Suppa A, Abbruzzese G, Berardelli A. Botulinum toxin changes intrafusal feedback in dystonia: A study with the tonic vibration reflex. *Mov Disord* (2006) 21(6):777–82. doi:10.1002/mds.20801

45. Suttrup I, Oberdiek D, Suttrup J, Osada N, Evers S, Marziniak M. Loss of sensory function in patients with idiopathic hand dystonia. *Mov Disord* (2011) 26(1):107–13. doi:10.1002/mds.23425

46. Conte A, Rocchi L, Ferrazzano G, Leodori G, Bologna M, Li Voti P, et al. Primary somatosensory cortical plasticity and tactile temporal discrimination in focal hand dystonia. *Clin Neurophysiol* (2014) 125(3):537–43. doi:10.1016/j.clinph.2013.08.006

47. Fiorio M, Tinazzi M, Bertolasi L, Aglioti SM. Temporal processing of visuotactile and tactile stimuli in writer's cramp. *Ann Neurol* (2003) 53(5):630–5. doi:10.1002/ana.10525

48. Sanger TD, Tarsy D, Pascual-Leone A. Abnormalities of spatial and temporal sensory discrimination in writer's cramp. *Mov Disord* (2001) 16(1):94–9. doi:10.1002/1531-8257(200101)16:1<94::aid-mds1020>3.0.co;2-o

49. Bara-Jimenez W, Shelton HM. Spatial discrimination is abnormal in focal hand dystonia. *Neurology* (2000) 55(12):1869–73. doi:10.1212/wnl.55.12.1869

50. Odergren T, Iwasaki N, Borg J, Forssberg H. Impaired sensory-motor integration during grasping in writer's cramp. *Brain* (1996) 119(2):569–83. doi:10.1093/brain/119.2.569

51. Serrien DJ, Burgunder JM, Wiesendanger M. Disturbed sensorimotor processing during control of precision grip in patients with writer's cramp. *Mov Disord* (2000) 15(5):965–72. doi:10.1002/1531-8257(200009)15:5<965::aid-mds1030>3.0.co;2-0

52. Nowak DA, Hermsdorfer J. Grip force behavior during object manipulation in neurological disorders: Toward an objective evaluation of manual performance deficits. *Mov Disord* (2005) 20(1):11–25. doi:10.1002/mds.20299

53. Bleton JP, Teremetz M, Vidailhet M, Mesure S, Maier MA, Lindberg PG. Impaired force control in writer's cramp showing a bilateral deficit in sensorimotor integration. *Mov Disord* (2014) 29(1):130–4. doi:10.1002/mds.25690

54. Prodoehl J, MacKinnon CD, Comella CL, Corcos DM. Rate of force production and relaxation is impaired in patients with focal hand dystonia. *Parkinsonism Relat Disord* (2006) 12(6):363–71. doi:10.1016/j.parkreldis.2006.01.008

55. Zeuner KE, Knutzen A, Pedack L, Hallett M, Deuschl G, Volkmann J. Botulinum neurotoxin treatment improves force regulation in writer's cramp.

Parkinsonism Relat Disord (2013) 19(6):611–6. doi:10.1016/j.parkreldis.2013.02.011

56. Bradley D, Whelan R, Walsh R, Reilly RB, Hutchinson S, Molloy F, et al. Temporal discrimination threshold: Vbm evidence for an endophenotype in adult onset primary torsion dystonia. *Brain* (2009) 132(9):2327–35. doi:10.1093/brain/awp156

57. Egger K, Mueller J, Schocke M, Brenneis C, Rinnerthaler M, Seppi K, et al. Voxel based morphometry reveals specific grey matter changes in primary dystonia. *Mov Disord* (2007) 22(11):1538–42. doi:10.1002/mds.21619

58. Etgen T, Muhlau M, Gaser C, Sander D. Bilateral grey-matter increase in the putamen in primary blepharospasm. *J Neurol Neurosurg Psychiatry* (2006) 77(9):1017–20. doi:10.1136/jnnp.2005.087148

59. Pantano P, Totaro P, Fabbrini G, Raz E, Contessa GM, Tona F, et al. A transverse and longitudinal mr imaging voxel-based morphometry study in patients with primary cervical dystonia. *AJNR Am J Neuroradiol* (2011) 32(1):81–4. doi:10.3174/ajnr.A2242

60. MacIver CL, Tax CMW, Jones DK, Peall KJ. Structural magnetic resonance imaging in dystonia: A systematic review of methodological approaches and findings. *Eur J Neurol* (2022) 29(11):3418–48. doi:10.1111/ene.15483

61. Berndt M, Li Y, Gora-Stahlberg G, Jochim A, Haslinger B. Impaired white matter integrity between premotor cortex and basal ganglia in writer's cramp. *Brain Behav* (2018) 8(10):e01111. doi:10.1002/brb3.1111

62. Delmaire C, Vidailhet M, Wassermann D, Descoteaux M, Valabregue R, Bourdain F, et al. Diffusion abnormalities in the primary sensorimotor pathways in writer's cramp. *Arch Neurol* (2009) 66(4):502–8. doi:10.1001/archneurol.2009.8

63. Preibisch C, Berg D, Hofmann E, Solymosi L, Naumann M. Cerebral activation patterns in patients with writer's cramp: A functional magnetic resonance imaging study. *J Neurol* (2001) 248(1):10–7. doi:10.1007/s004150170263

64. Wu CC, Fairhall SL, McNair NA, Hamm JP, Kirk IJ, Cunnington R, et al. Impaired sensorimotor integration in focal hand dystonia patients in the absence of symptoms. *J Neurol Neurosurg Psychiatry* (2010) 81(6):659–65. doi:10.1136/jnnp.2009.185637

65. Gallea C, Balas M, Bertasi E, Valabregue R, Garcia-Lorenzo D, Coynel D, et al. Increased cortico-striatal connectivity during motor practice contributes to the consolidation of motor memory in writer's cramp patients. *Neuroimage Clin* (2015) 8:180–92. doi:10.1016/j.nicl.2015.04.013

66. Castrop F, Dresel C, Hennenlotter A, Zimmer C, Haslinger B. Basal ganglia-premotor dysfunction during movement imagination in writer's cramp. *Mov Disord* (2012) 27(11):1432–9. doi:10.1002/mds.24944

67. Cho HJ, Hallett M. Non-invasive brain stimulation for treatment of focal hand dystonia: Update and future direction. *J Mov Disord* (2016) 9(2):55–62. doi:10.14802/jmd.16014

68. Gallea C, Herath P, Voon V, Lerner A, Ostuni J, Saad Z, et al. Loss of inhibition in sensorimotor networks in focal hand dystonia. *Neuroimage Clin* (2018) 17:90–7. doi:10.1016/j.nicl.2017.10.011

69. Gupta N, Pandey S. Treatment of focal hand dystonia: Current status. *Neurol Sci* (2021) 42(9):3561–84. doi:10.1007/s10072-021-05432-7

70. Hallett M, Benecke R, Blitzer A, Comella CL. Treatment of focal dystonias with botulinum neurotoxin. *Toxicon* (2009) 54(5):628–33. doi:10.1016/j.toxicon.2008.12.008

71. Lungu C, Nmashie A, George MC, Karp BI, Alter K, Shin S, et al. Comparison of ultrasound and electrical stimulation guidance for onabotulinum toxin-a injections: A randomized crossover study. *Mov Disord Clin Pract* (2022) 9(8):1055–61. doi:10.1002/mdc3.13546

72. Zakin E, Simpson DM. Botulinum toxin therapy in writer's cramp and musician's dystonia. *Toxins (Basel)* (2021) 13(12):899. doi:10.3390/toxins13120899

73. Lungu C, Karp BI, Alter K, Zolbrod R, Hallett M. Long-term follow-up of botulinum toxin therapy for focal hand dystonia: Outcome at 10 Years or more. *Mov Disord* (2011) 26(4):750–3. doi:10.1002/mds.23504

74. Zeuner KE, Bara-Jimenez W, Noguchi PS, Goldstein SR, Dambrosia JM, Hallett M. Sensory training for patients with focal hand dystonia. *Ann Neurol* (2002) 51(5):593–8. doi:10.1002/ana.10174

75. Zeuner KE, Hallett M. Sensory training as treatment for focal hand dystonia: A 1-year follow-up. *Mov Disord* (2003) 18(9):1044–7. doi:10.1002/mds.10490

76. Zeuner KE, Peller M, Knutzen A, Hallett M, Deuschl G, Siebner HR. Motor Re-training does not need to Be task specific to improve writer's cramp. *Mov Disord* (2008) 23(16):2319–27. doi:10.1002/mds.22222

77. Zeuner KE, Shill HA, Sohn YH, Molloy FM, Thornton BC, Dambrosia JM, et al. Motor training as treatment in focal hand dystonia. *Mov Disord* (2005) 20(3):335–41. doi:10.1002/mds.20314

78. Schenk T, Bauer B, Steidle B, Marquardt C. Does training improve writer's cramp? An evaluation of a behavioral treatment approach using kinematic analysis. *J Hand Ther* (2004) 17(3):349–63. doi:10.1197/j.jht.2004.04.005

79. Wissel J, Kabus C, Wenzel R, Klepsch S, Schwarz U, Nebe A, et al. Botulinum toxin in writer's cramp: Objective response evaluation in 31 patients. *J Neurol Neurosurg Psychiatry* (1996) 61(2):172–5. doi:10.1136/jnnp.61.2.172

80. Fahn S. Assessment of the primary dystonias. In: T Munsat, editor. *The quantification of neurologic deficit*. Boston: Butterworths (1989). p. 241–70.

81. Byl NN, Archer ES, McKenzie A. Focal hand dystonia: Effectiveness of a home program of fitness and learning-based sensorimotor and memory training. *J Hand Ther* (2009) 22(2):183–97. doi:10.1016/j.jht.2008.12.003

82. McKenzie AL, Goldman S, Barrango C, Shrime M, Wong T, Byl N. Differences in physical characteristics and response to rehabilitation for patients with hand dystonia: Musicians' cramp compared to writers' cramp. *J Hand Ther* (2009) 22(2):172–81. doi:10.1016/j.jht.2008.12.006

83. Bleton JP, Vidailhet M, Bourdain F, Ducorps A, Schwartz D, Delmaire C, et al. Somatosensory cortical remodelling after rehabilitation and clinical benefit of in writer's cramp. *J Neurol Neurosurg Psychiatry* (2011) 82(5):574–7. doi:10.1136/jnnp.2009.192476

84. Deepak KK, Behari M. Specific muscle emg biofeedback for hand dystonia. *Appl Psychophysiol Biofeedback* (1999) 24(4):267–80. doi:10.1023/a:1022239014808

85. Berger HJ, van der Werf SP, Horstink CA, Cools AR, Oyen WJ, Horstink MW. Writer's cramp: Restoration of striatal D2-binding after successful biofeedback-based sensorimotor training. *Parkinsonism Relat Disord* (2007) 13(3):170–3. doi:10.1016/j.parkreldis.2006.09.003

86. Baur B, Furholzer W, Marquardt C, Hermsdorfer J. Auditory grip force feedback in the treatment of writer's cramp. *J Hand Ther* (2009) 22(2):163–70. doi:10.1016/j.jht.2008.11.001

87. Siebner HR, Tormos JM, Ceballos-Baumann AO, Auer C, Catala MD, Conrad B, et al. Low-frequency repetitive transcranial magnetic stimulation of the motor cortex in writer's cramp. *Neurology* (1999) 52(3):529–37. doi:10.1212/wnl.52.3.529

88. Murase N, Rothwell JC, Kaji R, Urushihara R, Nakamura K, Murayama N, et al. Subthreshold low-frequency repetitive transcranial magnetic stimulation over the premotor cortex modulates writer's cramp. *Brain* (2005) 128(1):104–15. doi:10.1093/brain/awh315

89. Havrankova P, Jech R, Walker ND, Operto G, Tauchmanova J, Vymazal J, et al. Repetitive tms of the somatosensory cortex improves writer's cramp and enhances cortical activity. *Neuro Endocrinol Lett* (2010) 31(1):73–86.

90. Huang YZ, Lu CS, Rothwell JC, Lo CC, Chuang WL, Weng YH, et al. Modulation of the disturbed motor network in dystonia by multisession suppression of premotor cortex. *PLoS One* (2012) 7(10):e47574. doi:10.1371/journal.pone.0047574

91. Kimberley TJ, Borich MR, Arora S, Siebner HR. Multiple sessions of low-frequency repetitive transcranial magnetic stimulation in focal hand dystonia: Clinical and physiological effects. *Restor Neurol Neurosci* (2013) 31(5):533–42. doi:10.3233/RNN-120259

92. Bradnam LV, Graetz LJ, McDonnell MN, Ridding MC. Anodal transcranial direct current stimulation to the cerebellum improves handwriting and cyclic drawing kinematics in focal hand dystonia. *Front Hum Neurosci* (2015) 9:286. doi:10.3389/fnhum.2015.00286

93. Sadnicka A, Wiestler T, Butler K, Altenmuller E, Edwards MJ, Ejaz N, et al. Intact finger representation within primary sensorimotor cortex of musician's dystonia. *Brain* (2022) awac356. doi:10.1093/brain/awac356

DYSTONIA

TYPE Original Research
PUBLISHED 23 February 2023
DOI 10.3389/dyst.2023.11117

OPEN ACCESS

EDITED BY
Aasef Shaikh,
Case Western Reserve University,
United States

*CORRESPONDENCE
Terence Sanger,
terry@sangerlab.net

RECEIVED 09 December 2022
ACCEPTED 13 February 2023
PUBLISHED 23 February 2023

CITATION
Kasiri M, Javadzadeh S, Nataraj J, Seyyed Mousavi SA and Sanger T (2023), Correlated activity in globus pallidus and thalamus during voluntary reaching movement in three children with primary dystonia.
Dystonia 2:11117.
doi: 10.3389/dyst.2023.11117

Correlated activity in globus pallidus and thalamus during voluntary reaching movement in three children with primary dystonia

Maral Kasiri[1], Sina Javadzadeh[1], Jaya Nataraj[2], Seyyed Alireza Seyyed Mousavi[2] and Terence Sanger[1,2,3]*

[1]Department of Biomedical Engineering, University of California, Irvine, Irvine, CA, United States, [2]Department of Electrical Engineering and Computer Science, University of California, Irvine, Irvine, CA, United States, [3]Children's Health Orange County, Orange, CA, United States

Classical models of the physiology of dystonia suggest that involuntary muscle contractions are caused by inappropriately low activity in Globus Pallidus internus (GPi) that fails to adequately inhibit thalamic inputs to cortex. We test this prediction in three children with primary dystonia undergoing depth electrode recording in basal ganglia and thalamus during selection of targets for deep brain stimulation (DBS) implantation. We compare muscle activity to the power in the spectrogram of the local field potential, as well as to counts of identified spikes in GPi, subthalamic nucleus (STN), and the Ventral oralis (VoaVop) and Ventral Anterior (VA) subnuclei of the thalamus, while subjects are at rest or attempting to make active voluntary arm or leg reaching movements. In all three subjects, both spectrogram power and spike activity in GPi, STN, VoaVop, and VA are significantly positively correlated with movement. In particular, GPi and STN both increase activity during attempted movement. These results contradict the classical rate model of the physiology of dystonia, and support more recent models that propose abnormalities in the detailed pattern of activity rather than the overall lumped activity of pallidum and thalamus.

KEYWORDS

deep brain stimulation, basal ganglia, thalamus, primary dystonia, electrophysiology, rate model

Introduction

The classical "rate" model of basal ganglia physiology in dystonia developed by Albin and others has been built upon the known anatomical connections between striatum, pallidum, subthalamus, and thalamus (1–3). Inhibitory projection neurons originating in striatum and pallidum will hyperpolarize their targets in pallidum, subthalamus, and thalamus, while excitatory projection neurons in subthalamus and thalamus will depolarize their targets in pallidum and cortex. In primates, there is a division into

direct and indirect pathways. The direct pathway includes inhibitory projections from striatum to Globus Pallidus internus (GPi) and from GPi to thalamus, followed by excitatory projections from thalamus to cortex. The indirect pathway includes inhibitory projections from striatum to Globus Pallidus externus (GPe), from GPe to subthalamic nucleus (STN), and from GPi to thalamus, with excitatory projections from STN to GPi. Modifications of this model over the past decades have recognized the important role of a "hyperdirect" pathway from cortex to STN, as well as pathways from STN to GPe, GPi to STN, and medial thalamic nuclei to striatum. In all models, the final common pathway linking basal ganglia to thalamus remains the inhibitory projection from GPi to thalamus including the ventral oralis anterior and posterior (VoaVop) and ventral anterior (VA) subnuclei (4, 5).

The patterns of excitatory and inhibitory connections suggest what has been referred to as the classical "rate" model. This simplicity of this model has led to widespread adoption, and it has proven useful in the prediction of the physiology of Parkinson's disease, in which high firing rates in GPi are thought to cause inappropriate inhibition of thalamic outputs to cortex, thus leading to delayed movement initiation and decreased speed of movement (bradykinesia) (2). The finding of relatively lower firing rates in GPi during voluntary movement in some patients with dystonia has led to the suggestion that dystonia is due to the opposite problem: failure of inhibition of thalamic outputs to cortex (6), thus potentially leading to excessive involuntary muscle contractions (such as overflow, co-contraction, or hyperkinetic movements) (1, 7). This theory has been supported in recordings from healthy non-human primates showing that GPi activity is typically very high. It has also been supported by the observation that electrical stimulation in GPi can ameliorate symptoms in patients with dystonia.

However, important discrepancies in the application of the classical model to dystonia have been noted (7, 8). Perhaps the most significant is the observation that lesions in GPi also lead to amelioration of dystonia, whereas the model would predict that lesions would worsen dystonia. Another discrepancy is that if reduction in activity in GPi initiates movement in the healthy brain, then there is no mechanism for initiation of activity in a brain with baseline low activity in GPi. Another discrepancy is the observation that dystonic muscle activity is almost always caused by or worsened by active attempts at movement, whereas the classical model would predict the presence of dystonia at rest. And an important missing element of some models is the absence of a depolarizing (excitatory) input to thalamus (1); without such an input, thalamus will never activate and the hyperpolarizing (inhibitory) inputs from GPi will have no effect (3).

We examine the predictions of the classical rate model by making simultaneous recordings from high-impedance electrodes in GPi, STN, VoaVop, and VA in three children with primary dystonia. Recordings are performed as part of a previously-reported novel targeting method in which temporary externalized stereo electroencephalography (sEEG) depth electrodes are implanted in potential DBS targets, and children are tested with stimulation and recording while awake and unrestrained (9, 10). This method eliminates the effects of restrained movement (in the operating room with a headframe) and sedation and partial anesthesia, and permits prolonged testing with children awake, unrestrained, unmedicated, and performing routine tasks of daily living in a hospital room with parents and clinical staff present. Clinical outcomes from this targeting method have been reported elsewhere. Here we utilize recorded data obtained from the sEEG electrodes during voluntary arm or leg reaching movements in three children who previously underwent this procedure.

Between one and ten high-impedance (70–90 kΩ) contacts are present within each of the tested nuclei. Recordings are analyzed both in the frequency domain using the power spectral density (spectrogram) and in the time domain using analysis of the spike rate. Spectrogram power and spike rates are compared between rest and active movement.

Methods

Patient selection

Patients were selected for DBS surgery after being diagnosed with primary (genetic) dystonia by a pediatric movement disorder specialist (TDS) based on established criteria (11–13). All patients had confirmed failure of symptomatic medical therapies at adequate dosing, and potential stimulation target(s) were identifiable with magnetic resonance imaging (MRI). Patients or parents of minor patients provided Health Insurance Portability and Accountability Act (HIPAA) authorization for the research use of protected health information and written informed consent for surgical procedures conforming to standard hospital practice, and for research use of electrophysiological data before the procedure. The research use of data was approved by the institutional review board of the Children's Health, Orange County (CHOC) hospital. All surgical procedures and experiments took place at Children's Health Orange County (CHOC). In this study, we report data from three children with primary dystonia who have undergone DBS surgery in the Neuromodulation Unit (NMU). See Table 1 for subject demographics.

Depth recordings

Up to 10 temporary AdTech MM16C depth electrodes (AdTech Medical Instrument Corp., Oak Creek, WI,

TABLE 1 Subject demographics.

Subject	Mutation	Symptoms	Sex	Age	Bilateral depth electrode targets
S1	DYT1	Hypertonic and Hyperkinetic Dystonia	F	16	VIM, VoaVop, STN, VA, GPi anterior
S2	KMT2B	Hyperkinetic Dystonia	M	12	GPi anterior, GPi posterior, VIM, VA, VoaVop, STN
S3	KMT2B	Hyperkinetic Dystonia, Chorea	M	10	GPi anterior, GPi posterior, VA, VIM, VoaVop, STN

United States) were implanted in potential DBS targets using procedures reported previously (9). Potential stimulation targets were identified based on previous studies of clinical efficacy. Targets are named based on Hassler's terminology, and include subthalamic nucleus (STN), globus pallidus internus (GPi), in basal ganglia, ventral intermediate nucleus (VIM), ventral oralis anterior/posterior (VoaVop), and ventral anterior nucleus (VA), in thalamus. Each implanted electrode has ten high-impedance (70–90 kΩ) micro contacts (50-μm diameter) that are arranged in groups of two or three, spaced evenly around the circumference of the electrode shaft in four rows. The leads were connected to Adtech Cabrio™ connectors that include a custom unity-gain preamplifier for each micro contact to reduce noise and motion artifacts. All data used in this study were recorded at the micro contacts and sampled at 24 kHz by a custom recording system consisting of a PZ5M 256-channel digitizer, RZ2 processor, and RS4 high speed data storage (TDT, Tucker-Davis Technologies Inc., Alachua, FL, United States).

In addition to local field potential (LFP) recordings, we recorded muscle activity from 16 surface electromyography (EMG) Trigno™ Avanti (Delsys Incorporated, Natick, MA) sensors, attached to upper and lower extremities. We recorded EMG signals from biceps, triceps, flexor carpi ulnaris, extensor carpi radialis, gastrocnemius, tibialis, quadriceps, and hamstrings bilaterally, to track the changes in muscles activity with the brain activity. All EMG signals were sampled at 2 kHz and the EMG system was synchronized with the TDT using a pulse generator.

Movement task

Patients were asked to perform a voluntary reach to target task with their less impaired upper limb while depth electrode and EMG signals were recorded. In all cases, dystonia was present in the tested limb, as evidenced by the presence of dystonic postures interfering with expected performance of the task. The reaching task consisted of a one-to-two-minute period of voluntary reaching followed by 30 seconds of rest, for a total of four to six consecutive trials. Movement and rest onset and offset times were marked during the experiment. All data analysis was performed in MATLAB R2020a (The MathWorks, Inc., Natick, MA, United States).

EMG signal processing

EMG signals were notch-filtered to eliminate 60 Hz interference and band-pass filtered between 20 and 500 Hz. They were then rectified and low pass filtered at 1 Hz to extract the envelope of the EMG signal. Fourth-order Butterworth filters were used throughout.

Time-frequency analysis of LFP recordings

The microelectrode LFP recordings were notch-filtered at 60 Hz and the first five harmonics. They were then high pass filtered at 1 Hz to remove drift. The voltage difference between each pair of micro contacts in each of the four rows of a depth electrode were computed to remove common noise from the signals and reveal the underlying activity (bipolar montage) which results in eight different recordings per lead.

To compute the spectrograms of the recorded non-stationary signals, each signal was divided into segments with sixty percent overlap using a Kaiser window with time resolution of 3 seconds, and 0.7 leakage factor. Next, signals were transformed into the frequency domain using a short-time Fourier transform. Finally, the spectra of each segment were computed to build the spectrograms. The spectrograms were computed in two frequency ranges of 1–13 Hz (delta, theta, and alpha) and 13–35 Hz (beta). This specific frequency ranges are chosen as they are of standard frequency bands used in frequency analysis of brain activity. Additionally, the alpha and beta bands are important in other movement disorders such as Parkinson's disease, which involves abnormality in alpha and beta band oscillations (7).

Spike analysis of LFP recordings

Spike analysis was performed on the micro contact LFP recordings, using the bipolar montage, explained earlier. Signals are bandpass filtered between 350 and 3,000 Hz using an 8th order Butterworth filter. A non-linear energy operator (NEO) (14) was applied to the data to aid in spike detection by enhancing sharp peaks in bipolar LFP signals:

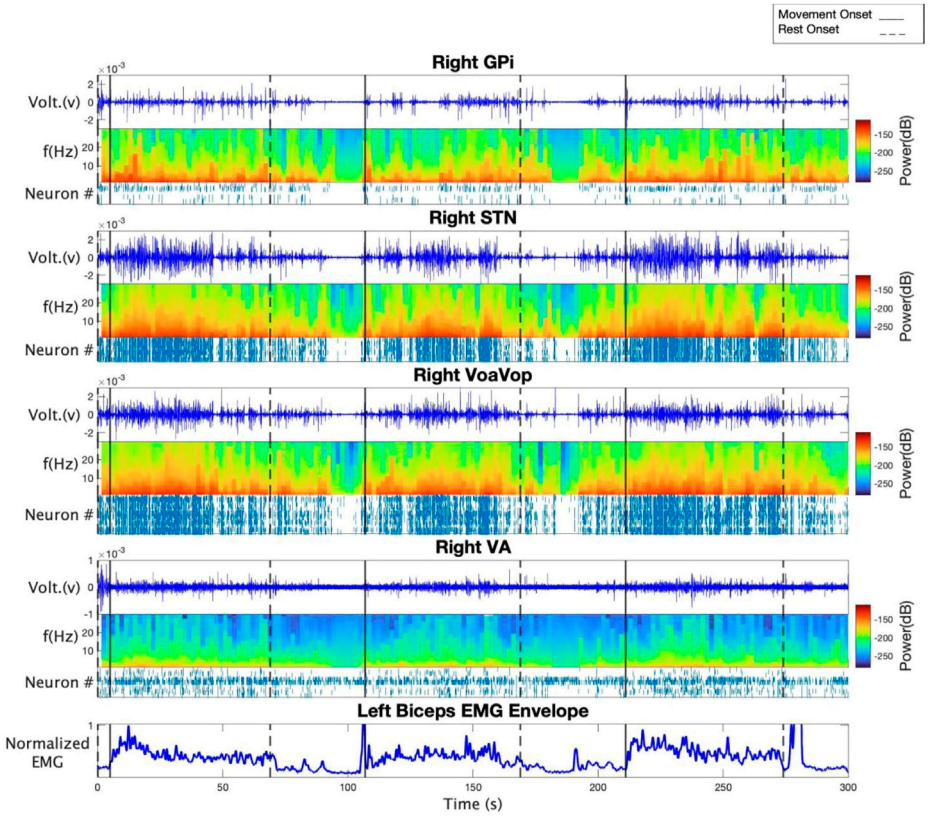

FIGURE 1
From top to bottom: raw LFP recording, spectrogram, and spike raster of GPi, STN, VoaVop, and VA for subject 1. The bottom plot demonstrates left biceps EMG recording as an example in order to highlight voluntary reaching task and rest periods. Spectrogram results show increased power in voluntary reaching task periods compared to resting periods. Spike rasters show increased neural activity in voluntary reaching task periods compared to resting periods.

$$y(t) = x^2(t) - x(t-1) \times x(t+1)$$

where x(t) is a sample of the waveform at time t and y(t) is the enhanced output. Spikes are characterized by localized high frequencies and sharp increases in instantaneous energy. These features are captured in the magnitude of the NEO, which is large only when the signal is high in power [x^2 (t) is large] and high in frequency [$x(t-1) \times x(t+1)$ is small].

Peak detection was performed on the NEO, where the amplitudes of detected peaks were between three and seventy times the standard deviation of the noise. Following event detection, wavelet decomposition was used to extract features from detected events and a Gaussian Mixture Model (GMM) was used to cluster detected events. Events with low probability of belonging to any clusters were removed. Events associated with the same cluster were identified as a "spike" belonging to the same originating neuron(s), and average spike rates were determined within the relevant intervals (movement or rest).

Because the impedance of the recording contacts is less than 100 kΩ, it is likely that the identified spikes correspond to multiple neuron clusters rather than to single units that would be recorded with higher impedance electrodes. Additionally, the spike clusters are identified by consistent shapes. If there were variability in the cluster, the overall shape would vary as well. A spike cluster likely represents a stereotyped firing pattern from a group of nearby neurons. Nevertheless, the spike rates are likely to parallel the neural activity that would be obtained from higher impedance recordings.

Statistical analysis

To measure the effect of movement on: 1) the average power in two frequency bands, and 2) average spike rate, a linear mixed effects model with repeated measures was fitted to both spike firing rate and power in each band. Repeated measures for the time-frequency analysis are the average power in each frequency band for every 5 s of each period of voluntary reaching and rest. Repeated measures for the spike analysis are

TABLE 2 Statistical results of the linear mixed-effect model for group analysis.

Group analysis results	Power analysis		Firing rate analysis	
	R^2	*p-value*	R^2	*p-value*
GPi	0.49	$p < 0.001$	0.42	$p < 0.001$
STN	0.76	$p = 0.001$	0.22	$p < 0.001$
VA	0.68	$p < 0.001$	0.53	$p < 0.001$
VoaVop	0.88	$p < 0.001$	0.34	$p < 0.001$

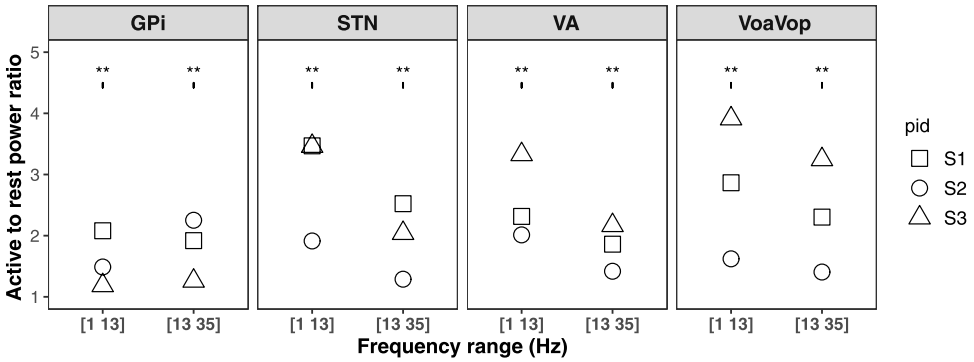

FIGURE 2
Ratio of active to rest average power in frequency ranges 1–13 Hz and 13–35 Hz for three patients are shown by different shapes in GPi, STN, VA, and VoaVop. The group analysis shows that log power ratio is significant for all of them.

the average firing rates for each voluntary reaching and rest period.

The model for the time frequency analysis consists of condition (active versus rest), frequency range ([1–13] and [13–35] Hz), and their interactions as fixed effects. Subject intercept was included as a random effect, and by-subject random slopes were the frequency range.

The model for average spike rate analysis consists of the condition as the fixed effect, while the random effect was assumed to be the subject intercept. All the statistical analyses were done using the lme4 (15) and emmeans (16) packages in R-studio (R core team, 2021).

Results

Figure 1 shows time-frequency and spike analyses of LFP recordings for subject 1. Raw bipolar LFP recordings, spectrograms, and spike rasters are displayed from top to bottom for contralateral GPi, STN, VoaVop, and VA. Figure 1 also includes an example EMG recording from the left biceps to highlight the voluntary reaching and rest period. Results from the spectrogram analysis suggest a clear trend in power, where power is increased during the reaching task in frequencies from 1 to 35 Hz and decreased in rest periods in all target locations. In particular, power starts to increase as the patient starts one period of voluntary reaching and subsequently decreases as the patient is in rest. Additionally, raster plots in all target locations illustrate increased spiking activity in voluntary reaching task periods in comparison to resting states. The observations are consistent among all the three subjects.

The linear mixed effects model was fitted on data from each brain region separately for group analysis. The explained variance of the models are shown in Table 2. We performed a pairwise comparison between the rest versus the active state to test for significance of increases in firing rates and power for each frequency range. Analysis of variance (ANOVA) using type II Wald chi-square test, with 95% confidence interval was performed on the linear models, and showed a significant difference between the active versus the resting state ($Pr_{(>chisq)} < 0.0001$) for all brain regions tested.

We then computed the log of the ratio between active and resting state powers for each frequency range. This measure is significantly different from zero for both frequency ranges. The results are shown in Figure 2 for each patient. The average spike rates in both active and resting states for all three patients are shown in Figure 3.

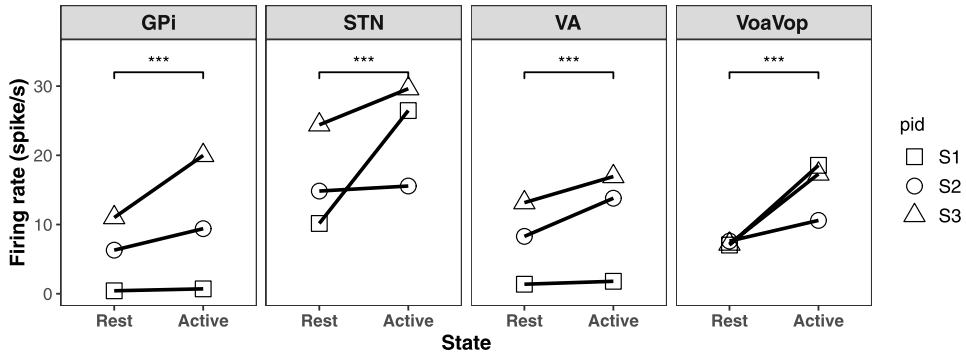

FIGURE 3
The average firing rate of resting versus voluntary reaching state for three subjects and the regression line in GPi, STN, VA, and VoaVop. The group analysis shows a significant increased firing rate during voluntary reaching period in GPi, STN, VA, and VoaVop.

Discussion

The classical rate model of basal ganglia function predicts that STN and GPi activity will be low and thalamic activity will be high during movement, and that STN and GPi activity will be high and thalamic activity will be low at rest (2, 17). While the predictions for VoaVop and VA subnuclei of the thalamus are supported by our results, the predictions for STN and GPi are contradicted. Our results are in agreement with prior results in monkeys showing increases in GPi activity from rest to movement, with maintained high GPi activity during movement and voluntary posture (18–21).

The rate model is known to have significant problems when applied to dystonia (7, 8), and we suggest several possible ways to address the results shown by our data. Most importantly, the classical model is incomplete because it does not posit a stimulatory (depolarizing) input to thalamus, and without excitation of thalamus, GPi inhibition would have no effect (There is no point in inhibiting a neuron that never fires.) Although GPi and GPe also receive primary inhibitory input from both striatum and pallidum, both structures also receive excitatory input from STN. The primary excitatory input to thalamus arises from cerebral cortex, and we suggest that augmenting the model with an excitatory cortical-thalamic-cortical loop provides an explanation for the increased thalamic firing during movement (7). In this case, the role of the GPi is to selectively inhibit this loop at the thalamus, effectively "sculpting" the thalamo-cortical loop. This mechanism is supported by lesion studies showing involuntary antagonist muscle activity resulting from lesions of GPi (22, 23). Dystonia could arise, similarly to the classical model, from insufficient inhibition of parts of this loop. In this augmented model, GPi would only need to inhibit the loop when thalamus is activated, consistent with our results. The deficit in dystonia would then be either insufficient inhibition (GPi increases rate with movement, but not enough) or an incorrect pattern of inhibition (7, 24) (GPi increases rate with movement but does not properly sculpt the thalamic activity). This proposal is consistent with the finding of abnormal sensory responses in thalamus, consistent with failure of inhibition of cortical inputs (25).

It is worth noting that the suggested dichotomy in which Parkinsonism represents decreased activity while dystonia represents increased activity is an oversimplification that may also be contributing to contradictions with the classical model (6). Although dystonia was originally classified as a hyperkinetic disorder, it shares features common to both hyperkinetic disorders (dyskinesia, Huntington's chorea) and hypokinetic disorders (rigidity, bradykinesia) (7). In children, a combination of parkinsonism and dystonia is typically present in conditions of low dopamine (e.g., dopa-responsive dystonia) or diffuse hypoxic injury (e.g., dyskinetic cerebral palsy) (26). EMG recordings from both Parkinsonism and dystonia demonstrate slow rates of contraction and change in contraction levels (27, 28) and both Parkinsonism and dystonia have hyperkinetic components that can include tremor and dyskinesia. Therefore, while electrophysiological data continue to support increased activity in GPi in parkinsonism compared with dystonia, both disorders may include a failure of appropriate inhibition of thalamo-cortical loops that includes both insufficient inhibition of unwanted movement and insufficient disinhibition of intended movement. Such similarities would be consistent with the observation that DBS in either GPi or STN as well as dopaminergic medication can ameliorate symptoms in both disorders.

Our results appear to contradict recordings from human and non-human primate models of dystonia that typically show very

high GPi activity at rest (1), inconsistent with the rate model. We suggest three hypotheses to explain this discrepancy. First, it is possible that non-human primates and humans have different patterns of activity in basal ganglia. Second, we only obtain recordings from human patients with severe disease, whereas the non-human primate recordings are typically made in healthy animals. Third, a non-human primate strapped into a recording apparatus with head immobilized may not be truly at rest, and ongoing isometric force exerted against the seating system and head immobilization system may not always be evident but could nevertheless lead to baseline activation of deep brain regions associated with movement or posture.

The results presented here include several important weaknesses. First, we tested only three children, and although all three have a genetic origin of their dystonia, the specific mutations are different. This suggests that the phenomena we observed are not confined to a single cause of primary dystonia, but whether this is a general feature of all patients (children and adults) with these or other forms of dystonia is not known. Second, we tested only reaching movements, and it is possible that patterns seen during other activities such as ambulation, speaking, eating, or isometric movements would be different. Third, the specific electrodes we use have impedances (70–90 kΩ) that are much less than typically used for extracellular recording (typically 1 MΩ or more) and thus could lead to different phenomena. In particular, the "spikes" that we observe probably do not represent single neuron depolarizations and are likely to be formed from stereotyped firing patterns of groups of neurons near the recording contacts. Fourth, we cannot determine the relationship between GPi firing and dystonic components of movement because it is not possible to separate dystonic from voluntary components of movement in our paradigm. From a theoretical point of view, our results do not shed light on the involvement of dopamine (29), sensory pathways (30–33), cerebellum (34–36), or other structures in the causes of dystonia.

Despite these limitations, our results support an overall increase in GPi firing from rest to movement in children with primary dystonia. This is an important observation for understanding the nature of dystonia and the mechanism of function of interventions including medications and DBS surgery. This finding is consistent with the hypothesis that it is the pattern of GPi outputs rather than the average firing rate that is abnormal in dystonia (7, 24), and that this pattern may include both inappropriate inhibition of desired thalamic activity as well as inappropriate disinhibition of unwanted thalamic activity. Confirmation of this hypothesis in a larger cohort of patients with more varied causes of dystonia will be important for further understanding and improved treatment of this debilitating disorder.

Data availability statement

The data analyzed in this study is subject to the following licenses/restrictions: The datasets were collected as part of DBS procedure for clinical and research purposes. They are considered protected health information under HIPAA. De-identified datasets may be available on request. Requests to access these datasets should be directed to Terence Sanger, terry@sangerlab.net.

Ethics statement

The studies involving human participants were reviewed and approved by CHOC Institutional Review Board—Research Institute. Written informed consent to participate in this study was provided by the participants' legal guardian/next of kin.

Author contributions

MK, SJ, JN, SS, and TS contributed to data acquisition, data analysis, data interpretation, and writing the manuscripts. MK contributed to statistical analysis. TS conceived the study. All authors have read and agreed to the published version of the manuscript.

Funding

This study is funded by Cerebral Palsy Alliance Research Foundation (PG02518) and The Crowley-Carter Foundation (CCF-562490).

Conflict of interest

The authors declare that the research was conducted in the absence of any commercial or financial relationships that could be construed as a potential conflict of interest.

Acknowledgments

We thank our volunteers and their parents for participating in this study. We also thank Jennifer Maclean for her assistance with neurologic examinations, as well as Jessica Vidmark for helping in data collection. We would also like to thank the reviewers for their insights.

References

1. Vitek JL, Chockkan V, Zhang JY, Kaneoke Y, Evatt M, DeLong MR, et al. Neuronal activity in the basal ganglia in patients with generalized dystonia and hemiballismus. *Ann Neurol* (1999) 46:22–35. doi:10.1002/1531-8249(199907)46:1<22:aid-ana6>3.0.co;2-z

2. Albin RL, Young AB, Penney JB. *The functional anatomy of basal ganglia disorders* (1989).

3. Delong MR. *Primate models of movement disorders of basal ganglia origin* (1989).

4. Devito JL, Anderson MEE. An autoradiographic study of efferent connections of the globus pallidus in *Macaca mulatta*. *Exp Brain Res* (1982) 46:107–17. doi:10.1007/BF00238104

5. Penney JB, Young AB. GABA as the pallidothalamic neurotransmitter: Implications for basal ganglia function. *Brain Res* (1981) 207:195–9. doi:10.1016/0006-8993(81)90693-4

6. Brüggemann N. Contemporary functional neuroanatomy and pathophysiology of dystonia. *J Neural Transm* (2021) 128:499–508. –508 Preprint at. doi:10.1007/s00702-021-02299-y

7. Vitek JL. Pathophysiology of dystonia: A neuronal model. *Move Disord* (2002) 17:S49–S62. Preprint at. doi:10.1002/mds.10142

8. Obeso JA, Lanciego JL. Past, present, and future of the pathophysiological model of the basal ganglia. Front Neuroanat *Preprint* (2011) 5:39. doi:10.3389/fnana.2011.00039

9. Sanger TD, Liker M, Arguelles E, Deshpande R, Maskooki A, Ferman D, et al. Pediatric deep brain stimulation using awake recording and stimulation for target selection in an inpatient neuromodulation monitoring unit. *Brain Sci* (2018) 8:135. doi:10.3390/brainsci8070135

10. Sanger TD, Robison A, Arguelles E, Ferman D, Liker M. Case report: Targeting for deep brain stimulation surgery using chronic recording and stimulation in an inpatient neuromodulation monitoring unit, with implantation of electrodes in GPi and vim in a 7-year-old child with progressive generalized dystonia. *J Child Neurol* (2018) 33:776–83. doi:10.1177/0883073818787741

11. Albanese A, Bhatia K, Bressman SB, Delong MR, Fahn S, Fung VSC, et al. Phenomenology and classification of dystonia: A consensus update. *Move Disord* (2013) 28:863–73. –873 Preprint at. doi:10.1002/mds.25475

12. Sanger TD, Delgado MR, Gaebler-Spira D, Hallett M, Mink JW. Classification and definition of disorders causing hypertonia in childhood. *Pediatrics* (2003) 111(1):e89–e97. doi:10.1542/peds.111.1.e89

13. Sanger TD, Chen D, Fehlings DL, Hallett M, Lang AE, Mink JW, et al. Definition and classification of hyperkinetic movements in childhood. *Move Disord* (2010) 25:25 1538–49. Preprint at. doi:10.1002/mds.23088

14. Kaiser JF. On a simple algorithm to calculate the 'energy' of a signal. In: *ICASSP, IEEE international conference on acoustics, speech and signal processing - proceedings*, 1 381–384. Publ by IEEE (1990).

15. Bates D, Mächler M, Bolker BM, Walker SC. Fitting linear mixed-effects models using lme4. *J Stat Softw* (2015) 67. doi:10.18637/jss.v067.i01

16. Searle SR, Speed FM, Milliken GA. Population marginal means in the linear model: An alternative to least squares means. *Am Statistician* (1980) 34:216–21. doi:10.2307/2684063

17. Penney JB, Young AB. Striatal inhomogeneities and basal ganglia function. *Move Disord* (1986) 1:3–15. –15 Preprint at. doi:10.1002/mds.870010102

18. Mink JW, Thach T. Basal ganglia motor control. II. Late pallidal timing relative to movement onset and inconsistent pallidal coding of movement parameters. *J Neurophysiol* (1991) 65(2):301–29. doi:10.1152/jn.1991.65.2.301

19. Mink JW, Thach T. Basal ganglia motor control. I. Nonexclusive relation of pallidal discharge to five movement modes. *J Neurophysiol* (1991) 65(2):273–300. doi:10.1152/jn.1991.65.2.273

20. Georgopoulos AP, Delong MR, Crutcher3 MD. Relations between parameters of step-tracking movements and single cell discharge in the globus pallidus and subthalamic nucleus of the behaving monkey'. *J Neurosci* (1983) 3:1586–98. doi:10.1523/JNEUROSCI.03-08-01586.1983

21. Mitchell SJ, Richardson RT, Baker FH, Delong MR. The primate nucleus basalis of meynert: Neuronal activity related to a visuomotor tracking task. *Exp Brain Res* (1987) 68:506–15. doi:10.1007/BF00249794

22. Mink JW, Thach T. Basal ganglia intrinsic circuits and their role in behavior. *Curr Opin Neurobiol* (1993) 3:950–7. doi:10.1016/0959-4388(93)90167-w

23. Thach WT. Basal ganglia motor control. III. Pallidal ablation: Normal reaction time, muscle cocontraction, and slow movement. *JOURNALOF NEUROPHYSIOLOGY* (2019) 65.

24. Mink JW. The basal ganglia: Focused selection and inhibition of competing motor programs. *Pergamorr Prog Neurobiol* (1996) 50:381–425. doi:10.1016/s0301-0082(96)00042-1

25. Lenz FA. *Thalamic single neuron activity in patients with dystonia: Dystonia-related activity and somatic sensory reorganization* (1999).

26. Sanger TD. *Annual review of neuroscience basic and translational neuroscience of childhood-onset dystonia: A control-theory perspective* (2018). doi:10.1146/annurev-neuro-080317

27. Fujita K, Eidelberg D. Imbalance of the direct and indirect pathways in focal dystonia: A balanced view. *Brain* (2017) 140:3075–7. doi:10.1093/brain/awx305

28. Malfait N, Sanger TD. Does dystonia always include co-contraction? A study of unconstrained reaching in children with primary and secondary dystonia. *Exp Brain Res* (2007) 176:206–16. doi:10.1007/s00221-006-0606-4

29. Ribot B, Aupy J, Vidailhet M, Mazere J, Pisani A, Bezard E, et al. Dystonia and dopamine: From phenomenology to pathophysiology. *Prog Neurobiol* (2019) 182:101678. Preprint at. doi:10.1016/j.pneurobio.2019.101678

30. Conte A, Defazio G, Hallett M, Fabbrini G, Berardelli A. The role of sensory information in the pathophysiology of focal dystonias. *Nat Rev Neurol* (2019) 15:224–33. –233 Preprint at. doi:10.1038/s41582-019-0137-9

31. Sanger TD, Kukke SN. Abnormalities of tactile sensory function in children with dystonic and diplegic cerebral palsy. *J Child Neurol* (2007) 22:289–93. doi:10.1177/0883073807300530

32. Sanger TD, Pascual-Leone A, Tarsy D, Schlaug G. Nonlinear sensory cortex response to simultaneous tactile stimuli in writer's cramp. *Move Disord* (2002) 17:17105–11. Preprint at. doi:10.1002/mds.1237

33. Sanger TD, Tarsy D, Pascual-Leone A. Abnormalities of spatial and temporal sensory discrimination in writer's cramp. *Move Disord* (2001) 16 94–9. Preprint at. doi:10.1002/1531-8257(200101)16:1<94:AID-MDS1020>3.0.CO;2-O

34. Fung WKW, Peall KJ. What is the role of the cerebellum in the pathophysiology of dystonia? *J Neurol* (2019) 266:1549–51. doi:10.1007/s00415-019-09344-7

35. Shakkottai VG, Batla A, Bhatia K, Dauer WT, Dresel C, Niethammer M, et al. Current opinions and areas of consensus on the role of the cerebellum in dystonia. *Cerebellum* (2017) 16 577:577–94. –594 Preprint at. doi:10.1007/s12311-016-0825-6

36. Prudente CN, Hess EJ, Jinnah HA. Dystonia as a network disorder: What is the role of the cerebellum? *Neuroscience* (2014) 260 23:23–35. doi:10.1016/j.neuroscience.2013.11.062

DYSTONIA

TYPE Original Research
PUBLISHED 01 February 2023
DOI 10.3389/dyst.2023.11019

OPEN ACCESS

EDITED BY
Daniela Popa,
INSERM U1024 Institut de biologie de l'Ecole Normale Supérieure, France

*CORRESPONDENCE
S. A. Norris,
norriss@wustl.edu

RECEIVED 31 October 2022
ACCEPTED 19 January 2023
PUBLISHED 01 February 2023

CITATION
Norris SA, Tian L, Williams EL and Perlmutter JS (2023), Transient dystonia correlates with parkinsonism after 1-methyl-4-phenyl-1,2,3,6-tetrahydropyridine in non-human primates.
Dystonia 2:11019.
doi: 10.3389/dyst.2023.11019

Transient dystonia correlates with parkinsonism after 1-methyl-4-phenyl-1,2,3,6-tetrahydropyridine in non-human primates

S. A. Norris[1,2]*, L. Tian[1], E. L. Williams[1] and J. S. Perlmutter[1,2,3,4,5]

[1]Department of Neurology, School of Medicine, Washington University in St. Louis, St. Louis, MO, United States, [2]Department of Radiology, School of Medicine, Washington University in St. Louis, St. Louis, MO, United States, [3]Department of Neuroscience, School of Medicine, Washington University in St. Louis, St. Louis, MO, United States, [4]Department of Physical Therapy, School of Medicine, Washington University in St. Louis, St. Louis, MO, United States, [5]Department of Occupational Therapy, School of Medicine, Washington University in St. Louis, St. Louis, MO, United States

Unilateral internal carotid artery 1-methyl-4-phenyl-1,2,3,6-tetrahydropyridine (MPTP) infusion in non-human primates produces transient contralateral hemi-dystonia followed by stable contralateral hemi-parkinsonism; the relationship between dystonia and parkinsonism remains unclear. We hypothesized that transient dystonia severity following MPTP correlates with parkinsonism severity. In male Macaca nemestrina (n = 3) and M. fascicularis (n = 17) we administered unilateral intra-carotid MPTP, then correlated validated blinded ratings of transient peak dystonia and delayed parkinsonism. We also correlated dystonia severity with post-mortem measures of residual striatal dopamine and nigral neuron counts obtained a mean 53 ± 15 days following MPTP, after resolution of dystonia but during stable parkinsonism. Median latency to dystonia onset was 1 day, and peak severity 2.5 days after MPTP; total dystonia duration was 13.5 days. Parkinsonism peaked a median of 19.5 days after MPTP, remaining nearly constant thereafter. Peak dystonia severity highly correlated with parkinsonism severity (r[18] = 0.82, $p < 0.001$). Residual cell counts in lesioned nigra correlated linearly with peak dystonia scores (r [18] = −0.68, p=<0.001). Dystonia was not observed in monkeys without striatal dopamine depletion (n = 2); dystonia severity correlated with striatal dopamine depletion when residual nigral cell loss was less than 50% ([11] r = −0.83, $p < 0.001$) but spanned a broad range with near complete striatal dopamine depletion, when nigral cell loss was greater than 50%. Our data indicate that residual striatal dopamine may not reflect dystonia severity. We speculate on mechanisms of transient dystonia followed by parkinsonism that may be studied using this particular NHP MPTP model to better understand relationships of transient dystonia to nigrostriatal injury and parkinsonism.

KEYWORDS

striatum, MPTP, plasticity, monkey, substantia nigra

Introduction

The neurotoxin 1-methyl-4-phenyl-1,2,3,6-tetrahydropyridine (MPTP) produces relatively selective dopaminergic nigrostriatal injury (1). Systemic MPTP exposure in non-human primates (NHP) causes diffuse nigrostriatal injury followed by subsequent stable dopa-responsive parkinsonism, modeling motor manifestations of people with idiopathic Parkinson disease (2–5). Single dose intra-carotid (IC) administration in untreated baboons, *Macaque nemestrina*, and *Macaque fascicularis* can cause contralateral acute transient dystonia followed by parkinsonism (6, 7). Unilateral IC MPTP is advantageous, given the un-injected side sustains no changes to presynaptic nigrostriatal dopaminergic neurons (8, 9) and provides an internal control (e.g. pathologic comparison of the affected and unaffected brain hemispheres) for studies of pathophysiological mechanisms. To date, no study has characterized the relationship of dystonia and parkinsonism in NHPs following acute IC administration of MPTP.

A study of nigrostriatal reserve in dopaminergic cell bodies and their terminal fields following IC MPTP administration in NHPs demonstrated that parkinsonism ratings correlated with striatal dopamine but only when nigral dopamine cell loss did not exceed 50%. When nigral cell loss exceeds 50%, striatal dopamine levels reached nearly complete loss despite continued increased severity of parkinsonism with additional loss of nigral cell bodies of dopaminergic neurons (9). As a result, striatal PET measures of presynaptic nigrostriatal neurons may only be a valid biomarker of disease severity in only mild MPTP induced parkinsonism. The relationship between parkinsonism and acute MPTP-induced transient dystonia remains to be determined. Study of this relationship may provide insight regarding the pathophysiology of dystonia, particularly given experimental evidence linking both dystonia and parkinsonism to striatal dopaminergic dysfunction.

In this analysis of cross-sectional data, we determine novel relationships of transient dystonia following acute IC administration of MPTP to a) degree of subsequent parkinsonism, b) loss of tyrosine hydroxylase (TH) immunoreactive neuronal cell bodies in substantia nigra pars compacta, and c) loss of striatal dopamine. The current approach expands upon our prior reports of transient dystonia followed by parkinsonism (6), now specifically testing the hypothesis that the degree of transient dystonia after acute IC MPTP administration in non-human primates correlates with the severity of parkinsonism, and thus correlates with the degree of nigral damage. Our observation of relationships between transient dystonia, parkinsonism, nigral cell count, and residual striatal dopamine prompts discussion regarding potential mechanisms underlying transient dystonia followed by parkinsonism, and future promise for this model in dystonia related research.

Materials and methods

Subjects

Acute MPTP induced dystonia

We retrospectively studied 20 male macaque monkeys, 17 *Macaca fascicularis* and 3 *Macaca. nemestrina* before and after unilateral internal carotid artery infusion of various doses of MPTP; two additional monkeys were included as controls that did not receive MPTP. All animals included in the current study were selected from an existing cohort utilized for an experimental paradigm previously conducted to test hypotheses relating to pathophysiological mechanisms of parkinsonism. These parent biomarker studies relied on the minimum number of animals necessary to achieve statistical power for respective *a-priori* hypotheses. From this existing cohort, animals with severe acute MPTP toxicity (10) or exposure to dopaminergic medications or carboxyfullerene were excluded for the current analysis (11, 12). Furthermore, as the current study aimed to determine the relationship between peak acute transient dystonia and degree of parkinsonism, animals euthanized prior to anticipated peak parkinsonism were excluded. Two *nemestrina* animals had microelectrode penetrations in the globus pallidus on the infusion side before and after MPTP administration. Otherwise, no animals received intracranial manipulations during the experimental period. Animals were always able to care for themselves. The mean age of all animals was 7.3 ± 1.4 years (range, 4.9–9.6 years). Behavioral measures for a portion of these animals were previously reported (9), although blinded behavioral ratings of videos were repeated in the current study to maintain consistency across all animals since the prior blinded reviewer was no longer available. Data for all animals are presented in Table 1.

In accordance with the recommendations of the Weatherall report "The Use of Non-Human Primates in Research," all steps were taken to ameliorate suffering in these studies. Guidelines prescribed by the NIH Guide for the Care and Use of Laboratory Animals (NIH Publications No. 8023, revised 1978) were followed in the parent biomarker studies, and all studies were approved by the institutional animal care and use committee at Washington University in St Louis.

MPTP infusion

We infused the right internal carotid artery with MPTP in anesthetized animals using angiographic guidance as previously described (6). Briefly, animals fasted overnight and underwent anesthesia induction with ketamine and glycopyrrolate followed by intubation with a soft-cuffed endotracheal tube. Anesthesia was maintained with isoflurane inhalation. A 20-gauge catheter was placed into a femoral artery followed by fluoroscopic guidance of an 80-cm catheter guided into the right internal

carotid artery over a guidewire. Cerebral angiogram prior to infusion confirmed proper placement of the catheter and good distal blood flow.

To obtain a dose response curve, a randomized dose between 0 and 0.25 mg/kg of MPTP (Sigma, St. Louis, MO) diluted in normal saline was infused IC in a concentration of 0.1 mg/mL at a rate no faster than 1 mL per minute. The mean absolute dose of MPTP administered was 1.28 mg ± 0.71 across monkeys injected (10). A repeat angiogram was performed following infusion of MPTP to document maintenance of proper positioning and distal blood flow. After the procedure, animals were continuously observed until able to care for themselves. Safety precautions were followed for handling MPTP and all contaminated tissues and waste products (13).

Behavioral evaluations

Video was obtained at the same time of day (early morning) in the first 3 days following MPTP infusion, then several times per week after MPTP until euthanasia. The behavioral protocol included a) walking 15 feet toward, then away from the camera three times in a straight corridor, b) walking in a circle of approximately 7 feet diameter, 3 times clockwise then 3 times counterclockwise, and c) reaching 10 times with each hand for a food item held by the trainer at arm's length from the animal. A single observer blinded to each animal's treatment status rated each video clip, which was presented in a random order, using a scale previously developed and validated for non-human primate studies (7). Behavioral evaluations of parkinsonism and dystonia are consistent with those previously described (6, 7, 9).

Dystonic posturing was defined as extensor posturing of an upper or lower extremity and was clearly distinguished from the more typical parkinsonian flexed posture of the limb. Briefly, ratings for dystonia included a 0–3 scale (0 = unaffected, 1 = mildly affected, 2 = moderately affected, and 3 = severely affected) for dystonia occurring in each limb: 1) with the animal sitting at rest, 2) with movement of the rated limb (i.e., during gait or when reaching for a food item), and 3) movement of the contralateral limb. The ratings were scored for each side separately, producing a composite with a maximum dystonia rating of 18 per side. Ratings for parkinsonism included a 0–3 scale (0 = unaffected, 1 = mildly affected, 2 = moderately affected, and 3 = severely affected) for bradykinesia, tremor, and/or flexed posturing. The maximum score for parkinsonism ratings was also 18 per side. Behavioral raters were blind to *in vitro* measures (described below) and MPTP dose. Parkinsonism and dystonia ratings from some animals have been previously published (6, 9), but rating scores were reestablished to maintain rater consistency across all animals as the prior rater was no longer available to extend ratings to newly acquired animals.

In vitro measures

Animals were euthanized with intravenous pentobarbital (100 mg/kg; Somnasol Euthanasia, Butler Schein Animal Health, Dublin, OH) at completion of the parent study. The brain was removed within 10 min. Details regarding animal euthanasia, brain retrieval and preparation, tyrosine hydroxylase immunohistochemistry and stereology, and striatal dopamine measurement protocols are described elsewhere (9), but we provide a brief overview here.

For substantia nigra tyrosine hydroxylase immunohistochemistry, the midbrain was fixed in 4% paraformaldehyde in 0.1 M phosphate buffered solution for 7 days, transferred to 30% sucrose for 7 days, and then cut on a freezing microtome in serial 50 µm-thick transverse sections after 7 days. Every 6th section was processed for tyrosine hydroxylase immunocytochemistry and sections were counterstained with cresyl violet for unbiased stereological counts of nigral neurons obtained *via* microscope digital image acquisition. Substantia nigra pars compacta was defined as the region ventral to medial lemniscus and lateral to the third cranial nerve fibers, and TH-stained nigral cells were counted using the Visiopharm Integrator System (version 3.2.10.0).

For striatal dopamine measures, separated hemispheres were sliced in the coronal plane at the time of euthanasia followed by collection of standard punch biopsies from caudate and putamen bilaterally which were frozen on dry ice snow and stored at −80°C until dopamine was assayed. High-performance liquid chromatography with electrochemical detection was applied to measure striatal dopamine levels, expressed in microgram per Gram of wet tissue.

All *in vitro* measurements were performed by a rater blinded to MPTP dose and behavioral measures. Select *in vitro* measures from animals included here have been published in-part elsewhere (9).

Statistics

Mean, standard deviation, is reported for continuous variables of interest, while median is reported for ordinal data. Two-sample paired t-tests were used to compare continuous variables of interest between the MPTP-treated and control sides. We correlated non-parametric validated blinded ratings of transient peak dystonia scores with that of subsequent peak parkinsonism, *in vitro* measures of striatal dopamine, and unbiased stereologic counts of nigral neurons with TH by calculating a one-tailed Spearman's coefficient (rho) in SPSS (IBM, version 22). Prior to data analysis, we conservatively defined the threshold of behavioral dystonia as a score of at least two points to avoid possible overlap with normal behavior, similar to our prior strategy with respect to parkinsonism (9).

TABLE 1 Animal characteristics and outcome measures.

Monkey	Species	Sex	Age (yrs)	Animal	MPTP dose	MPTP dose	Euthanasia	Parkinsonism	Parkinsonism	Parkinsonism	Dystonia	Dystonia	Dystonia	Dystonia	SN TH	Striatal DA
			At MPTP	Weight (kg)	(mg/kg)	(mg)	(days)	Peak rating	Onset (days)	Plateau (days)	Peak rating	Onset (days)	Peak (Days)	Duration (days)	(inj/ uninject)	(inj/ uninject)
1	Nemestrina	M	5.1	5.1	0.12	0.61	56	3	13	20	4	1	3	12	0.73	0.50
2	Nemestrina	M	5.6	5.6	0.06	0.34	56	3	16	20	1	1	1	13	0.81	0.86
3	Nemestrina	M	7.8	7.8	0.18	1.41	56	7	4	28	3	1	5	20	0.40	0.01
4	Fasicularis	M	6.5	6.45	0	0	56	0	N/A	N/A	0	N/A	N/A	N/A	0.78	1.07
5	Fasicularis	M	7.5	7.5	0.25	1.88	58	6	2	21	4	3	9	14	0.16	0.03
6	Fasicularis	M	5.6	5.6	0.12	0.672	56	4	9	11	4	1	1	5	0.86	0.84
7	Fasicularis	M	8.9	8.9	0.18	1.6	60	6	2	14	5	1	2	9	0.84	0.06
8	Fasicularis	M	7.0	6.95	0.06	0.417	56	3	8	18	3	1	3	10	0.68	0.37
9	Fasicularis	M	7.3	7.3	0.25	1.825	56	7	16	24	6	1	2	17	0.46	0.02
10	Fasicularis	M	7.0	7	0	0	57	0	N/A	N/A	0	N/A	N/A	N/A	0.88	1.03
11	Fasicularis	M	7.5	7.45	0.14	1.043	56	4	1	15	5	1	3	9	0.79	0.59
12	Fasicularis	M	8.2	8.2	0.14	1.148	57	9	1	24	12	1	1	7	0.06	0.02
13	Fasicularis	M	6.9	6.9	0.11	0.69	60	5	1	23	5	1	3	14	0.50	0.01
14	Fasicularis	M	8.9	8.9	0.14	1.25	57	8	1	18	9	2	4	15	0.20	0.01
15	Fasicularis	M	5.7	5.7	0.12	0.684	57	0	N/A	N/A	0	N/A	N/A	N/A	0.87	0.64
16	Fasicularis	M	4.9	4.9	0.06	0.294	57	0	N/A	N/A	0	N/A	N/A	N/A	0.94	0.86
17	Fasicularis	M	9.5	9.5	0.25	2.38	22	11	1	17	8	1	2	15	0.57	0.01
18	Fasicularis	M	9.0	9	0.25	2.25	21	7	6	20	4	1	1	15	0.55	0.01
19	Fasicularis	M	8.4	8.35	0.25	2.09	25	6	8	16	8	1	3	16	0.23	0.00
20	Fasicularis	M	9.6	9.55	0.25	2.39	87	4	5	19	5	1	2	8	0.07	0.01
Mean/Median[†]			7.3	7.33	0.16[a]	1.28[a]	53.3	5.5[†a]	4.5[†]	19.5[†]	4.5[†a]	1[†]	2.5[†]	13.5[†]	0.57	0.35
Standard Deviation			1.4	1.45	0.07[a]	0.71[a]	14.9								0.42	0.41

[a]Does not include 2 animals that did not receive MPTP.

[†]denotes median values; all others in the row are mean values.

SN TH, substantia nigra tyrosine hydroxylase; DA, dopamine; inj/uninjected = ratio of the left (MPTP injected) to right (uninjected) sides.

10.3389/dyst.2023.11019

10.3389/dyst.2023.11019

Results

Table 1 summarizes animal characteristics, behavioral, biochemical, and morphological profiles for all monkeys included in this study.

Behavioral response to MPTP

The typical behavioral response to unilateral MPTP injection included recovery from anesthesia followed within hours to days by contralateral transient hemi-dystonia. Hemi-dystonia was observed in 16/18 MPTP injected monkeys as extension of the fore- and hind-limbs at the shoulder/hip, elbow/knee, and wrist/ankle with external rotation at the shoulder/hip that often worsened with attempted use of the affected limbs (either walking-worse when walking in circles with the affected side on the inner diameter- or reaching for objects). There was no postural tremor at onset of dystonic features in any of the observed monkeys. Four animals (two that did not receive MPTP) did not exhibit any dystonia or parkinsonism following MPTP administration, before euthanasia. The mean times following MPTP to onset of dystonic manifestations, peak dystonia and duration of dystonia are presented in Table 1. Hemi-dystonia gradually resolved after peak dystonia with overlapping onset of hemi-parkinsonism (Figure 1). At euthanasia, no animals had dystonic manifestations.

Peak dystonia score correlated with peak parkinsonism ([18],r = 0.82, $p < 0.001$, Figure 2A). Mean time following MPTP to onset and plateau of parkinsonism at peak parkinsonism severity are presented in Table 1. The parkinsonian phase typically began with flexed posturing of the affected upper and lower extremity with bradykinesia. Some ambiguity existed with regard to scores of bradykinesia since severe dystonia often caused bradykinesia. In some animals, extensor dystonic posturing of the lower or upper extremity persisted when bradykinesia developed. Only two animals had tremor during the parkinsonian phase.

Correlation of dystonia with delayed measures of nigral injury

Quantification of TH-stained nigral neurons was obtained a mean of 53 days following MPTP, in all cases acute transient dystonia resolved. The percent of residual nigral cell counts correlates with the prior peak dystonia rating scores ([18],r = −0.63, $p = 0.002$, Figure 2B). The threshold of nigral cell loss remains unknown given timing of TH-nigral measures in relation to dystonia, but monkey 6 represents the lowest threshold of injured nigra at 14% with associated dystonia, a similar level to that previously observed for parkinsonism (9).

Correlation of dystonia with subsequent percent residual striatal dopamine

The peak dystonia rating score correlated linearly with the percent residual striatal dopamine obtained a mean of 53 days after MPTP (r = −0.81, $p < 0.001$), when nigral injury was less than 50%. When nigral injury exceeded 50%, the percent residual striatal dopamine was essentially zero across the entire measured range of dystonia scores. Data for residual striatal dopamine are displayed in Figure 2C; we only correlate data where nigral injury is less than 50% to avoid false representation of what appear as independent clusters. The threshold of striatal dopamine loss that corresponded to transient dystonia also remains unknown given timing of striatal dopamine measures in relation to dystonia, but the lowest threshold of striatal dopamine depletion was 14%–36% with associated prior transient dystonia, similar to that previously reported for parkinsonism (9). We averaged post-mortem striatal measures of dopamine for the caudate and putamen as the mean caudate dopamine concentrations did not differ from putamen measures on the control side (mean 11.9 ± 6.5 ug/g versus 12.1 ± 5.1 ug/g of wet tissue, respectively; two-sample paired t-test: t = −0.13, $p = 0.90$) and MPTP-lesioned side (5.4 ± 7.3 ug/g versus 5.4 ± 6.2 ug/g of wet tissue, respectively; two-sample paired t-test: t = −0.03, $p = 0.97$). Similarly, the mean caudate percent residual dopamine concentration did not differ from the putamen concentrations (41 ± 42% versus 43.7 ± 44%, respectively; two-sample paired t-test: t = −0.53, $p = 0.61$).

Discussion

Our data build upon evidence that unilateral IC MPTP in non-human primates causes acute transient hemi-dystonia followed by stable parkinsonism, (6, 7) demonstrating that dystonia severity correlates with severity of parkinsonism. Our data further indicate that residual striatal dopamine does not reflect dystonia severity when nigral injury exceeds 50%, although measures of striatal depletion occurred after resolution of dystonia. Yet, dystonia severity strongly correlates with measures of dopaminergic nigral cell body injury, supporting a common mechanism underlying dystonia and parkinsonism that involves nigrostriatal injury (9). Interpretation of these data must be done with caution since the nigral measures were obtained following resolution of transient dystonia. Specifically, our results cannot be generalized to transient dystonia alone. Nevertheless, the relation of parkinsonism and nigral injury with transient dystonia offers clues that may guide future testable hypotheses aimed at understanding mechanisms of acute transient dystonia followed by parkinsonism in this non-human primate MPTP model.

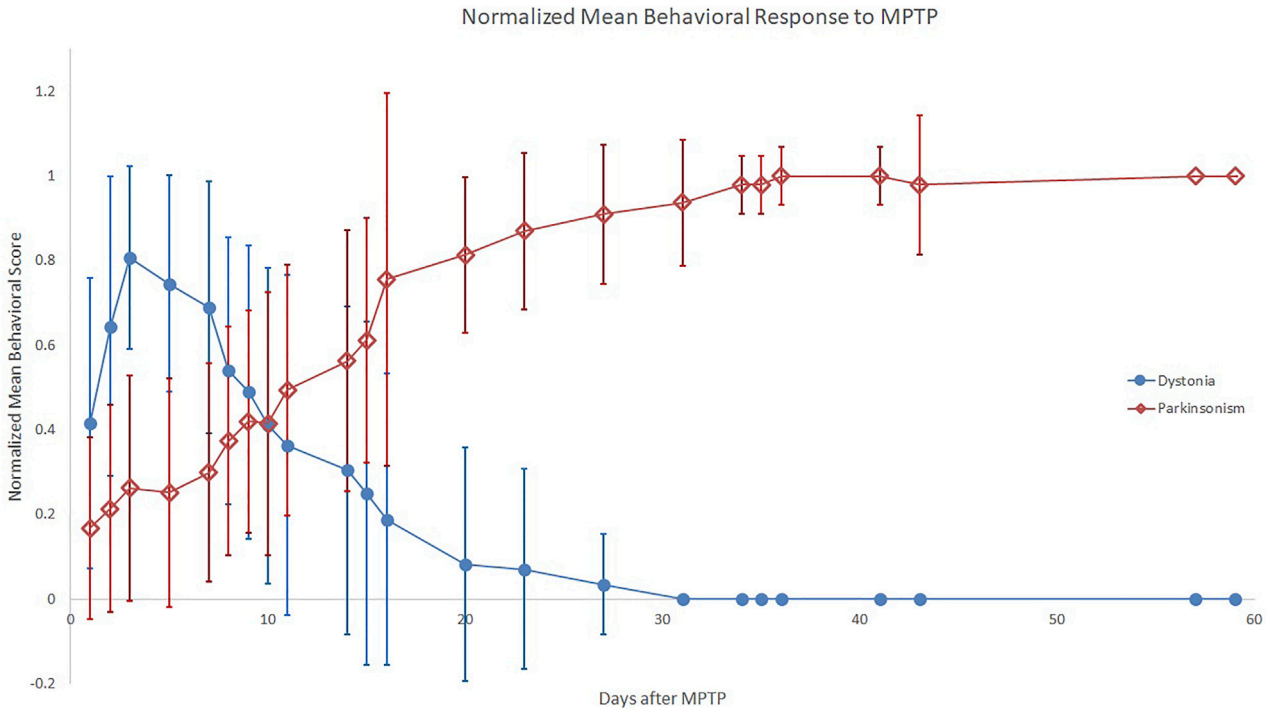

FIGURE 1
Normalized Mean Behavioral Response to MPTP. The plot displays mean ratios, across all monkeys per time bin, of individual dystonia (circle) or parkinsonism (diamond) scores divided by the individual monkey's respective peak measure. Error bars represent standard deviation of the ratios across monkeys for each time bin.

Relationship of transient dystonia and parkinsonism in the NHP MPTP model

Dystonia is not consistently reported before parkinsonism in primates treated with MPTP. Variability in MPTP primate models may contribute to this, including use of different ages of old- and new-world primates and variable administration and dosing methods that includes intracarotid, intramuscular, subcutaneous, or intravenous as a single dose or repeatedly over a few days, weeks, or months (14–22). Regardless, IC MPTP administration in baboons, *Macaca nemestrina*, and *Macaca fasicularis* has consistently caused transient dystonia followed by chronic parkinsonism (6, 7). It remains unclear whether differences in observed behavior results from methodology, or rather, lack of recognition and/or reporting of the early dystonic manifestation. The high correlation of dystonia and parkinsonian severity strengthens the association of MPTP with transient dystonia, strengthening support of this model for the study of pathophysiologic mechanisms and nigrostriatal function.

It is unlikely that subjective rating errors occurred when distinguishing phenomenology of dystonia and parkinsonism (i.e., mistaking early, more severe parkinsonism for dystonia) since the scores on these two rating scales clearly diverged as demonstrated in Figure 1. Also, a key rating observation helped to distinguish the dystonic from parkinsonian phase; we defined dystonia as extensor posturing of an extremity while flexion indicated parkinsonism.

Striatal dopamine is an inadequate biomarker for transient dystonia

Animal studies have previously implicated the basal ganglia in dystonia [see reviews: (23–25)]. Selective striatal lesions with 6-hydroxydopamine or 3-nitropropionic acid and MPTP caused dystonia in rodents (26, 27) and non-human primates (6, 7, 28, 29). MPTP demonstrates selective preference to injure dopaminergic neurons (30–32). During the dystonic phase in baboons previously treated with IC MPTP, putaminal dopamine D2-like specific binding sites decreased about 30% (measured as soon as 10 days after MPTP) with associated striatal dopamine deficiency of about 97%–98% (33). In macaques, during the dystonic phase, striatal dopamine decreased about 66% in the first day ($n = 2$), 98% at day 3 ($n = 1$) and 99% at 2–4 months ($n = 5$) (6). Striatal FDOPA uptake decreased approximately 70%, a loss maintained 2–4 months following infusion (6). Thus, the dystonic phase begins, continues and ends during a period of

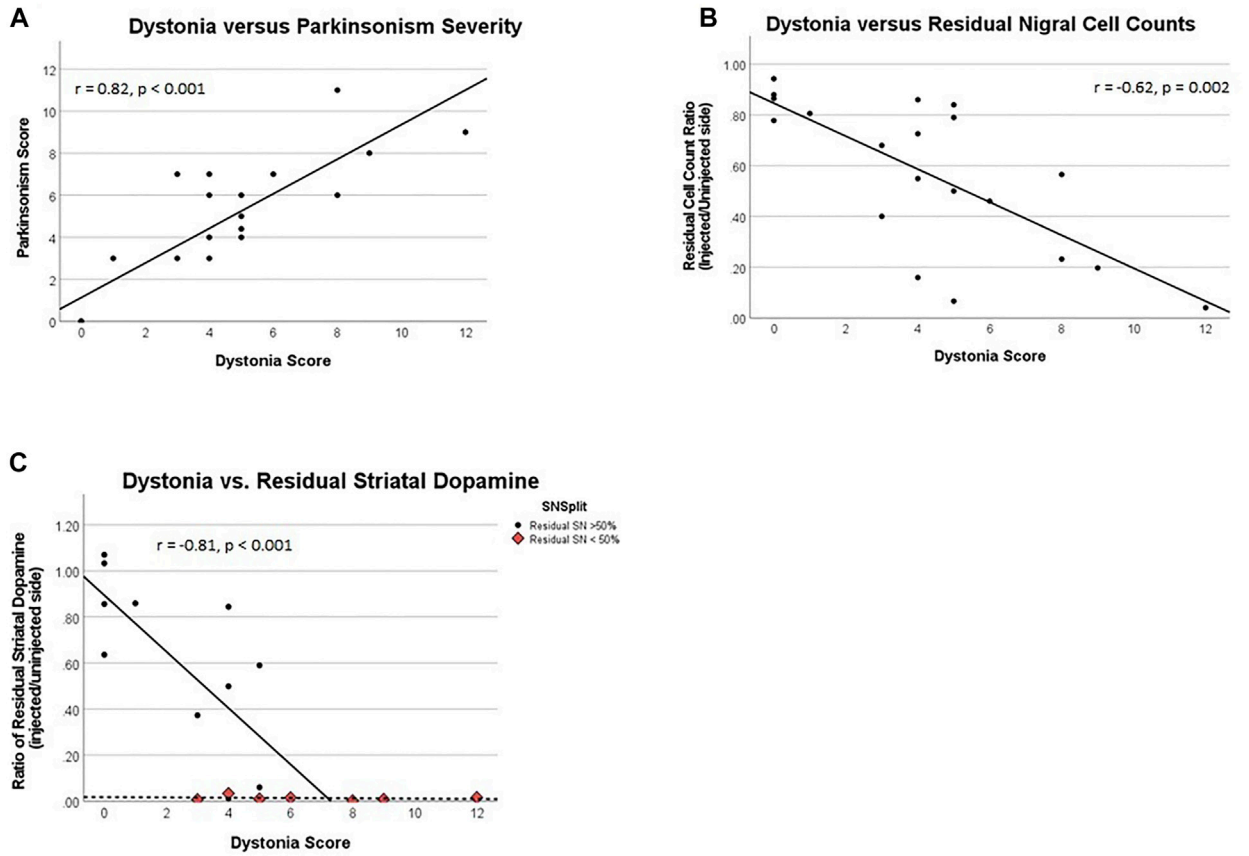

FIGURE 2
(A) Dystonia rating score vs. parkinsonism rating score, **(B)** Dystonia score vs. the ratio of residual substantia nigra cells, and **(C)** Dystonia vs. residual striatal dopamine. Correlation represents only data where residual SN > 50%, a distinct data cluster from that of SN < 50%. **(B, C)**: All ratios represent their respective measures on the brain side injected with MPTP over similar measures for the un-injected side.

sustained striatal dopamine deficiency. Based on our observations that transient dystonia occurs in context of incomplete, low intensity persistent striatal dopamine depletion is of particular interest regarding pathophysiology given that striatal healing is unlikely. Our findings indicate that striatal dopamine alone does not reflect dystonia severity in this model through the full range of severity.

Macaque nemestrina and *Macaque fascicularis* animals that develop dystonia following IC MPTP (0.1–0.4 mg/kg) have quicker drops in striatal dopamine during the dystonic phase (6) than squirrel monkeys systemically administered MPTP for which dystonia was not reported (34). The squirrel monkeys have only modest drops in putamen dopamine at day 1 following subcutaneous administration of 2.5 mg/kg followed by further decreases at day 5 in both caudate and putamen. Thus, the rapid changes induced by IC MPTP that is completely extracted on first pass through the brain circulation may be critical to induce dystonia, above and beyond striatal dopamine deficiency alone.

Correlations of nigral injury and dystonia severity warrants cautious interpretation

The temporal dissociation of transient dystonia and biochemical measures limits our ability to speculate regarding the correlation of dystonia severity with residual nigral cell counts. This association may reflect changes in the effects of dopamine transmission and/or receptor configuration in downstream striatal terminals, for which future studies are required to understand the timing of nigral injury in relation to transient dystonia.

Potential for future applications of the NHP MPTP dystonia model

A critical question in our non-human primate IC MPTP model relates to what causes dystonia to recover whereas parkinsonism does not. Alterations in striatal dopaminergic

signaling relate to the pathophysiology of both dystonia and parkinsonism (35, 36). Reports regarding the effects of MPTP on dopamine receptors vary. In general, there appears relatively little change in D1-like receptor numbers. Some report decreased dopamine D2-like receptors, but others report no change or an increase (37–41). As multiple dopamine receptors are the products of separate genes (42), it is possible that changes in D2-like receptor binding described in prior studies may be attributable to changes in the expression of a single receptor subtype or to complex changes in the expression of D2, D3, or D4 receptors. Future studies focused on potentially adaptive relationships of various dopamine receptors during the transition from dystonia to parkinsonism, particularly differentiating the direct and indirect pathway, may be valuable to understand the role of such receptors in altered neural plasticity and phenotypic conversion from dystonia to parkinsonism. Changes in other modulators of the direct and indirect pathways such as such as dynorphin, enkephalin, substance P and PDE10a may also play a role in development of dystonia, and future molecular studies measuring their levels in this NHP model during and after transient dystonia may prove informative regarding pathophysiologic mechanisms of transient dystonia.

Acute transient dystonia in the current NHP model may also relate to abnormal cortico-striatal neural plasticity (43). In rodents, MPTP induced nigro-striatal injury produces immediate striatal release of dopamine and its metabolites (44, 45). Early profound dopaminergic efflux likely stimulates D1 and D2-like dopamine receptors simultaneously, possibly causing acute alterations in glutamatergic sensitivity *via* altered synaptic long term potentiation and long term depression at medium spiny neurons (46). Thus, IC MPTP may cause a sudden flood of available dopamine followed by marked reduction (6). This rapid dopaminergic striatal efflux followed by relative dopaminergic paucity mimics the clinical scenario of human cocaine exposure (i.e., striatal dopaminergic priming), where those exposed are more prone to drug-induced dystonia following dopamine receptor blockade (47). Acute dopamine depletion may produce more excitable medium-sized spiny neurons, less excitable GABAergic interneurons and increased cholinergic cell excitability (48, 49); thus, dopamine depleted striatal circuits exhibit pathological hyperactivity. Longitudinal neurophysiological, PET, and functional neuroimaging experiments flanking development and resolution of transient dystonia in this NHP MPTP model may unravel potential links between biochemical and circuit-level dysfunction contributing to altered cortico-striatal plasticity.

Each of these potentially contributing mechanisms of altered striatal plasticity requires future study, but the most intriguing relates to cholinergic interneurons (ChI). ChIs show hyperactivity with bursts and silences in the dopamine depleted striatum, where hyperactivity also relates to extrinsic synaptic inputs targeting ChIs *via* glutaminergic and GABAergic inputs. The latter is essential for sustaining ChI hyperactivity, but MPTP induced dopamine loss alters substantia nigra pars compacta signaling which reduces glutamate co-excitation of dorsolateral striatal ChIs due to downregulation of mGluR1 (50). As the relative ratio of striatal acetylcholine/dopamine relates to acute dystonia in mice treated with acute reserpine, one might anticipate that this ratio would normalize with downregulation of mGluR1, potentially translating to the end of the dystonic phase. This speculation supports growing data that ChIs play a role in dystonia and may serve as the main drivers of pathological hyperactivity in the striatum secondary to dopamine depletion and altered extrinsic synaptic inputs (51). Post-mortem histopathological measures of choline acetyltransferase (ChAT) or *in vivo* PET measures of [18F]fluoroethoxybenzovesamicol, (-)-[18F] FEOBV,(-)-(2R,3R)-trans-2-hydroxy-3-(4- phenylpiperidino)-5-(2-[18F]fluoroethoxy)-1,2,3,4-tetralin (52) or (-)-(1-(8-(2-[(18)F) fluoroethoxy)-3-hydroxy-1,2,3,4-tetrahydronaphtalen-2-yl)-pi peridi n -4 -yl) (4-fluorophenyl)methanone([18F]VAT) (53) may provide clues with respect to altered ChI activity during the transient dystonia phase in this NHP MPTP model.

Future studies are critical to tease out mechanistic components in the NHP model of transient dystonia which may include shifting neurotransmitter levels, immunomodulatory effects secondary to cellular injury, direct nigrostriatal influence versus indirect downstream effects, receptor auto regulation, altered transcription pathways, or shifts in network-level synchronicity.

Synaptic sprouting does not explain phenomenological evolution

Given the acute nature of IC MPTP in our animals, one might speculate that initial terminal field injury causes dystonia with recovery of function (i.e. sprouting of terminal fields), relieving dystonia. However, there is no evidence in our animals to support sprouting of terminal fields that produces any functional activity or neuronal recovery during the dystonic phase or beyond (54).

Conclusion

Severity of transient IC MPTP induced dystonia correlates with subsequent parkinsonism severity, supporting common pathways with respect to mechanistic consideration. The degree of dystonia correlates with subsequent nigral cell injury across the entire spectrum of severity, where striatal dopamine measures do not. There are limitations to interpreting the nigral cell counts, but sustained striatal dopamine depletion is not sufficient as a biomarker for transient dystonia. Although the dystonic phase is discrete and short lived in *Macaca fasiculata* and *Macaca nemestrina*, it is consistent and sufficient in duration to permit analysis of behavioral response in relation to

physiological parameters, particularly with regard to studying dystonia independent of, or in relation to parkinsonism in unmedicated animals.

Data availability statement

Animal videos will only be released upon institutional approval to researchers qualified and trained in conjunction with an appropriate institutional animal care and use committee. Requests to access the datasets should be directed to JP, perlmutterjoel@wustl.edu.

Ethics statement

The animal study was reviewed and approved by Institutional Animal Care and Use Committee (IACUC), Washington University School of Medicine.

Author contributions

SN and JP contributed to conception and design of the study; SN, JP, EW, and LT assisted with conduct of experiments. EW and LT managed and organized the database; SN and LT performed statistical analysis. SN drafted the manuscript. All authors contributed to manuscript revision, read and approved the submitted version.

Funding

This work was supported by NIH NINDS/NIA (NS039821, NS075321, NS41509, NS058714, NS124789); the Barnes Jewish Hospital Foundation (Elliot Stein Family Fund and Parkinson Disease Research Fund); the American Parkinson Disease Association; the Barbara & Sam Murphy Fund; the McDonnell Center for Systems Neuroscience; and the Oertli Fund for Parkinson Disease Research.

Conflict of interest

The authors declare that the research was conducted in the absence of any commercial or financial relationships that could be construed as a potential conflict of interest.

Acknowledgments

The authors would like to thank Susan Loftin, John Hood, Darryl Craig, Samar Tabbal, and Emily Flores for their roles in this research.

References

1. D'Amato RJ, Lipman ZP, Snyder SH. Selectivity of the parkinsonian neurotoxin MPTP: Toxic metabolite MPP+ binds to neuromelanin. *Science* (1986) 231(4741): 987–9. doi:10.1126/science.3080808

2. Jenner P. The MPTP-treated primate as a model of motor complications in PD: Primate model of motor complications. *Neurology* (2003) 61(6):S4–11. doi:10.1212/wnl.61.6_suppl_3.s4

3. Burns RS, Chiueh CC, Markey SP, Ebert MH, Jacobowitz DM, Kopin IJ. A primate model of parkinsonism: Selective destruction of dopaminergic neurons in the pars compacta of the substantia nigra by N-methyl-4-phenyl-1,2,3,6-tetrahydropyridine. *Proc Natl Acad Sci U S A* (1983) 80(14):4546–50. doi:10.1073/pnas.80.14.4546

4. Ballard PA, Tetrud JW, Langston JW. Permanent human parkinsonism due to 1-methyl-4-phenyl-1,2,3,6-tetrahydropyridine (MPTP): Seven cases. *Neurology* (1985) 35(7):949–56. doi:10.1212/wnl.35.7.949

5. Boyce S, Rupniak NM, Steventon MJ, Iversen SD. Characterisation of dyskinesias induced by L-dopa in MPTP-treated squirrel monkeys. *Psychopharmacology (Berl)* (1990) 102(1):21–7. doi:10.1007/BF02245739

6. Tabbal SD, Mink JW, Antenor JA, Carl JL, Moerlein SM, Perlmutter JS. 1-Methyl-4-phenyl-1,2,3,6-tetrahydropyridine-induced acute transient dystonia in monkeys associated with low striatal dopamine. *Neuroscience* (2006) 141(3): 1281–7. doi:10.1016/j.neuroscience.2006.04.072

7. Perlmutter JS, Tempel LW, Black KJ, Parkinson D, Todd RD. MPTP induces dystonia and parkinsonism. Clues to the pathophysiology of dystonia. *Neurology* (1997) 49(5):1432–8. doi:10.1212/wnl.49.5.1432

8. Karimi M, Tian L, Brown CA, Flores HP, Loftin SK, Videen TO, et al. Validation of nigrostriatal positron emission tomography measures: Critical limits. *Ann Neurol* (2013) 73(3):390–6. doi:10.1002/ana.23798

9. Tabbal SD, Tian L, Karimi M, Brown CA, Loftin SK, Perlmutter JS. Low nigrostriatal reserve for motor parkinsonism in nonhuman primates. *Exp Neurol* (2012) 237(2):355–62. doi:10.1016/j.expneurol.2012.07.008

10. Norris SA, White H, Tanenbaum A, Williams EL, Cruchaga C, Tian L, et al. Severe acute neurotoxicity reflects absolute intra-carotid 1-methyl-4-phenyl-1,2,3,6-tetrahydropyridine dose in non-human primates. *J Neurosci Methods* (2022) 366:109406. doi:10.1016/j.jneumeth.2021.109406

11. Hardt JI, Perlmutter JS, Smith CJ, Quick KL, Wei L, Chakraborty SK, et al. Pharmacokinetics and Toxicology of the Neuroprotective e,e,e-Methanofullerene(60)-63-tris Malonic Acid [C3] in Mice and Primates. *Eur J Drug Metab Pharmacokinet* (2018) 43(5):543–54. doi:10.1007/s13318-018-0464-z

12. Dugan LL, Tian L, Quick KL, Hardt JI, Karimi M, Brown C, et al. Carboxyfullerene neuroprotection postinjury in Parkinsonian nonhuman primates. *Ann Neurol* (2014) 76(3):393–402. doi:10.1002/ana.24220

13. Tian L, Karimi M, Loftin SK, Brown CA, Xia H, Xu J, et al. No differential regulation of dopamine transporter (DAT) and vesicular monoamine transporter 2 (VMAT2) binding in a primate model of Parkinson disease. *PloS one* (2012) 7(2): e31439. doi:10.1371/journal.pone.0031439

14. Benazzouz A, Gross C, Feger J, Boraud T, Bioulac B. Reversal of rigidity and improvement in motor performance by subthalamic high-frequency stimulation in MPTP-treated monkeys. *Eur J Neurosci* (1993) 5(4):382–9. doi:10.1111/j.1460-9568.1993.tb00505.x

15. Langston JW, Langston EB, Irwin I. MPTP-induced parkinsonism in human and non-human primates--clinical and experimental aspects. *Acta Neurol Scand Suppl* (1984) 100:49–54.

16. Bezard E, Dovero S, Bioulac B, Gross C. Effects of different schedules of MPTP administration on dopaminergic neurodegeneration in mice. *Exp Neurol* (1997) 148(1):288–92. doi:10.1006/exnr.1997.6648

17. Bezard E, Dovero S, Prunier C, Ravenscroft P, Chalon S, Guilloteau D, et al. Relationship between the appearance of symptoms and the level of nigrostriatal degeneration in a progressive 1-methyl-4-phenyl-1,2,3,6-tetrahydropyridine-lesioned macaque model of Parkinson's disease. *J Neurosci* (2001) 21(17): 6853–61. doi:10.1523/JNEUROSCI.21-17-06853.2001

18. Di Monte DA, McCormack A, Petzinger G, Janson AM, Quik M, Langston WJ. Relationship among nigrostriatal denervation, parkinsonism, and dyskinesias in the MPTP primate model. *Mov Disord* (2000) 15(3):459–66. doi:10.1002/1531-8257(200005)15:3<459:AID-MDS1006>3.0.CO;2-3

19. Iravani MM, Jackson MJ, Kuoppamaki M, Smith LA, Jenner P. 3,4-methylenedioxymethamphetamine (ecstasy) inhibits dyskinesia expression and normalizes motor activity in 1-methyl-4-phenyl-1,2,3,6-tetrahydropyridine-treated primates. *J Neurosci* (2003) 23(27):9107–15. doi:10.1523/JNEUROSCI.23-27-09107.2003

20. Meissner W, Prunier C, Guilloteau D, Chalon S, Gross CE, Bezard E. Time-course of nigrostriatal degeneration in a progressive MPTP-lesioned macaque model of Parkinson's disease. *Mol Neurobiol* (2003) 28(3):209–18. doi:10.1385/MN:28:3:209

21. Belanger N, Gregoire L, Hadj Tahar A, Bedard PJ. Chronic treatment with small doses of cabergoline prevents dopa-induced dyskinesias in parkinsonian monkeys. *Mov Disord* (2003) 18(12):1436–41. doi:10.1002/mds.10589

22. Rose S, Nomoto M, Jackson EA, Gibb WR, Jaehnig P, Jenner P, et al. Age-related effects of 1-methyl-4-phenyl-1,2,3,6-tetrahydropyridine treatment of common marmosets. *Eur J Pharmacol* (1993) 230(2):177–85. doi:10.1016/0014-2999(93)90800-w

23. Richter A, Loscher W. Pathology of idiopathic dystonia: Findings from genetic animal models. *Prog Neurobiol* (1998) 54(6):633–77. doi:10.1016/s0301-0082(97)00089-0

24. Jinnah HA, Hess EJ, Ledoux MS, Sharma N, Baxter MG, Delong MR. Rodent models for dystonia research: Characteristics, evaluation, and utility. *Mov Disord* (2005) 20(3):283–92. doi:10.1002/mds.20364

25. Guehl D, Cuny E, Ghorayeb I, Michelet T, Bioulac B, Burbaud P. Primate models of dystonia. *Prog Neurobiol* (2009) 87(2):118–31. doi:10.1016/j.pneurobio.2008.10.003

26. Fernagut PO, Diguet E, Stefanova N, Biran M, Wenning GK, Canioni P, et al. Subacute systemic 3-nitropropionic acid intoxication induces a distinct motor disorder in adult C57Bl/6 mice: Behavioural and histopathological characterisation. *Neuroscience* (2002) 114(4):1005–17. doi:10.1016/s0306-4522(02)00205-1

27. Winkler C, Kirik D, Bjorklund A, Cenci MA. L-DOPA-induced dyskinesia in the intrastriatal 6-hydroxydopamine model of Parkinson's disease: Relation to motor and cellular parameters of nigrostriatal function. *Neurobiol Dis* (2002) 10(2):165–86. doi:10.1006/nbdi.2002.0499

28. Palfi S, Ferrante RJ, Brouillet E, Beal MF, Dolan R, Guyot MC, et al. Chronic 3-nitropropionic acid treatment in baboons replicates the cognitive and motor deficits of Huntington's disease. *J Neurosci* (1996) 16(9):3019–25. doi:10.1523/JNEUROSCI.16-09-03019.1996

29. Burns LH, Pakzaban P, Deacon TW, Brownell AL, Tatter SB, Jenkins BG, et al. Selective putaminal excitotoxic lesions in non-human primates model the movement disorder of Huntington disease. *Neuroscience* (1995) 64(4):1007–17. doi:10.1016/0306-4522(94)00431-4

30. Jenner P, Marsden CD. The actions of 1-methyl-4-phenyl-1,2,3,6-tetrahydropyridine in animals as a model of Parkinson's disease. *J Neural Transm Suppl* (1986) 20:11–39.

31. Pifl C, Schingnitz G, Hornykiewicz O. Effect of 1-methyl-4-phenyl-1,2,3,6-tetrahydropyridine on the regional distribution of brain monoamines in the rhesus monkey. *Neuroscience* (1991) 44(3):591–605. doi:10.1016/0306-4522(91)90080-8

32. Przedborski S, Jackson-Lewis V, Djaldetti R, Liberatore G, Vila M, Vukosavic S, et al. The parkinsonian toxin MPTP: Action and mechanism. *Restorative Neurol Neurosci* (2000) 16(2):135–42.

33. Todd RD, Carl J, Harmon S, O'Malley KL, Perlmutter JS. Dynamic changes in striatal dopamine D2 and D3 receptor protein and mRNA in response to 1-methyl-4-phenyl-1,2,3,6-tetrahydropyridine (MPTP) denervation in baboons. *J Neurosci* (1996) 16(23):7776–82. doi:10.1523/JNEUROSCI.16-23-07776.1996

34. Irwin I, DeLanney LE, Forno LS, Finnegan KT, Di Monte DA, Langston JW. The evolution of nigrostriatal neurochemical changes in the MPTP-treated squirrel monkey. *Brain Res* (1990) 531(1-2):242–52. doi:10.1016/0006-8993(90)90780-f

35. Karimi M, Perlmutter JS. The role of dopamine and dopaminergic pathways in dystonia: Insights from neuroimaging. *Tremor and other hyperkinetic movements* (2015) 5:280. doi:10.7916/D8J101XV

36. Zhai S, Tanimura A, Graves SM, Shen W, Surmeier DJ. Striatal synapses, circuits, and Parkinson's disease. *Curr Opin Neurobiol* (2018) 48:9–16. doi:10.1016/j.conb.2017.08.004

37. Falardeau P, Bedard PJ, Di Paolo T. Relation between brain dopamine loss and D2 dopamine receptor density in MPTP monkeys. *Neurosci Lett* (1988) 86(2):225–9. doi:10.1016/0304-3940(88)90575-7

38. Gagnon C, Bedard PJ, Di Paolo T. Effect of chronic treatment of MPTP monkeys with dopamine D-1 and/or D-2 receptor agonists. *Eur J Pharmacol* (1990) 178(1):115–20. doi:10.1016/0014-2999(90)94802-5

39. Lau YS, Fung YK. Pharmacological effects of 1-methyl-4-phenyl-1,2,3,6-tetrahydropyridine (MPTP) on striatal dopamine receptor system. *Brain Res* (1986) 369(1-2):311–5. doi:10.1016/0006-8993(86)90541-x

40. Weihmuller FB, Bruno JP, Neff NH, Hadjiconstantinou M. Dopamine receptor plasticity following MPTP-induced nigrostriatal lesions in the mouse. *Eur J Pharmacol* (1990) 180(2-3):369–72. doi:10.1016/0014-2999(90)90324-y

41. Alexander GM, Brainard DL, Gordon SW, Hichens M, Grothusen JR, Schwartzman RJ. Dopamine receptor changes in untreated and (+)-PHNO-treated MPTP parkinsonian primates. *Brain Res* (1991) 547(2):181–9. doi:10.1016/0006-8993(91)90960-4

42. Grandy DK, Civelli O. G-protein-coupled receptors: The new dopamine receptor subtypes. *Curr Opin Neurobiol* (1992) 2(3):275–81. doi:10.1016/0959-4388(92)90115-2

43. Mink JW. Basal ganglia mechanisms in action selection, plasticity, and dystonia. *Eur J Paediatr Neurol* (2018) 22(2):225–9. doi:10.1016/j.ejpn.2018.01.005

44. Tadano T, Satoh N, Sakuma I, MaTsumura T, Kisara K, Arai Y, et al. Behavioral and biochemical changes following acute administration of MPTP and MPP+. *Life Sci* (1987) 40(13):1309–18. doi:10.1016/0024-3205(87)90588-1

45. Pileblad E, Fornstedt B, Clark D, Carlsson A. Acute effects of 1-methyl-4-phenyl-1,2,3,6-tetrahydropyridine on dopamine metabolism in mouse and rat striatum. *J Pharm Pharmacol* (1985) 37(10):707–11. doi:10.1111/j.2042-7158.1985.tb04947.x

46. Calabresi P, Picconi B, Tozzi A, Di Filippo M. Dopamine-mediated regulation of corticostriatal synaptic plasticity. *Trends Neurosci* (2007) 30(5):211–9. doi:10.1016/j.tins.2007.03.001

47. van Harten PN, van Trier JC, Horwitz EH, Matroos GE, Hoek HW. Cocaine as a risk factor for neuroleptic-induced acute dystonia. *J Clin Psychiatry* (1998) 59(3):128–30. doi:10.4088/jcp.v59n0307

48. McKinley JW, Shi Z, Kawikova I, Hur M, Bamford IJ, Sudarsana Devi SP, et al. Dopamine deficiency reduces striatal cholinergic interneuron function in models of Parkinson's disease. *Neuron* (2019) 103(6):1056–72. doi:10.1016/j.neuron.2019.06.013

49. Fino E, Glowinski J, Venance L. Effects of acute dopamine depletion on the electrophysiological properties of striatal neurons. *Neurosci Res* (2007) 58(3):305–16. doi:10.1016/j.neures.2007.04.002

50. Cai Y, Nielsen BE, Boxer EE, Aoto J, Ford CP. Loss of nigral excitation of cholinergic interneurons contributes to parkinsonian motor impairments. *Neuron* (2021) 109(7):1137–49.e5. doi:10.1016/j.neuron.2021.01.028

51. Padilla-Orozco M, Duhne M, Fuentes-Serrano A, Ortega A, Galarraga E, Bargas J, et al. Synaptic determinants of cholinergic interneurons hyperactivity during parkinsonism. *Front Synaptic Neurosci* (2022) 14:945816. doi:10.3389/fnsyn.2022.945816

52. Mulholland GK, Wieland DM, Kilbourn MR, Frey KA, Sherman PS, Carey JE, et al. [18F]fluoroethoxy-benzovesamicol, a PET radiotracer for the vesicular acetylcholine transporter and cholinergic synapses. *Synapse* (1998) 30(3):263–74. doi:10.1002/(SICI)1098-2396(199811)30:3<263:AID-SYN4>3.0.CO;2-9

53. Yue X, Bognar C, Zhang X, Gaehle GG, Moerlein SM, Perlmutter JS, et al. Automated production of [^{18}F]VAT suitable for clinical PET study of vesicular acetylcholine transporter. *Appl Radiat Isot* (2016) 107:40–6. doi:10.1016/j.apradiso.2015.09.010

54. Tian L, Karimi M, Brown CA, Loftin SK, Perlmutter JS. *In vivo* measures of nigrostriatal neuronal response to unilateral MPTP treatment. *Brain Res* (2014) 1571:49–60. doi:10.1016/j.brainres.2014.05.009

DYSTONIA

TYPE Original Research
PUBLISHED 02 February 2023
DOI 10.3389/dyst.2023.10974

OPEN ACCESS

EDITED BY
Daniela Popa,
INSERM U1024 Institut de biologie de l'Ecole Normale Supérieure, France

*CORRESPONDENCE
Timothy J. Ebner,
ebner001@umn.edu
Russell E. Carter,
recarter@umn.edu

†These authors have contributed equally to this work

RECEIVED 14 October 2022
ACCEPTED 17 January 2023
PUBLISHED 02 February 2023

CITATION
Gray MM, Naik A, Ebner TJ and Carter RE (2023), Altered brain state during episodic dystonia in tottering mice decouples primary motor cortex from limb kinematics.
Dystonia 2:10974.
doi: 10.3389/dyst.2023.10974

Altered brain state during episodic dystonia in tottering mice decouples primary motor cortex from limb kinematics

Madelyn M. Gray[1†], Anant Naik[2†], Timothy J. Ebner[1*] and Russell E. Carter[1*]

[1]Department of Neuroscience, University of Minnesota, Minneapolis, MN, United States, [2]Department of Biomedical Engineering, University of Minnesota, Minneapolis, MN, United States

Episodic Ataxia Type 2 (EA2) is a rare neurological disorder caused by a mutation in the *CACNA1A* gene, encoding the P/Q-type voltage-gated Ca^{2+} channel important for neurotransmitter release. Patients with this channelopathy exhibit both cerebellar and cerebral pathologies, suggesting the condition affects both regions. The *tottering* (*tg*/*tg*) mouse is the most commonly used EA2 model due to an orthologous mutation in the *cacna1a* gene. The *tg*/*tg* mouse has three prominent behavioral phenotypes: a dramatic episodic dystonia; absence seizures with generalized spike and wave discharges (GSWDs); and mild ataxia. We previously observed a novel brain state, transient low-frequency oscillations (LFOs) in the cerebellum and cerebral cortex under anesthesia. In this study, we examine the relationships among the dystonic attack, GSWDs, and LFOs in the cerebral cortex. Previous studies characterized LFOs in the motor cortex of anesthetized *tg*/*tg* mice using flavoprotein autofluorescence imaging testing the hypothesis that LFOs provide a mechanism for the paroxysmal dystonia. We sought to obtain a more direct understanding of motor cortex (M1) activity during the dystonic episodes. Using two-photon Ca^{2+} imaging to investigate neuronal activity in M1 before, during, and after the dystonic attack, we show that there is not a significant change in the activity of M1 neurons from baseline through the attack. We also conducted simultaneous, multi-electrode recordings to further understand how M1 cellular activity and local field potentials change throughout the progression of the dystonic attack. Neither putative pyramidal nor inhibitory interneuron firing rate changed during the dystonic attack. However, we did observe a near complete loss of GSWDs during the dystonic attack in M1. Finally, using spike triggered averaging to align simultaneously recorded limb kinematics to the peak Ca^{2+} response, and *vice versa*, revealed a reduction in the spike triggered average during the dystonic episodes. Both the loss of GSWDs and the reduction in the coupling suggest that, during the dystonic attack, M1 is effectively decoupled from other structures. Overall, these results indicate that the attack is not initiated or controlled in M1, but elsewhere in the motor circuitry. The findings also highlight that LFOs, GSWDs, and dystonic attacks represent three brain states in *tg*/*tg* mice.

KEYWORDS

episodic ataxia type 2, calcium imaging, generalized spike-and-wave discharges, absence seizures, P/Q-type calcium channel

Introduction

Dystonia encompasses a spectrum of neurological disorders characterized by involuntary movements or postures resulting from sustained muscle contractions [for reviews see (1–3)]. The current classification scheme is organized along two axes (4). Axis I is based on the clinical findings and presentation. Axis II is whether the dystonia is isolated or combined, that is without or with other neurological or systemic manifestations. Just as the clinical presentations of dystonia are manifold, the etiologies are varied and range from acquired or inherited structural or degenerative nervous system lesions, drugs/toxins, and inherited forms. The prevalence of idiopathic and inherited dystonia is estimated at over 300 individuals per million (5–7).

A large number of genetic disorders have dystonia as the sole symptom or as part of the phenotype (1). Several present with episodic dystonia such as paroxysmal kinesigenic dyskinesia (PKD) due to mutations in proline-rich transmembrane protein 2 (PRRT) (8), exercise-induced dystonia owing to mutations in *SLC2A1 (glucose transporter type 1)* (9), and dystonic episodes in *ATP1A3* spectrum disorders (10). The channelopathies are group of neurological disorders due to mutations in genes encoding for ion channels and are characterized by episodic symptoms [for reviews see (11–15)]. One of the Ca^{2+} channelopathies, and the focus of this study, results in episodic ataxia type 2 (EA2). EA2 is caused by dominant mutations of the *CACNA1A* gene that encodes the α_{1A}, pore-forming subunit of the $Ca_v2.1$ (P/Q-type) voltage gated Ca^{2+} channel (11, 16–20). Patients with EA2 suffer from episodic motor dysfunction consisting of limb and gait ataxia and oscillopsia, consistent with a cerebellar origin (11, 16, 17, 21). Interictally, patients may exhibit nystagmus and progressive cerebellar dysfunction linked to cerebellar atrophy (16, 17, 22). Different families have a spectrum of other episodic symptoms that suggest cerebral cortex involvement including migraine, hemiplegic paralysis, dystonia, and cognitive disturbances (11, 16, 18, 23–26). As for all channelopathies, a fundamental question is the mechanism by which a permanent abnormality in an ion channel leads to transient nervous system dysfunction (15).

The *tottering* mouse (*tg*/*tg*) is the most commonly used murine model for EA2 and harbors a missense mutation in *Cacna1a*, the ortholog for the human *CACNA1A* gene that results in a substitution of leucine for proline (P1802L) in the pore lining region of the P/Q-type Ca^{2+} channel (27). The *tg*/*tg* mouse has three major behavioral phenotypes. First, absence seizures defined by bilateral, synchronous 6–7 per second cortical generalized spike-and-wave discharges (GSWDs) in electroencephalographic recordings (EEG) accompanied by sudden movement arrest, twitching of the whiskers, and a fixed stare (28–33). Second, mild ataxia that particularly involves the hindlimbs, tail, and head movements with a wobbly gait and poorly coordinated movements (31, 34). Third, a paroxysmal motor attack, referred to as paroxysmal dyskinesia or episodic dystonia, that lasts 60–90 min with a characteristic progression along the body axis that starts in the hindlimbs (31, 35). As for the episodic cerebellar disturbances in EA2 patients, attacks in *tg*/*tg* mice are evoked by stress, caffeine, and ethanol (35, 36).

It is well established that the cerebellum plays a central role in the episodic dystonia by immediate early gene expression, mutant mouse models, and lesion studies (36–40). One possible mechanism underlying the attacks in *tg*/*tg* mice are the episodic, low-frequency oscillations (LFOs) of ~0.04–0.1 Hz, initially observed in the cerebellar cortex (41). The cerebellar LFOs occur spontaneously, can propagate to neighboring regions, last approximately 30–120 min, and are both P/Q-type channel and Ca^{2+} dependent. During the episodic dystonia, bursts of electromyographic (EMG) activity occur at the same low frequencies and are coherent with LFOs in the cerebellum (41). Similar low-frequency oscillations are also prominent in the *tg*/*tg* cerebral cortex (42).

We hypothesized that the LFOs provide a mechanism for generating the episodic dystonia in the *tg*/*tg* mouse (41, 42). While the episodic dystonia is cerebellar dependent, the presence of the LFOs in cerebral cortex as well as the role of the motor cortex in controlling movements suggests the LFOs in the cerebral cortex could contribute to the motor attacks. Importantly, two effective treatments for EA2, 4-amino pyridine (4-AP) and acetazolamide (ACTZ) (43, 44), dramatically decrease the LFOs in the cerebral cortex (42). Another striking feature of a *tg*/*tg* dystonic attack is the characteristic topographic progression of the simultaneous contractions of agonist and antagonist muscle groups, with the first contractions occurring in the hindlimbs, followed by spread to the torso, forelimbs, and finally the head. In the final phase, the mice regain control of their hindlimbs, while contractions of the forepaw and facial muscles continue (31, 35). This orderly progression and recovery are reminiscent of a Jacksonian epileptic march involving the motor cortex and suggests involvement of a body map as found in the primary motor cortex. Finally, recent views of the pathophysiology emphasize dystonia is a network disorder involving the basal ganglia, cerebellum, and motor cortices [for reviews see (1, 45, 46)].

Therefore, here we investigate this possibility using two-photon (2P) Ca^{2+} imaging and multiple single cell electrophysiological recordings before, during, and after an evoked episodic dystonia attack. Unexpectedly, the results suggest that motor cortical LFOs are not involved in the

episodic dystonia. Instead, the findings show that the motor cortex coupling to limb movements decreases during the motor attack. Furthermore, the GSWD is nearly abolished during the episodic dystonia.

Methods

Animal care and husbandry

All animal studies were performed under protocols approved by the Institutional Animal Care and Use Committee of the University of Minnesota. Male and female *tg*/*tg* mice on a C57BL/6 background, as well as their wild type (WT) counterparts, were housed in University of Minnesota Research Animal Resources Facilities. Homozygous *tg*/*tg* mice were obtained by crossing a mouse line containing the *tg*/*tg* allele and closely linked semidominant allele *Os*, which causes oligosyndactalism. Genotyping of homozygous *tg*/*tg* mice was performed during weaning by confirming the absence of oligosyndactalism and was further verified *via* behavioral observation of episodic dystonia.

Overview of experimental design

The study involved three separate experiments using three different cohorts of mice for each portion of the study: anesthetized, awake two-photon Ca^{2+} imaging, and awake electrophysiology recordings. Each procedure utilized a different cranial window preparation, as described below, and therefore could not be performed in the same set of animals. For the anesthetized experiments, we used 8 *tg*/*tg* (3 male, 5 female) and 5 WT (2 male, 3 female) mice. For the awake two-photon Ca^{2+} imaging, we recorded from 6 *tg*/*tg* (4 male, 2 female) and 4 WT (2 male, 2 female) mice, however one *tg*/*tg* mouse was excluded from the attack and recovery period due to unsuccessful limb tracking. Finally, for the awake electrophysiology recordings we used a total of 4 *tg*/*tg* (2 male, 2 female) and 4 WT (2 male, 2 female) mice.

Anesthetized two-photon surgical preparation and image acquisition

Animals were anesthetized with acepromazine (2.0 mg/kg, i.p.) and urethane (2.0 mg/kg, i.p.), supplemented with 1.5 mg/kg urethane as needed. Once the animal was unresponsive to toe pinch, the skin covering the dorsal surface of the skull was removed, and a custom made imaging headplate was attached using a combination of Gel Superglue (Loctite) and Dental Cement (Dentsply Caulk). The animal then underwent a tracheotomy, was mechanically ventilated (120 breaths/min), and was then attached to a custom stereotax. Body temperature was maintained at 37°C using a feedback controlled heating pad. A 3 mm craniotomy was drilled over the left motor cortex (0 mm rostral, 1.5 mm lateral to bregma). Care was taken to avoid any bleeding and the dura was left intact. To image Ca^{2+} activity, 500 μM OGB-1 was then pressure injected using a fine-tipped glass micropipette at 3-4 sites in the craniotomy. An aqueous solution of 250 μM SR101 (Sigma) was placed on the surface of the brain to label astrocytes. Finally, the craniotomy was covered with a thin layer of agar and sealed with a glass coverslip and dental cement.

After surgical preparation was complete, the custom stereotax was secured to an xyz stage under a Leica SP5 multi-photon microscope with a MaiTai DeepSee laser tuned to 810 nm. Image series (3000 frames, 10 Hz) were taken over in randomly selected locations in M1. Some locations were imaged over multiple series to detect changes in LFOs over time. After imaging, mice were transcardially perfused using PBS and fixed with 4% paraformaldehyde.

Chronic window implantation

Mice used for chronic imaging were implanted with a transparent skull window (47). Due to the notable phenotypic difference in head size between *tg*/*tg* and WT mice, custom windows for each strain were used [for fabrication methods, see (47)]. Each implant was designed such that motor, somatosensory, barrel, and the rostral portions of the visual cortices could be imaged. However, this study recorded only in the motor cortex. The implant consisted of two pieces: a 3D-printed polymethyl methacrylate (PMMA) frame with a polyethylene terephthalate (PET) film, and a titanium head plate to attach to a custom disk treadmill for head-fixed imaging.

Four hours prior to surgery start, mice were injected with 1 mg/kg slow-release Buprenorphene and 2 mg/kg Meloxicam. Adult mice, 3–8 months of age, were anesthetized using Isofluorane (5% induction, 0.75%–3% maintenance), and head-fixed in a stereotaxic frame. Body temperature was maintained at 37°C using a feedback controlled heating pad. The dorsal region of the skin was removed to expose the skull. Craniotomy coordinates were determined by tracing the implant on the exposed skull. Before the craniotomy was removed, three burr holes were drilled over the right motor cortex for delivery of AAV1-hSyn-GCaMP6f-WPRE (Penn Vector Core). At each injection site, 200 nL of virus was delivered (50 nL/min, 0.7 mm from the cortical surface) through a Nanofil syringe (World Precision Instruments) using an automated injector (UMP3, World Precision Instruments). The syringe was withdrawn after 5 min following each injection.

A single bone screw was placed over the cerebellum to give stability to the implant during attachment. Great care was taken to avoid blood loss during the skull removal. The PMMA portion of the implant was then attached with Vetbond (3M) and dental cement (C&B Metabond, Parkell Inc.). Once fully cured, the titanium head plate was attached to the implant using screws, and

further secured with dental cement. A cap was affixed to the implant using Kwik-Sil (World Precision Instruments) to prevent damage to the brain from photobleaching as well as damage to the PET film from cage debris. Surgical attachment of the imaging window took roughly 4 h in total. Mice were allowed to recover from surgery for 3–4 days before experimentation.

Awake two-photon image acquisition and data processing

Mice were head fixed to the disk treadmill and secured to the xyz stage under the SP5 microscope. The xyz positions were logged so that the precise location of each imaging field could be determined. A wavelength of 920 nm was used to excite GCaMP6f (48). Image series (6000 frames, 20 Hz) were acquired for 5 min. Behavioral data was collected using an IR-sensitive camera (DMK 33UP1300, Image Source) at 20 Hz. After recording 1 hour of baseline activity, episodic dystonia was evoked *via* injection of caffeine (15 mg/kg, I.P., in saline). Mice were imaged through the duration of the attack and 1 hour into recovery. The imaging software sent out an initial trigger pulse to an external pulse generator which then triggered the behavior camera acquisition at the same frame rate as the two-photon Ca^{2+} imaging. As the behavior cameras are IR sensitive, we are able to see the two-photon laser in the behavior images, and the behavior frames were then accurately aligned to the start and stop of the laser illumination.

The raw signal of individual neurons in M1 was obtained using ImageJ (NIH). In brief, xy motion artifact was corrected using the moco plugin (49), and cells were identified using the cell magic wand plugin (50). Raw fluorescence signals were extracted for each region of interest (ROI), imported into MATLAB 2016b (Mathworks) and detrended. Fluorescence data was converted into $\Delta F/F_0$, where F_0 was defined as the 20th percentile of the overall fluorescence (51).

Low-frequency oscillation analysis

To evaluate traces for evidence of LFOs, the spectral profile of each trace was obtained *via* the Welch's power spectral density estimate in MATLAB (*pwelch*, 1000-point window, 100-point overlap, resolution of 4096). Setting the threshold for the high-power state was as described previously (41, 42). In brief, the threshold for high-power activity was set as 3 standard deviations above the WT mean in the 0.035–0.11 Hz band. In order to determine the degree of synchrony between high-power cells in a single time series, three analyses were performed. First, the local maxima of the frequency spectra of the cells were determined to probe maximally elevated frequency bands. If two local maxima were found within 10 data points of each other, the larger point was recorded. Second, the cross coherence between all high- and low-power traces in a time series was computed separately. The maximum coherence coefficient and frequency at which it occurred were extracted. To determine synchronicity in the time domain, cross correlation was computed separately for high- and low-power traces and the maximum correlation coefficient and time at which it occurred were extracted. Results from anesthetized data were used to set criteria within these parameters for LFO determination in the awake state.

Simultaneous two-photon Ca^{2+} imaging and behavioral analysis during attack

To determine what changes in M1 paralleled attack behavior, we calculated the peak number, peak amplitude, coherence and correlation of traces in each stack using built in MATLAB functions. Behavior tracking was performed using DeepLabCut1.0 (52) with three points per paw. All movement analyses were performed using limb speed, for which position data was differentiated and converted to polar coordinates. Behavior coupling to Ca^{2+} data was determined by aligning ±1 s of behavior data to each Ca^{2+} peak. Periods of movement and rest were manually defined, and three standard deviations above the mean-aligned rest traces was used to define movement. If movement defined by these parameters occurred within 100 ms of the Ca^{2+} peak, cells were determined to encode movement.

Awake electrophysiology surgical preparation and data acquisition

For experimentation, a separate cohort of *tg*/*tg* and WT C57BL/6 (Jackson Laboratories) were anaesthetized and prepared for surgery as described above. A 3–4 mm craniotomy was drilled over the motor cortex and a custom 3D-printed chamber was implanted over the craniotomy, affixed to the skull with dental screws and cement. The chamber was filled with sterile agarose gel and saline and sealed with Kwik-Sil. After surgery, mice recovered for 3–4 days prior to training. Mice were acclimatized to head-fixation on a custom freely moving recording wheel every other day for increasing durations to reduce the stress of being head-fixed and potential confounds with inducing the dystonic attack.

On recording days, up to 16 glass-gated platinum iridium microelectrodes were loaded into a multi-electrode array (System Eckhorn Microdrive, 100 µm spacing, Thomas Recording, GMBH), and were individually lowered. Electrophysiological signals were recorded at 24 KHz using a 32-channel pre-amp (PZ2-32, Tucker Davis Technologies) and RZ2 amplifier (Tucker Davis Technologies). Following 15–20 min of baseline activity, 15 mg/kg (i.p.) caffeine was injected to trigger the dystonic attack. Mice were continuously monitored for attack onset and duration (53).

Electrophysiology data analysis

Raw signals were either filtered using a 150th order FIR low-pass filter (200 Hz) and down-sampled by a factor of 8 to obtain local field potentials (LFPs) or using a 150th order FIR bandpass filter (800–5,000 Hz) to obtain single units. Generalized spike-and-wave discharges (GSWDs) were isolated using a custom algorithm. Briefly, the short-time Fourier Transform (1 s window, 875 ms overlap, NFFT of 24,000) was computed and the product of the maximum powers for the first three resonant peaks (5–8, 13–17, and 19–24 Hz) were determined and thresholded against one standard deviation of the mode power. GSWDs were excluded if the duration was less than 1 s (54). Positive GSWD events were combined if two GSWDs occurred within 1 s of each other. Algorithm performance was approximately 95.9% accurate, with 0 false positives and 4.1% false negatives.

For single unit analysis, an amplitude threshold was selected to identify isolated action potentials. This was done using a standard outlier detection approach previously described (55), found to be 5 times the probable error of the overall signal. A waveform forming a 2-millisecond window around the identified peak was extracted. Three commonly used methods for feature extraction were applied to each identified waveform, include wavelet decomposition (56), Linear Discriminant Analysis (57, 58), and differential features including first and second derivatives (59). Features were first ordered by a modified Kolmogorov-Smirnov test for unimodality (56). For each feature, a KS-test was performed between the original distribution and a unimodal distribution of the same mean and standard deviation. Significant features ($p < 0.05$) were then ordered based on the obtained p-value. All significant features were then used to manually cluster the data.

Subsequently, unique units in each recording were subclassified as either interneurons or pyramidal cells using previously published methodology (60). Briefly, this was done by reducing the dimension of five parameters (mode interspike interval, mean firing rate, cell burst index, waveform asymmetry score, and waveform trough-to-peak latency) using t-distributed Stochastic Network Embedding (t-SNE) (61), a non-parametric method that computes the variability across each input dimension to assign a weight that retains the n-dimensional nearest-neighbor spatial arrangement of the data set. The output variables have arbitrary units but represent a weighted combination of the original features of the data. This classification system yielded two separable clusters with unique firing properties. To verify the classification, the firing properties of the cells were determined and compared to the literature values (62–64) including the firing rates and autocorrelation properties. Firing rhythmicity was characterized by the 2nd-order coefficient of variance (CV_2), the ratio of the standard deviation to the mean squared, that shows the extent of variability in relation to the mean of the population (65, 66).

Statistical evaluations

All statistics were performed in MATLAB and GraphPad Prism 8.0, and significance was set at $p > 0.05$. Data is reported as mean ± standard deviation. The mean correlation and coherence coefficients for *tg*/*tg* high-power, *tg*/*tg* low-power, and WT cells were compared using one-way ANOVA with Bonferroni *post hoc* test. Effect size (Cohen's d) was calculated for all significant effects, and only significant effects with medium (>0.5, dashed lines) and large (>0.8, solid lines) effect sizes are shown in the figures. We report effect size to emphasize the magnitude of any changes, as small changes could result in significant but small effects given the large "n" values of the data sets. In the remainder of the manuscript, we only highlight comparisons that were both significant and passed these effect size criteria. All statistics are reported in Table 1.

Results

Low-frequency oscillations (LFOs) of movement kinematics during episodic dystonia in *tg*/*tg* mice

To test our hypothesis that the LFOs observed in macroscopic brain imaging in the anesthetized *tg*/*tg* mouse are related to the attack, we performed high-speed video tracking of limb movements before, during, and after the attack (Figure 1A). Spectral analysis of DeepLabCut tracked limb movements showed increased rhythmicity of limb speed in the LFO band of interest (0.035–0.11 Hz) during the attack, as shown for example data (Figure 1B, red trace). This increase in power was significant and large in magnitude when compared to baseline and recovery across all mice, while wild-type mice showed no evidence of oscillation following caffeine challenge (Figure 1C). These results support earlier observations of LFO in the EMG activity of *tg*/*tg* during episodic dystonia (41) and suggest that the LFOs in the limb movement may be coupled to LFOs in the cerebral cortex and/or cerebellar cortex (42).

Ca^{2+} imaging of motor cortical neurons reveals high-power LFOs in the anesthetized *tg*/*tg* mice but not during awake behavior or attack

Previous studies of the LFOs in *tg*/*tg* mice were performed under anesthesia using flavoprotein imaging (41, 42), which uses metabolic activity as a surrogate of cellular activation. However,

TABLE 1 Statistical testing results and effect sizes.

	Tukey's multiple comparisons test	Adjusted *p*-value	Effect size (Cohen's d)
Figure 1C	Baseline *tg/tg* vs. Attack *tg/tg*	0.03	0.57
	Baseline *tg/tg* vs. Recovery *tg/tg*	0.92	0.39
	Attack *tg/tg* vs. Recovery *tg/tg*	0.02	0.89
	Baseline WT vs. Caff WT	0.72	Ns
	Baseline WT vs. Recovery WT	0.96	Ns
	Caff WT vs. Recovery WT	0.56	Ns
	n = 6 attacks from 5 tg/tg mice, 4 caffeine administrations in 4 WT mice		
Figure 2D	Anesthetized *tg/tg* vs. Awake *tg/tg*	<0.0001	2.5
	Anesthetized *tg/tg* vs. Awake WT	<0.0001	2.81
	Anesthetized *tg/tg* vs. Attack *tg/tg*	<0.0001	2.68
	Anesthetized *tg/tg* vs. WT caff	<0.0001	2.65
	Awake *tg/tg* vs. Awake WT	0.78	Ns
	Awake *tg/tg* vs. Attack *tg/tg*	0.97	Ns
	Awake *tg/tg* vs. Caff WT	0.98	Ns
	Awake WT vs. Attack *tg/tg*	>0.99	Ns
	Awake WT vs. Caff WT	>0.99	Ns
	Attack *tg/tg* vs. Caff WT	>0.99	Ns
Figure 2E	Anesthetized *tg/tg* vs. Awake *tg/tg*	0.81	Ns
	Anesthetized *tg/tg* vs. Awake WT	<0.0001	1.93
	Anesthetized *tg/tg* vs. Attack *tg/tg*	0.65	Ns
	Anesthetized *tg/tg* vs. WT caff	0.2	Ns
	Awake *tg/tg* vs. Awake WT	<0.0001	1.4
	Awake *tg/tg* vs. Attack *tg/tg*	0.083	Ns
	Awake *tg/tg* vs. Caff WT	0.028	Ns
	Awake WT vs. Attack *tg/tg*	<0.0001	1.76
	Awake WT vs. Caff WT	<0.0001	2.47
	Attack *tg/tg* vs. Caff WT	0.83	Ns
Figure 2F	Anesthetized *tg/tg* vs. Awake *tg/tg*	0.044	1.70
	Anesthetized *tg/tg* vs. Awake WT	0.96	Ns
	Anesthetized *tg/tg* vs. Attack *tg/tg*	0.0078	2.45
	Anesthetized *tg/tg* vs. WT caff	0.15	Ns
	Awake *tg/tg* vs. Awake WT	0.0009	0.87
	Awake *tg/tg* vs. Attack *tg/tg*	0.71	Ns
	Awake *tg/tg* vs. Caff WT	>0.9999	Ns
	Awake WT vs. Attack *tg/tg*	<0.0001	1.25
	Awake WT vs. Caff WT	0.13	Ns
	Attack *tg/tg* vs. Caff WT	0.93	Ns
	*Anesthetized WT had 0 high power cells		
	Number of recordings with high power cells/number of high-power cells		
	Anesthetized *tg/tg*: 8 recordings/81 cells		
	Anesthetized WT: 0 recordings/0cells (13 overall recordings)		
	Awake *tg/tg*: 22 recordings/574 cells		
	Awake WT: 11 recordings/222 cells		
	Attack *tg/tg*: 6 recordings/233 cells		
	WT caffeine: 4 recordings/57 cells		
Figure 3A	Baseline *tg/tg* vs. Attack *tg/tg*	0.14	Ns
	Baseline *tg/tg* vs. Recovery *tg/tg*	>0.9999	Ns
	Attack *tg/tg* vs. Recovery *tg/tg*	0.59	Ns

(Continued on following page)

TABLE 1 (*Continued*) Statistical testing results and effect sizes.

	Tukey's multiple comparisons test	Adjusted *p*-value	Effect size (Cohen's d)
	Baseline WT vs. Caff WT	<0.0001	0.38
	Baseline WT vs. Recovery WT	0.91	Ns
	Caff WT vs. Recovery WT	<0.0001	0.3
	Baseline *tg/tg* vs. Baseline WT	<0.0001	0.8
	Attack *tg/tg* vs. Caff WT	0.026	0.11
	Recovery *tg/tg* vs. Recovery WT	0.001	0.32
Figure 3B	Baseline *tg/tg* vs. Attack *tg/tg*	<0.0001	0.16
	Baseline *tg/tg* vs. Recovery *tg/tg*	0.0004	0.74
	Attack *tg/tg* vs. Recovery *tg/tg*	<0.0001	0.41
	Baseline WT vs. Caff WT	>0.9999	Ns
	Baseline WT vs. Recovery WT	>0.9999	Ns
	Caff WT vs. Recovery WT	>0.9999	Ns
	Baseline *tg/tg* vs. Baseline WT	<0.0001	1.03
	Attack *tg/tg* vs. Caff WT	0.0002	0.21
	Recovery *tg/tg* vs. Recovery WT	<0.0001	0.76
Figure 3C	Baseline *tg/tg* vs. Attack *tg/tg*	<0.0001	0.41
	Baseline *tg/tg* vs. Recovery *tg/tg*	<0.0001	0.42
	Attack *tg/tg* vs. Recovery *tg/tg*	<0.0001	0.82
	Baseline WT vs. Caff WT	<0.0001	0.48
	Baseline WT vs. Recovery WT	<0.0001	0.46
	Caff WT vs. Recovery WT	>0.9999	Ns
	Baseline *tg/tg* vs. Baseline WT	0.023	0.2
	Attack *tg/tg* vs. Caff WT	0.97	Ns
	Recovery *tg/tg* vs. Recovery WT	<0.0001	0.71
	For Figures 3A–C: *n* = 692 *tg/tg* cells from 6 animals, 351 WT cells from 4 animals		
Figure 3F	WT Firing Rate Pyr vs. Int	0.0036	1.14
	WT CV2 Pyr vs. Int	0.4463	Ns
	n= 16 pyramidal cells, 19 interneurons		
Figure 3G	Firing Rate Int Baseline vs. Attack	0.56	Ns
	Firing Rate Int Baseline vs. Recovery	0.93	Ns
	Firing Rate Int Recovery vs. Attack	0.64	Ns
	Firing Rate Py Baseline vs. Attack	0.57	Ns
	Firing Rate Py Baseline vs. Recovery	0.63	Ns
	Firing Rate Py Recovery vs. Attack	0.46	Ns
	CV2 Int Baseline vs. Attack	0.37	Ns
	CV2 Int Baseline vs. Recovery	0.75	Ns
	CV2 Int Recovery vs. Attack	0.46	Ns
	CV2 Py Baseline vs. Attack	0.48	Ns
	CV2 Py Baseline vs. Recovery	>0.99	Ns
	CV2 Py Recovery vs. Attack	0.35	Ns
Figure 4C	Baseline vs. Attack	0.01	1.64
	Baseline vs. Recovery	0.51	Ns
	Attack vs. Recovery	0.069	Ns
Figure 4E	Baseline vs. Attack	<0.0001	0.54
	Baseline vs. Recovery	0.4	Ns
	Attack vs. Recovery	<0.0001	0.51
	n = 334 cells from 5 animals		
Figure 5D	GSWD/min Baseline vs. Attack	<0.001	1.27

(Continued on following page)

TABLE 1 (*Continued*) Statistical testing results and effect sizes.

Tukey's multiple comparisons test	Adjusted *p*-value	Effect size (Cohen's d)
GSWD/min Baseline vs. Recovery	0.38	Ns
GSWD/min Recovery vs. Attack	<0.001	2.38
Interictal Time Baseline vs. Attack	<0.001	0.47
Interictal Time Baseline vs. Recovery	0.8	Ns
Interictal Time Recovery vs. Attack	<0.001	0.53

flavoprotein imaging cannot distinguish signals from different cell types or the activity of single neurons. To test whether LFOs occur at the neuronal level in the *tg*/*tg* mouse, we first performed single cell two-photon (2P) imaging under two conditions in layer II/III of the primary motor cortex (M1): 1) under urethane-anesthesia using the Ca^{2+} indicator OGB-1 (Figure 2A); and 2) in awake mice using virally injected GCaMP6f (Figures 2B, C; see *Methods*). Example single cell activity and spectral analysis are shown for a sample of cells identified in the image (Figure 2A, right). Using the previously established criteria of high-power LFO activity in anesthetized *tg*/*tg* mice (3 standard deviations above the mean of WT mice (Cramer et al., 2015)), we identified 49.36 ± 19.01% of cells in each of 8 mice recorded with high-power activity, while no cells recorded in the anesthetized WT mouse that exhibited high-power LFO activity (Figure 2D). Thus, the anesthetized WT condition was excluded from the remainder of LFO analysis as there were no cells with high-power LFOs identified. Analysis of the activity of the *tg*/*tg* high-power cells in the frequency domain reveals a high degree of maximum coherence (Figure 2E). Furthermore, the mean peak frequency of the *tg*/*tg* high-power cells (0.23 ± 0.14 Hz) is within the LFO band of interest.

We next performed awake two-photon imaging of head-fixed *tg*/*tg* mice before, during, and following caffeine (15 mg/kg I.P.) induced episodic dystonia. Example single cell activity and spectral analysis are shown for a sample of cells identified in the image (Figures 2B, C, right). Using the same LFO detection criteria as in the anesthetized recordings, we identified less than 12% of cells with high-power activity in awake and attack *tg*/*tg* conditions (Figure 2D). While the coherence amplitude was high across high-power cells from the different groups, with some differences (Figure 2E), the maximum coherence was in the LFO band of interest only for neurons recorded in the anesthetized *tg*/*tg* mouse (0.23 ± 0.14 Hz, Figure 2F). Taken together, these results confirm that LFOs are present in *tg*/*tg* M1 neurons and the Ca^{2+} transients in these cells are highly synchronized under anesthesia. Injections of caffeine in WT mice did not result in an increase in LFOs in motor cortex neurons, therefore caffeine itself does not produce the oscillations. However, in awake, behaving *tg*/*tg* mice, we observed only a small percentage of neurons with LFOs, in either the baseline or episodic dystonia state.

Neuronal firing rate and variability do not change during episodic dystonia

Although the activity of *tg*/*tg* M1 neurons did not display synchronized LFOs during episodic dystonia, we examined if there were any other changes in Ca^{2+} activity. No significant changes with a large enough effect size were observed in the amplitude of Ca^{2+} events in *tg*/*tg* mice throughout the recordings (Figure 3A). There was a significant increase (large effect size) in both the amplitude (Figure 3A) and number (Figure 3B) of Ca^{2+} events during baseline between *tg*/*tg* and WT mice, likely attributed to the mutated P/Q-type Ca^{2+} channels. The number of Ca^{2+} events did remain significantly larger (medium effect size) in the recovery period compared to baseline in *tg*/*tg* mice (Figure 3B), and an increase in the correlation of cells in local M1 networks following but not during the attack (Figure 3C), suggesting some long-lasting alterations in M1 cells following an episodic dystonia attack. Taken together, these results suggest that these modest, non-specific changes in Ca^{2+} event metrics in layers II/III M1 neurons may be insufficient to attribute a major role for the primary motor cortex in the episodic dystonia.

As 2P Ca^{2+} imaging is predominantly restricted to the upper layers of the cerebral cortex, does not directly measure neural spiking, and is not cell type specific unless using targeted expression systems, we performed multielectrode extracellular recordings in the motor cortex before, during, and following the episodic dystonia in *tg*/*tg* mice. To first examine for neuronal specific type specific changes, pyramidal cells and inhibitory interneurons were classified in WT mice using the established approaches detailed in the Methods (Figures 3D–F). Applying these classification criteria to the neurons recorded in *tg*/*tg* mice revealed 38 excitatory and 84 inhibitory neurons during baseline, 33 and 68 during the attack, and 36 and 52 during recovery. Due to the nature of the large dystonic movements, some cells were lost during the attack and into the recovery period. Importantly, neither the firing rate or CV_2 of either cell type in *tg*/*tg* mice significantly changed during the episodic dystonia. The lack of any electrophysiological changes not only confirms, but extends the 2P imaging results, and suggest a lack of motor cortical involvement in the dystonic attack.

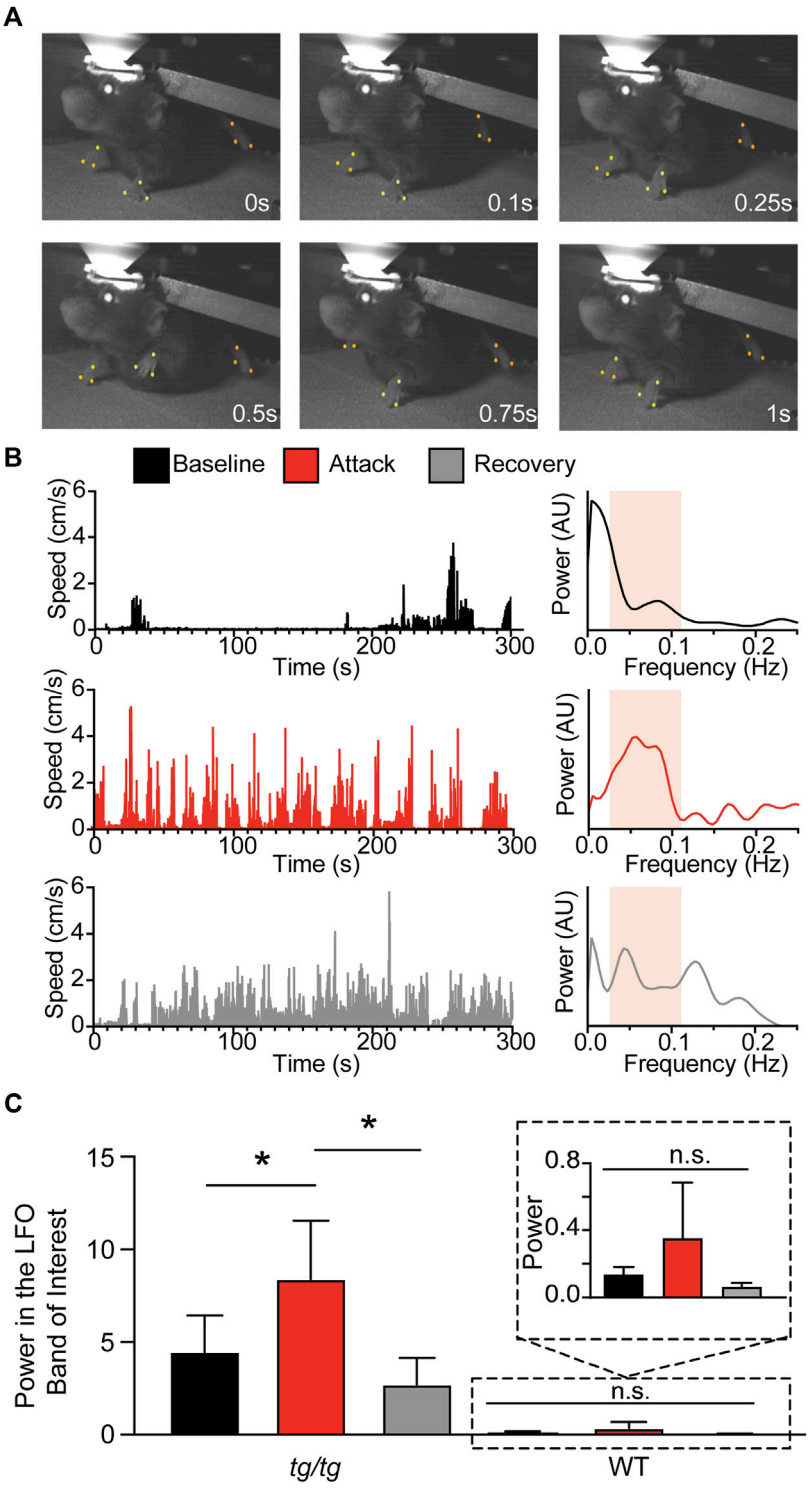

FIGURE 1
Presence of LFO in tg/tg limb kinematics during episodic dystonia. **(A)** Sample recording of a head-fixed *tg/tg* mouse with point tracking on right and left forelimbs and left hindlimb. **(B)** Speed analysis from the left hindlimb, calculated as the center of each paw from the three points indicated in ***A***, from baseline, during, and recovery from episodic dystonia. Spectral analysis from each time period shows an increase in the LFO band of interest (0.035–0.11 Hz) during the attack. Band of interest is denoted by the beige shaded area in the power spectrum plots. **(C)** Quantification of the power from the left hindlimb showing significantly increased power differences between baseline-attack and attack-recovery. Inset shows zoomed in view of power from WT mice. Data includes 6 episodic dystonia attacks from 5 *tg/tg* mice, and 4 sessions from 4 WT mice, all administered caffeine. Significant differences with large effect sizes indicated by a solid line.

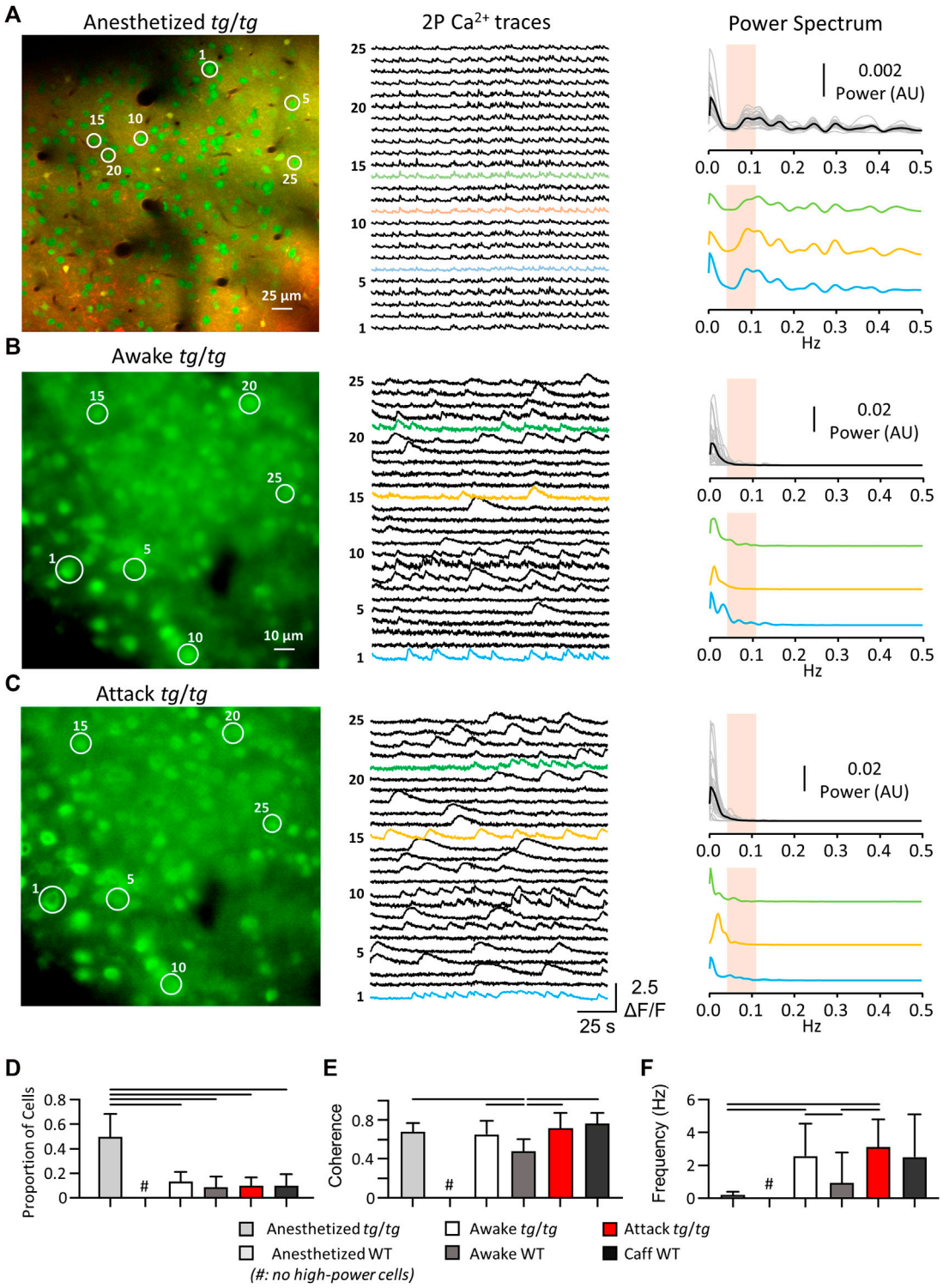

FIGURE 2
Single-cell Ca^{2+} activity reveals LFO present in *tg/tg* mice only under anesthesia. **(A)** Sample OGB-1/SR101 (green/red, respectively; overlap in yellow) recording from a *tg/tg* mouse under urethane anesthesia, with individual single-cell Ca^{2+} activity and spectral density plots (each cell power spectra in grey, mean in black) for the color-coded traces. **(B)** Sample GCaMP6f recordings and spectral plots from *tg/tg* motor cortex during awake, baseline behavior. **(C)** Sample GCaMP6f recording and spectral plots from the same mouse and cells as in ***B*** during an evoked episodic dystonia attack. Band of interest is denoted by the beige shaded area in the power spectrum plots in **(A–C)**. **(D)** Proportion of cells that experience the high-power state. **(E)** Changes in the largest magnitude-squared coherence between cells in different animals and states. **(F)** Quantification of the frequency at maximum coherence. For **(D,F)**, significant differences with large (solid line) effect sizes are shown. Data collected from 8 *tg/tg* (3 male, 5 female) and 5 WT (2 male, 3 female) mice for the anesthetized recordings, and 6 *tg/tg* (4 male, 2 female) and 4 WT (2 male, 2 female) mice for the awake recordings.

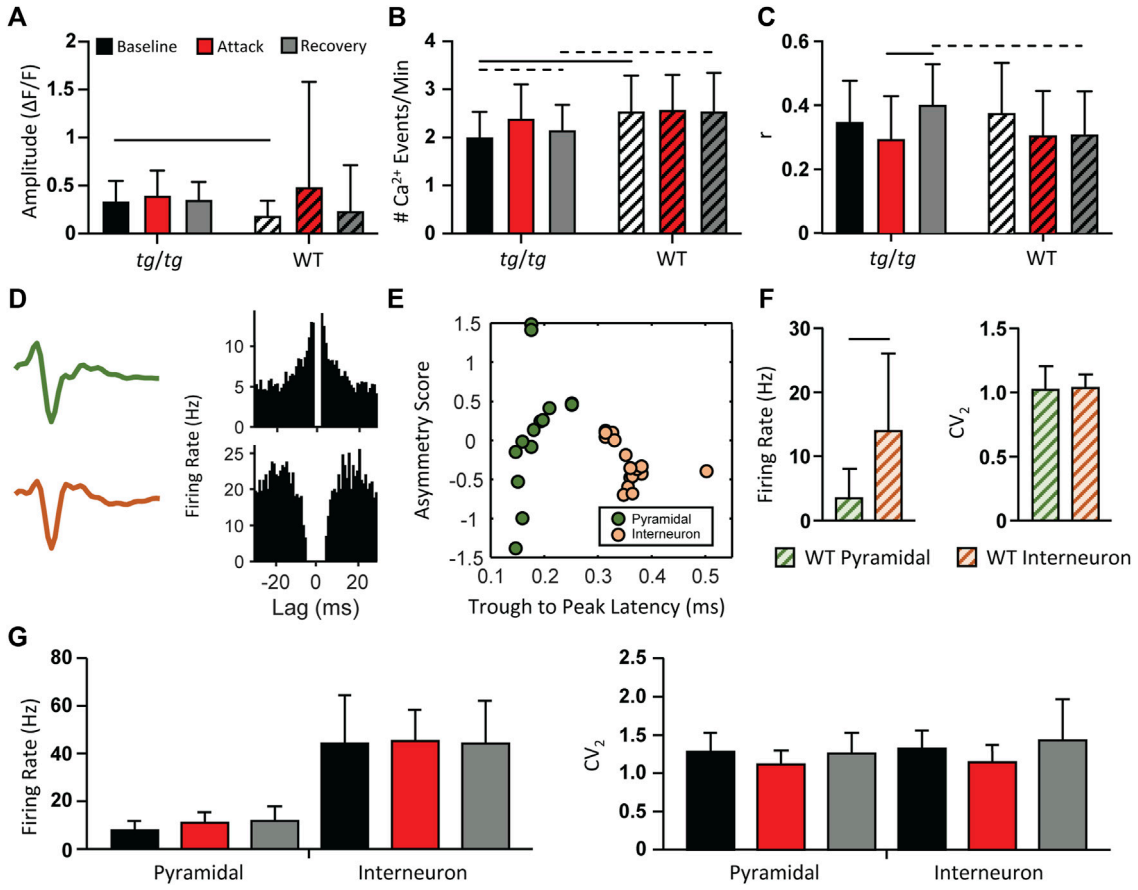

FIGURE 3
Minimal changes in *tg/tg* motor cortex single-cell Ca^{2+} and extracellular single-unit activity between baseline, attack, and recovery. **(A)** Quantification of ΔF/F GCaMP6f amplitude from caffeine injected *tg/tg* and WT mice. **(B)** Number of Ca^{2+} events per minute. **(C)** Average between-cell correlation (r) of ΔF/F activity. **(D)** Sample extracellular single-unit waveform and autocorrelogram of their firing rate from a putative pyramidal (green, top) and inhibitory (orange, bottom) cell in a WT mouse. **(E)** Visualization of metrics used for WT pyramidal and interneuron classification. **(F)** Quantification of firing rate and CV_2 differences between WT pyramidal and interneurons. **(G)** Firing rate (left) and CV_2 (right) quantification in *tg/tg* mice reveal no significant change in either parameter from pyramidal or interneurons between baseline, attack, or recovery. For **(A–C, F)**, significant differences with medium (dashed line) or large (solid line) effect sizes are shown. Data collected from 6 *tg/tg* (4 male, 2 female) and 4 WT (2 male, 2 female) mice for the awake Ca^{2+} recordings, and from 4 *tg/tg* (2 male, 2 female) and 4 WT (2 male, 2 female) mice for the awake electrophysiology recordings.

Spike triggered coupling to kinematics decreases during episodic dystonia

The lack of overt, dystonic-like changes in either the Ca^{2+} activity or the spike firing statistics of M1 neurons of the *tg/tg* mouse suggests that M1 may partially decouple from the downstream movements during the dystonic attack. To test this hypothesis, we performed a spike triggered behavior inspired approach in which for each neuron we aligned forelimb kinematics (Figure 4A, top) to the Ca^{2+} peaks (Figure 4A, bottom) during periods of movement and rest (Figure 4B). Cells that had limb speed during movement that was 3 standard deviations above the rest mean 100 ms on either side of Ca^{2+} peaks were considered 'movement cells' and assumed to encode limb behavior. This is illustrated for an example movement cell, showing that the Ca^{2+} peak was coupled to and led the limb speed (Figure 4B). The proportion of movement cells significantly decreased during the dystonic attack and significantly increased during the recovery period, but not quite returning to baseline levels (Figure 4C). Aligning the Ca^{2+} ΔF/F to movement onset revealed a strong relationship with Ca^{2+} activity to movement during the baseline period, that significantly decreased during the attack (Figures 4D,E) and recovered to baseline levels in the recovery period, suggesting that M1 partially decouples from behavioral output during the motor attack.

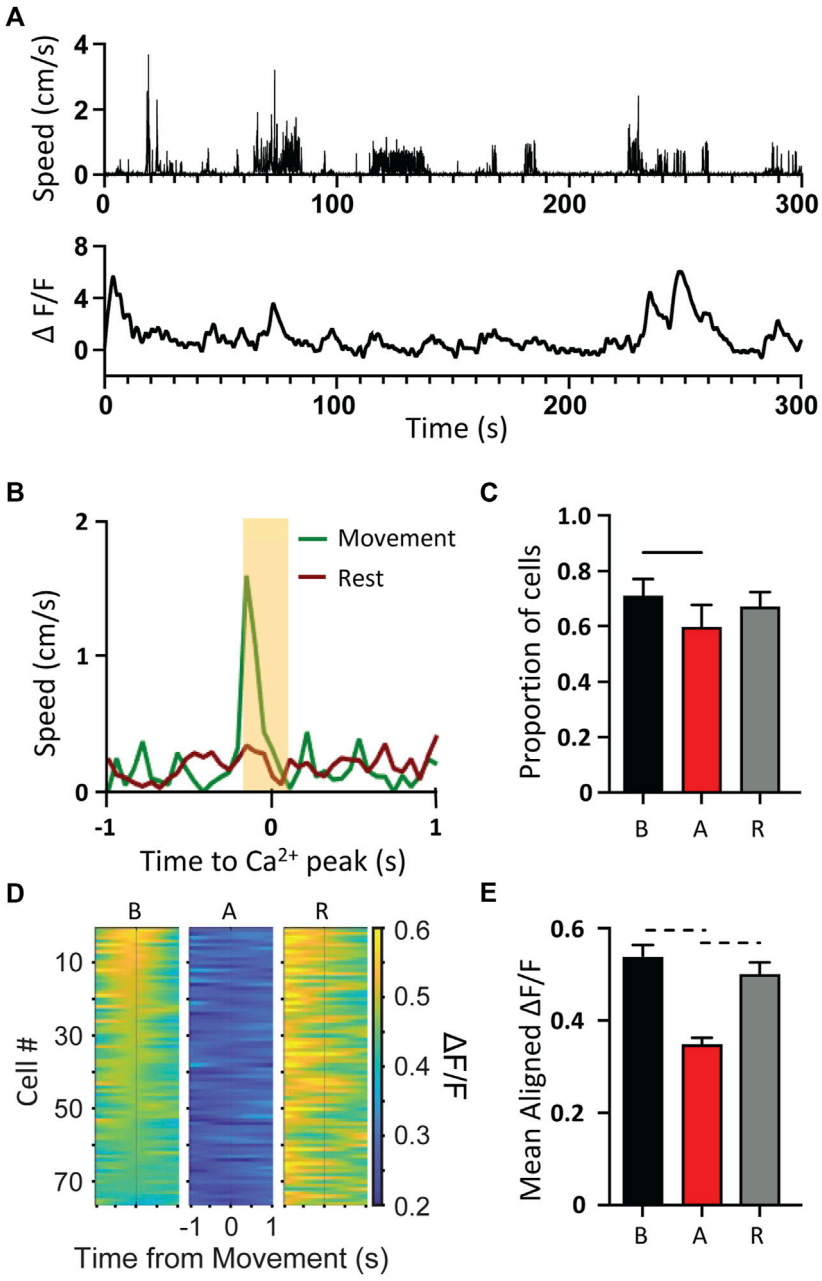

FIGURE 4
Decoupling of Ca^{2+} activity to movement kinematics during *tg/tg* attack. **(A)** Sample movement speed of forelimb (top) and 2P single-cell Ca^{2+} ΔF/F trace (bottom) from a *tg/tg* mouse during baseline conditions. **(B)** Example trace from classified "movement" cell. **(C)** Quantification of the proportion of movement cells from baseline to attack and recovery. **(D)** Movement onset aligned PSTH for left forelimb for representative session. **(E)** Quantification of average fluorescence 200 ms surrounding movement onset for all attacks. For **(C, E)**, significant differences with medium (dashed line) or large (solid line) effect sizes are shown. Data collected from 5 *tg/tg* (3 male, 2 female) mice.

Generalized spike-and-wave discharges are abolished during episodic dystonia

The *tg/tg* mice exhibit generalized spike-and-wave discharges (GSWDs) that are an underlying mechanism of absence seizures and one of the major phenotypes of the mutation in the *cacna1a* gene. However, the relationship between GSWDs and the episodic dystonia are not well understood. As the Ca^{2+} imaging shows that M1 is partially decoupled from behavior, we reasoned that the

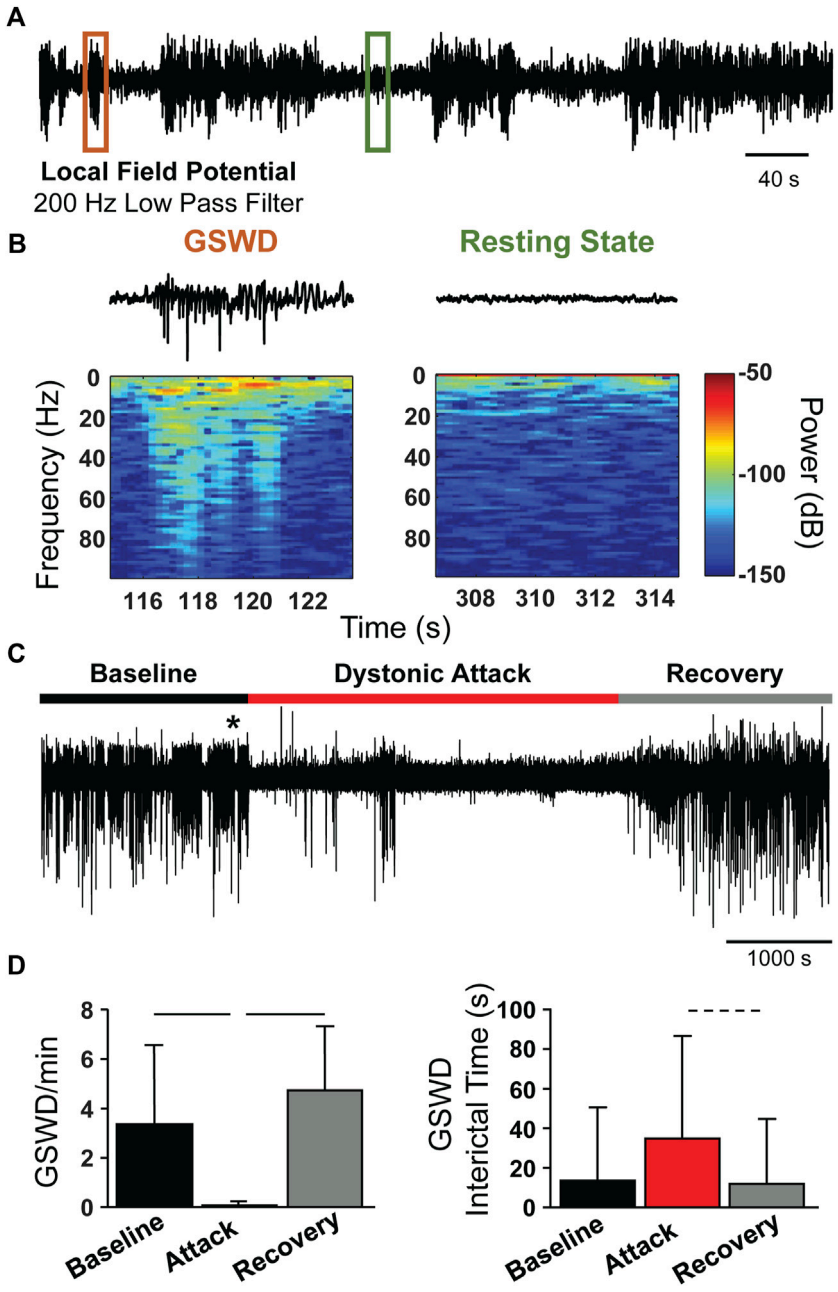

FIGURE 5
Loss of GSWDs during episodic dystonia attack in *tg/tg* mice. **(A)** Example motor cortex LFP trace from an awake *tg/tg* mouse. **(B)** Zoomed in views of the LFP trace from the color-coded regions in **(A)**, showing an example GSWD and resting period (top) and the corresponding spectral content (bottom). **(C)** Continuous motor cortex LFP recording from a *tg/tg* mouse during baseline, caffeine-evoked episodic dystonia attack, and recovery. * denotes time of caffeine injection. **(D)** Quantification of GSWD occurrence rate (left) and interictal time (right) during all recordings. Significant differences with medium (dashed line) or large (solid line) effect sizes are shown. Data collected from 4 *tg/tg* (2 male, 2 female) and 4 WT (2 male, 2 female) mice.

GSWDs in the cerebral cortex may be similarly affected. Therefore, we recorded the local field potentials (LFPs) from *tg/tg* mice and determined the presence and timing of GSWDs (Figure 5A) in relation to a dystonic attack. A GSWD event is characterized by the high amplitude deflections in the LFP trace and increased power (Figure 5B) compared to the resting state (no GSWDs present). During the dystonic attack, GSWDs were almost completely abolished. As shown for a representative LFP recording during the course of a caffeine-evoked episodic

dystonia attack, there are negligible GSWDs during the attack (Figure 5C), while prominent GSWDs occur during both the baseline and recovery periods.

Quantification of the average GSWD rate (per minute) during the baseline, attack, and recovery periods show a marked decrease in GSWD rate during the attack, compared to baseline and recovery periods (Figure 5D, left). Correspondingly, the GSWD interictal time significantly increased during the attack period (Figure 5D, right), but did not quite reach a medium effect size (Cohen's d = 0.47), likely due to the extremely small number of GSWD events during the attack. The loss of GSWDs, as well as the uncoupling of Ca^{2+} activity to movement kinematics, suggests that the episodic dystonic attack induces a different brain state in *tg*/*tg* mice.

Discussion

Our past work highlighting the presence of transient LFOs in the cerebral cortex of the anesthetized *tg*/*tg* mouse that are markedly reduced by ACTZ and 4-AP, two of the major treatments for EA2 (Cramer et al., 2015), lead us to hypothesize a central role for the these rather unique oscillations in the dystonic attack in this EA2 mouse model. Here we tested this hypothesis, using 2P Ca^{2+} imaging and electrophysiological recordings of single neurons, as well as LFPs, before, during, and following caffeine-triggered dystonic attacks.

Presence of LFOs in limb kinematics during dystonic attack

Further extending our hypothesis that brain LFOs are central to the dystonic attack in awake, behaving *tg*/*tg* mice, we observed that limbs movements are characterized by frequencies within the cortical LFO band of interest throughout the dystonic attack. This finding confirms earlier observations of EMG activity at these low frequencies (41). As a similar magnitude increase did not occur in WT mice, even when caffeine was administered, this change is likely attributable to the caffeine-triggered neural mechanisms that underlie the *tg*/*tg* attack, but not the caffeine itself. Given that neuronal firing in M1 has long been linked to limb kinematics [for reviews see (67, 68)], we hypothesized that the LFOs would be reflected in M1 activity during the motor attack in awake, behaving *tg*/*tg* mice.

Two-photon Ca^{2+} imaging during an episodic dystonic attack

Previous wide-field imaging studies using flavoprotein as a surrogate for neuronal activation observed the LFOs in cerebellum and cerebral cortex (41, 42). These studies were unable to attribute this activity to single cells or specific subtypes of cells/neurons. Here, we observed LFOs in the Ca^{2+} transients of individual layer II/III M1 neurons in the anesthetized *tg*/*tg* mouse. This cellular level activity exhibited high spectral coherence in the LFO band of interest, consistent with earlier, wide-field flavoprotein optical recordings of LFOs in the cerebral cortex (42). This confirms that LFOs are present at the single cell level in anesthetized *tg*/*tg* mice.

Surprisingly, we did not find evidence for LFOs in the Ca^{2+} fluorescence signals in M1 neurons in the awake *tg*/*tg* mouse, at rest or during a dystonic attack. In addition to assessing for the presence of LFOs, we evaluated changes in the number, amplitude, and correlation of Ca^{2+} transients in relation to a dystonic attack. No significant changes or effect sizes were observed in either the amplitude or number of Ca^{2+} events comparing baseline to the attack state, with only a medium effect size in the number of Ca^{2+} events between baseline and recovery, and a large effect size in the between-cell correlation from the attack to recovery. In our view, these changes in M1 neurons are not consistent with the magnitude of the abnormal limb movements in the LFO band of interest during the attack. Taken together, the 2P imaging results do not support our original hypothesis that LFOs in the activity of M1 neurons have a major role in the episodic dystonia in the *tg*/*tg* mouse.

LFP and single cell recordings during a dystonic attack

While we did not observe LFOs or large changes in the Ca^{2+} events in M1 neurons during the episodic dystonia, our 2P imaging was restricted to recording neurons in layers II/III. There is a possibility that layer V output neurons would exhibit large changes in firing that contribute to the motor attack. Therefore, we recorded ensembles of M1 neurons that spanned all cortical layers, sorted into excitatory and inhibitory classes based on discharge properties, and tested for changes in firing statistics. Notably, both classes of neurons showed no significant changes in firing statistics during the dystonic attack, further underscoring our interpretation of the Ca^{2+} data and highlighting a remarkable lack of activity changes in M1 neurons during the dystonic attack in *tg*/*tg* mice.

M1 activity decouples from limb kinematics during dystonic attack

Given a lack of pronounced firing and activity changes across M1 layers in *tg*/*tg* mice during the dystonic attack, despite very pronounced changes in limb kinematic patterns, we performed additional analysis to quantify the relationship of M1 activity to limb motor output before, during, and after the dystonic attack. Aligning either movement onset to identified Ca^{2+} peaks, or aligning

Ca^{2+} activity to identified movement onset revealed a significant decrease in the number of movement cells and Ca^{2+} activity surrounding movement onset during the attack, respectively. Taken together, these findings suggest that M1 activity decouples from movement output during the dystonic attack. This is consistent with EA2 patient reports that although they are conscious, the dystonic limb movements are involuntary (69). While the findings support a decoupling of the motor cortex from the motor output, we acknowledge that other explanations need to be considered. One possibility is that non-cortical structures are driving the dystonia, providing a powerful drive to the spinal cord and alpha motor neuron pools that overwhelms any descending inputs from M1. Another explanation is that afferent input to M1 is disrupted, not the output. Additional studies are needed to test the various possibilities.

Loss of GSWD during dystonic attack

We also investigated a second hallmark of the *tg*/*tg* phenotype, GSWD. During the attack period, we consistently observed a near complete loss of the GSWDs that returns to baseline-like levels during the recovery period. It is well established that the thalamo-cortical circuitry plays a critical role in both GSWD and absence seizures [for reviews see (70, 71)]. In the *tg*/*tg* mouse, cerebellar involvement with GSWDs has been shown by phase-locking of nuclear neuron firing and GSWDs in the cerebral cortex. Further, GSWD can be modulated by the cerebellum, as optogenetic inhibition of the cerebellar nuclei to the thalamus suppresses GSWDs (54, 72). When coupled with the present observations, GSWD loss during the episodic dystonia suggests that connectivity between the cerebellum and motor cortex, *via* the thalamus, is causally disrupted during the attack.

Distinct brain and behavioral states in the *tg*/*tg* mouse

The present results highlight disparate brain and behavior states within the *tg*/*tg* mouse model of EA2. Mice display a baseline behavioral state marked by GSWDs and absence seizures, mild ataxia, and coupling between M1 activity and limb behavior. Under anesthesia, LFOs are present throughout the dorsal cerebral cortex and the cerebellar cortex (41, 42). The attack state is marked by notable differences in behavior and brain activity. Behaviorally, animals are racked with strong dystonic limb movements that are characterized by LFOs. During a dystonic attack, the cerebellar cortex exhibits LFOs, while neuronal activity in M1 changes very little. Furthermore, the normally ubiquitous GSWDs are largely absent and M1 neuronal activity is significantly decoupled from motor output. Following the motor attack, mice return to the baseline behavioral state. Therefore, there are multiple brain states due to the mutation in the *cacna1a* gene in the mouse that underlie the behavioral phenotypes.

One of these brain states is the dramatic high-power LFOs in cerebral cortex of anesthetized *tg*/*tg* mice, but these cortical LFOs are not present in the awake animal or during the dystonic attack. These oscillations are consistent with observations that anesthesia induces highly correlated, brain-wide, low-frequency oscillations in the mouse (73, 74). As shown recently in wide-field Ca^{2+} imaging, these oscillations include waves of activity that spread across the dorsal cerebral cortex (74). In wild-type mice, the frequency of these oscillations ranges from 0.75 to 2 Hz, compared to the much lower frequencies observed in *tg*/*tg* mice. We speculate that the mutation in the P/Q-type Ca^{2+} channel shifts the excitability of neurons in the cerebral cortex to synchronize at these very low frequencies, the same frequencies observed in the limb movements.

The second brain state is the loss of both GSWDs and decoupling of M1 from the limb movements during the dystonic attack. However, during the attack, LFOs are present in the cerebellar cortex and increase in coherence with the limb EMG activity (41). Therefore, the cerebral cortex and cerebellum have fundamentally different excitatory states, and therefore roles, during the episodic dystonia. In the cerebellar cortex, the synchronization and propagation of the LFOs occur over 30–120 min (41), similar to the duration of the episodic dystonia (29, 31, 53). We have hypothesized that the oscillations in Purkinje cell output will be transmitted downstream to the cerebellar nuclei and their targets in the brainstem that project to the spinal cord (Campbell and Hess, 1998), potentially supplying a powerful input to muscles that is expressed as the episodic dystonia. As described above, the loss of GSWDs upstream in the cerebral cortex may also be due to the abnormal cerebellar output. A major remaining question is whether the lack of LFOs in the cerebral cortex and decoupling from the dystonic movements actually facilitates the abnormal movements by allowing the cerebellar output to modulate downstream pathways without interference from descending cerebral cortical activity.

Support has increased for cerebellar involvement in several dystonias [for reviews see (45, 46)] and would be the focus of future investigations. We would determine if the LFOs in the cerebellar cortex are driving the episodic dystonia, by testing whether blocking cerebellar cortical LFOs stopped an ongoing motor attack. A complementary test would be to determine if initiating LFOs in the cerebellar cortex generates an attack. It would be important to test if the two main treatments for EA2, 4-AP and ACTZ, when applied to the cerebellum block the LFOs and control the attacks. Further investigations would assess how the different classes of neurons in the cerebellum are modulated during an attack, as well as the involvement of mossy fiber inputs and climbing fiber input from the inferior olive. Also, probing cerebellar output pathways during the episodic dystonia, including the cerebellar nuclei and their brainstem targets, would be important to understand how the LFOs are propagated. If

cerebellar LFOs could be firmly established as the origin of the motor attacks, this would suggest future therapeutic targets.

Regardless of the mechanism that provided the switch between baseline and attack states, this work establishes a new role for M1 in the generation of the dystonic attack in *tg*/*tg* mice. Future interventions to correct the *tg*/*tg* dystonic phenotype (and perhaps EA2 itself) may hinge upon preventing the emergence of the 'attack' brain phenotype that includes decoupling of M1 from the motor output.

Data availability statement

The raw data supporting the conclusion of this article will be made available by the authors, without undue reservation.

Ethics statement

The animal study was reviewed and approved by Institutional Animal Care and Use Committee of the University of Minnesota.

Author contributions

MG, RC, and TE designed the calcium imaging studies. AN, RC, and TE designed the electrophysiology studies. RC performed anesthetized Ca^{2+} imaging studies. MG performed awake Ca^{2+} imaging studies. AN and RC performed electrophysiology studies. MG analyzed the Ca^{2+} data. AN analyzed the electrophysiology data. MG, AN, RC, and TE wrote the manuscript.

Funding

This work was supported in part by NH grant NS18338 to TE and from the Max E. and Mary LaDue Pickworth Endowed Chair in Neuroscience to TE. This work was supported by the resources and staff at the University of Minnesota University Imaging Centers (UIC) SCR_020997.

Conflict of interest

The authors declare that the research was conducted in the absence of any commercial or financial relationships that could be construed as a potential conflict of interest.

References

1. Balint B, Mencacci NE, Valente EM, Pisani A, Rothwell J, Jankovic J, et al. *Dystonia Nat Rev Dis Primers* (2018) 4(1):25. doi:10.1038/s41572-018-0023-6

2. Grütz K, Klein C. Dystonia updates: Definition, nomenclature, clinical classification, and etiology. *J Neural Transm (Vienna)* (2021) 128(4):395–404. doi:10.1007/s00702-021-02314-2

3. Barbosa P, Warner TT. Dystonia, *Handb Clin Neurol* (2018) 159:229–36. doi:10.1016/B978-0-444-63916-5.00014-8

4. Albanese A, Bhatia K, Bressman SB, Delong MR, Fahn S, Fung VS, et al. Phenomenology and classification of dystonia: A consensus update. *Mov Disord* (2013) 28(7):863–73. doi:10.1002/mds.25475

5. Nutt JG, Muenter MD, Aronson A, Kurland LT, Melton LJ. Epidemiology of focal and generalized dystonia in Rochester, Minnesota. *Mov Disord* (1988) 3(3): 188–94. doi:10.1002/mds.870030302

6. Epidemiological Study of Dystonia in Europe (ESDE) Collaborative Group. A prevalence study of primary dystonia in eight European countries. *J Neurol* (2000) 247(10):787–92. doi:10.1007/s004150070094

7. Medina A, Nilles C, Martino D, Pelletier C, Pringsheim T. The prevalence of idiopathic or inherited isolated dystonia: A systematic review and meta-analysis. *Mov Disord Clin Pract* (2022) 9(7):860–8. doi:10.1002/mdc3.13524

8. Cao L, Huang X, Wang N, Wu Z, Zhang C, Gu W, et al. Recommendations for the diagnosis and treatment of paroxysmal kinesigenic dyskinesia: An expert consensus in China. *Transl Neurodegener* (2021) 10(1):7. doi:10.1186/s40035-021-00231-8

9. De Giorgis V, Veggiotti P. GLUT1 deficiency syndrome 2013: Current state of the art. *Seizure* (2013) 22(10):803–11. doi:10.1016/j.seizure.2013.07.003

10. Brashear A, Dobyns WB, de Carvalho Aguiar P, Borg M, Frijns CJ, Gollamudi S, et al. The phenotypic spectrum of rapid-onset dystonia-parkinsonism (RDP) and mutations in the ATP1A3 gene. *Brain* (2007) 130(3):828–35. doi:10.1093/brain/awl340

11. Jen J, Kim GW, Baloh RW. Clinical spectrum of episodic ataxia type 2. *Neurology* (2004) 62(1):17–22. doi:10.1212/01.wnl.0000101675.61074.50

12. Ptacek LJ, Fu YH. Channelopathies: Episodic disorders of the nervous system. *Epilepsia* (2001) 42(5):35–43. doi:10.1046/j.1528-1157.2001.0420s5035.x

13. Pietrobon D, Ca V. CaV2.1 channelopathies. *Pflugers Arch* (2010) 460(2): 375–93. doi:10.1007/s00424-010-0802-8

14. Kullmann DM. The neuronal channelopathies. *Brain* (2002) 125(6):1177–95. doi:10.1093/brain/awf130

15. Ryan DP, Ptacek LJ. Episodic neurological channelopathies. *Neuron* (2010) 68(2):282–92. doi:10.1016/j.neuron.2010.10.008

16. Jen JC, Graves TD, Hess EJ, Hanna MG, Griggs RC, Baloh RW, et al. Primary episodic ataxias: Diagnosis, pathogenesis and treatment. *Brain* (2007) 130(10): 2484–93. doi:10.1093/brain/awm126

17. Baloh RW, Yue Q, Furman JM, Nelson SF. Familial episodic ataxia: Clinical heterogeneity in four families linked to chromosome 19p. *AnnNeurol* (1997) 41(1): 8–16. doi:10.1002/ana.410410105

18. Rajakulendran S, Schorge S, Kullmann DM, Hanna MG. Dysfunction of the Ca(V)2.1 calcium channel in cerebellar ataxias. *F1000 Biol Rep* (2010) 2:4. doi:10.3410/B2-4

19. Ophoff RA, Terwindt GM, Vergouwe MN, van Eijk R, Oefner PJ, Hoffman SM, et al. Familial hemiplegic migraine and episodic ataxia type-2 are caused by mutations in the Ca 2+ channel gene CACNL1A4. *Cell* (1996) 87:543–52. doi:10.1016/s0092-8674(00)81373-2

20. Kramer PL, Yue Q, Gancher ST, Nutt JG, Baloh R, Smith E, et al. A locus for the nystagmus-associated form of episodic ataxia maps to an 11-cM region on chromosome 19p. *AmJ HumGenet* (1995) 57(1):182–5.

21. Rajakulendran S, Kaski D, Hanna MG. Neuronal P/Q-type calcium channel dysfunction in inherited disorders of the CNS. *NatRevNeurol* (2012) 8(2):86–96. doi:10.1038/nrneurol.2011.228

22. Denier C, Ducros A, Vahedi K, Joutel A, Thierry P, Ritz A, et al. High prevalence of CACNA1A truncations and broader clinical spectrum in episodic ataxia type 2. *Neurology* (1999) 52(9):1816–21. doi:10.1212/wnl.52.9.1816

23. Jouvenceau A, Eunson LH, Spauschus A, Ramesh V, Zuberi SM, Kullmann DM, et al. Human epilepsy associated with dysfunction of the brain P/Q-type calcium channel. *Lancet* (2001) 358(9284):801–7. doi:10.1016/S0140-6736(01)05971-2

24. Ducros A, Denier C, Joutel A, Cecillon M, Lescoat C, Vahedi K, et al. The clinical spectrum of familial hemiplegic migraine associated with mutations in a neuronal calcium channel. *Nenglj Med* (2001) 345(1):17–24. doi:10.1056/NEJM200107053450103

25. Spacey SD, Materek LA, Szczygielski BI, Bird TD. Two novel CACNA1A gene mutations associated with episodic ataxia type 2 and interictal dystonia. *Arch Neurol* (2005) 62(2):314–6. doi:10.1001/archneur.62.2.314

26. Kinder S, Ossig C, Wienecke M, Beyer A, von der Hagen M, Storch A, et al. Novel frameshift mutation in the CACNA1A gene causing a mixed phenotype of episodic ataxia and familiar hemiplegic migraine. *Eur J Paediatr Neurol* (2015) 19(1):72–4. doi:10.1016/j.ejpn.2014.10.005

27. Fletcher CF, Lutz CM, O'Sullivan TN, Shaughnessy JD, Jr., Hawkes R, Frankel WN, et al. Absence epilepsy in tottering mutant mice is associated with calcium channel defects. *Cell* (1996) 87(4):607–17. doi:10.1016/s0092-8674(00)81381-1

28. Heller AH, Dichter MA, Sidman RL. Anticonvulsant sensitivity of absence seizures in the tottering mutant mouse. *Epilepsia* (1983) 24(1):25–34. doi:10.1111/j.1528-1157.1983.tb04862.x

29. Noebels JL, Sidman RL. Inherited epilepsy: Spike-wave and focal motor seizures in the mutant mouse tottering. *Science* (1979) 204(4399):1334–6. doi:10.1126/science.572084

30. Song I, Kim D, Choi S, Sun M, Kim Y, Shin HS. Role of the alpha1G T-type calcium channel in spontaneous absence seizures in mutant mice. *J Neurosci* (2004) 24(22):5249–57. doi:10.1523/JNEUROSCI.5546-03.2004

31. Green MC, Sidman RL. Tottering--a neuromusclar mutation in the mouse. And its linkage with oligosyndacylism. *J Hered* (1962) 53:233–7. doi:10.1093/oxfordjournals.jhered.a107180

32. Meier H, MacPike AD. Three syndromes produced by two mutant genes in the mouse. Clinical, pathological, and ultrastructural bases of tottering, leaner, and heterozygous mice. *J Hered* (1971) 62(5):297–302. doi:10.1093/oxfordjournals.jhered.a108176

33. Seyfried TN, Glaser GH. A review of mouse mutants as genetic models of epilepsy. *Epilepsia* (1985) 26(2):143–50. doi:10.1111/j.1528-1157.1985.tb05398.x

34. Scholle HC, Jinnah HA, Arnold D, Biedermann FH, Faenger B, Grassme R, et al. Kinematic and electromyographic tools for characterizing movement disorders in mice. *Mov Disord* (2010) 25(3):265–74. doi:10.1002/mds.22933

35. Fureman BE, Jinnah HA, Hess EJ. Triggers of paroxysmal dyskinesia in the calcium channel mouse mutant tottering. *PharmacolBiochemBehav* (2002) 73(3):631–7. doi:10.1016/s0091-3057(02)00854-7

36. Campbell DB, Hess EJ. Cerebellar circuitry is activated during convulsive episodes in the tottering (tg/tg) mutant mouse. *Neuroscience* (1998) 85(3):773–83. doi:10.1016/s0306-4522(97)00672-6

37. Campbell DB, Hess EJ. L-type calcium channels contribute to the tottering mouse dystonic episodes. *Mol Pharmacol* (1999) 55(1):23–31. doi:10.1124/mol.55.1.23

38. Campbell DB, North JB, Hess EJ. Tottering mouse motor dysfunction is abolished on the Purkinje cell degeneration (pcd) mutant background. *Exp Neurol* (1999) 160(1):268–78. doi:10.1006/exnr.1999.7171

39. Abbott LC, Isaacs KR, Heckroth JA. Co-localization of tyrosine hydroxylase and zebrin II immunoreactivities in Purkinje cells of the mutant mice, tottering and tottering/leaner. *Neuroscience* (1996) 71(2):461–75. doi:10.1016/0306-4522(95)00444-0

40. Neychev VK, Fan X, Mitev VI, Hess EJ, Jinnah HA. The basal ganglia and cerebellum interact in the expression of dystonic movement. *Brain* (2008) 131(9):2499–509. doi:10.1093/brain/awn168

41. Chen G, Popa LS, Wang X, Gao W, Barnes J, Hendrix CM, et al. Low frequency oscillations in the cerebellar cortex of the tottering mouse. *J Neurophysiol* (2009) 101:234–45. doi:10.1152/jn.90829.2008

42. Cramer SW, Popa LS, Carter RE, Chen G, Ebner TJ. Abnormal excitability and episodic low-frequency oscillations in the cerebral cortex of the tottering mouse. *J Neurosci* (2015) 35(14):5664–79. doi:10.1523/JNEUROSCI.3107-14.2015

43. Strupp M, Kalla R, Claassen J, Adrion C, Mansmann U, Klopstock T, et al. A randomized trial of 4-aminopyridine in EA2 and related familial episodic ataxias. *Neurology* (2011) 77(3):269–75. doi:10.1212/WNL.0b013e318225ab07

44. Strupp M, Kalla R, Dichgans M, Freilinger T, Glasauer S, Brandt T. Treatment of episodic ataxia type 2 with the potassium channel blocker 4-aminopyridine. *Neurology* (2004) 62(9):1623–5. doi:10.1212/01.wnl.0000125691.74109.53

45. Jinnah HA, Sun YV. Dystonia genes and their biological pathways. *Neurobiol Dis* (2019) 129:159–68. doi:10.1016/j.nbd.2019.05.014

46. Shakkottai VG, Batla A, Bhatia K, Dauer WT, Dresel C, Niethammer M, et al. Current opinions and areas of consensus on the role of the cerebellum in dystonia. *Cerebellum* (2017) 16(2):577–94. doi:10.1007/s12311-016-0825-6

47. Ghanbari L, Carter RE, Rynes ML, Dominguez J, Chen G, Naik A, et al. Cortex-wide neural interfacing via transparent polymer skulls. *Nat Commun* (2019) 10(1):1500. doi:10.1038/s41467-019-09488-0

48. Akerboom J, Chen TW, Wardill TJ, Tian L, Marvin JS, Mutlu S, et al. Optimization of a GCaMP calcium indicator for neural activity imaging. *JNeurosci* (2012) 32(40):13819–40. doi:10.1523/JNEUROSCI.2601-12.2012

49. Dubbs A, Guevara J, Yuste R. moco: Fast motion correction for calcium imaging. *Front Neuroinform* (2016) 10:6. doi:10.3389/fninf.2016.00006

50. Wilson DE, Smith GB, Jacob AL, Walker T, Dimidschstein J, Fishell G, et al. GABAergic neurons in ferret visual cortex participate in functionally specific networks. *Neuron* (2017) 93(5):1058–65. doi:10.1016/j.neuron.2017.02.035

51. Tischbirek C, Birkner A, Jia H, Sakmann B, Konnerth A. Deep two-photon brain imaging with a red-shifted fluorometric Ca2+ indicator. *Proc Natl Acad Sci U S A* (2015) 112(36):11377–82. doi:10.1073/pnas.1514209112

52. Mathis A, Mamidanna P, Cury KM, Abe T, Murthy VN, Mathis MW, et al. DeepLabCut: Markerless pose estimation of user-defined body parts with deep learning. *Nat Neurosci* (2018) 21(9):1281–9. doi:10.1038/s41593-018-0209-y

53. Carter RE, Ebner TJ. The tottering mouse. In: DL Gruol, N Koibuchi, M Manto, M Molinari, JD Schmahmann, Y Shen, editors. *Essentials of cerebellum and cerebellar disorders: A primer for graduate students*. Cham: Springer International Publishing (2016). p. 437–42.

54. Kros L, Eelkman Rooda OH, Spanke JK, Alva P, van Dongen MN, Karapatis A, et al. Cerebellar output controls generalized spike-and-wave discharge occurrence. *Ann Neurol* (2015) 77(6):1027–49. doi:10.1002/ana.24399

55. Quiroga RQ, Garcia H, Rabinowicz A. Frequency evolution during tonic-clonic seizures. *Electromyogr Clin Neurophysiol* (2002) 42(6):323–31.

56. Quiroga RQ, Nadasdy Z, Ben-Shaul Y. Unsupervised spike detection and sorting with wavelets and superparamagnetic clustering. *Neural Comput* (2004) 16(8):1661–87. doi:10.1162/089976604774201631

57. Keshtkaran MR, Yang Z. Noise-robust unsupervised spike sorting based on discriminative subspace learning with outlier handling. *J Neural Eng* (2017) 14(3):036003. doi:10.1088/1741-2552/aa6089

58. Keshtkaran MR, Yang Z. Unsupervised spike sorting based on discriminative subspace learning. *Annu Int Conf IEEE Eng Med Biol Soc* (2014) 2014:3784–8. doi:10.1109/EMBC.2014.6944447

59. Yang Z, Zhao Q, Liu W. Improving spike separation using waveform derivatives. *J Neural Eng* (2009) 6(4):046006. doi:10.1088/1741-2560/6/4/046006

60. Gold C, Henze DA, Koch C, Buzsáki G. On the origin of the extracellular action potential waveform: A modeling study. *J Neurophysiol* (2006) 95(5):3113–28. doi:10.1152/jn.00979.2005

61. Maaten LvdH G. Visualizing data using t-SNE. *J Machine Learn Res* (2008)(9) 26.

62. Kawaguchi Y Distinct firing patterns of neuronal subtypes in cortical synchronized activities. *J Neurosci* (2001) 21(18):7261–72. doi:10.1523/JNEUROSCI.21-18-07261.2001

63. Senzai Y, Fernandez-Ruiz A, Buzsáki G. Layer-specific physiological features and interlaminar interactions in the primary visual cortex of the mouse. *Neuron* (2019) 101(3):500–13. doi:10.1016/j.neuron.2018.12.009

64. Petersen PC, Siegle JH, Steinmetz NA, Mahallati S, Buzsáki G. CellExplorer: A framework for visualizing and characterizing single neurons. *Neuron* (2021) 109(22):3594–608.e2. doi:10.1016/j.neuron.2021.09.002

65. Graf M, Nair A, Wong KLL, Tang Y, Augustine GJ. Identification of mouse claustral neuron types based on their intrinsic electrical properties. *eNeuro* (2020) 7(4):0216. doi:10.1523/ENEURO.0216-20.2020

66. Holt GR, Softky WR, Koch C, Douglas RJ. Comparison of discharge variability *in vitro* and *in vivo* in cat visual cortex neurons. *J Neurophysiol* (1996) 75(5):1806–14. doi:10.1152/jn.1996.75.5.1806

67. Johnson MT, Ebner TJ. Processing of multiple kinematic signals in the cerebellum and motor cortices. *Brain Res Brain Res Rev* (2000) 33(2-3):155–68. doi:10.1016/s0165-0173(00)00027-8

68. Georgopoulos AP, Carpenter AF. Coding of movements in the motor cortex. *Curr Opin Neurobiol* (2015) 33:34–9. doi:10.1016/j.conb.2015.01.012

69. Thompson VB, Jinnah HA, Hess EJ. Convergent mechanisms in etiologically-diverse dystonias. *Expert Opin Ther Targets* (2011) 15(12):1387–403. doi:10.1517/14728222.2011.641533

70. Kostopoulos GK. Involvement of the thalamocortical system in epileptic loss of consciousness. *Epilepsia* (2001) 42(3):13–9. doi:10.1046/j.1528-1157.2001.042suppl.3013.x

71. Fogerson PM, Huguenard JR. Tapping the brakes: Cellular and synaptic mechanisms that regulate thalamic oscillations. *Neuron* (2016) 92(4):687–704. doi:10.1016/j.neuron.2016.10.024

72. Eelkman Rooda OHJ, Kros L, Faneyte SJ, Holland PJ, Gornati SV, Poelman HJ, et al. Single-pulse stimulation of cerebellar nuclei stops epileptic thalamic activity. *Brain Stimul* (2021) 14(4):861–72. doi:10.1016/j.brs.2021.05.002

73. Fontanini A, Spano P, Bower JM. Ketamine-xylazine-induced slow (<1.5 Hz) oscillations in the rat piriform (olfactory) cortex are functionally correlated with respiration. *J Neurosci* (2003) 23(22):7993–8001. doi:10.1523/JNEUROSCI.23-22-07993.2003

74. Donaldson PD, Navabi ZS, Carter RE, Fausner SML, Ghanbari L, Ebner TJ, et al. Polymer skulls with integrated transparent electrode arrays for cortex-wide opto-electrophysiological recordings. *Adv Healthc Mater* (2022) 11(18):e2200626. doi:10.1002/adhm.202200626

DYSTONIA

TYPE Original Research
PUBLISHED 24 August 2023
DOI 10.3389/dyst.2023.11487

OPEN ACCESS

EDITED BY
Aasef Shaikh,
Case Western Reserve University,
United States

*CORRESPONDENCE
Roy V. Sillitoe,
sillitoe@bcm.edu

RECEIVED 17 April 2023
ACCEPTED 11 August 2023
PUBLISHED 24 August 2023

CITATION
Salazar Leon LE and Sillitoe RV (2023), Disrupted sleep in dystonia depends on cerebellar function but not motor symptoms in mice.
Dystonia 2:11487.
doi: 10.3389/dyst.2023.11487

Disrupted sleep in dystonia depends on cerebellar function but not motor symptoms in mice

Luis E. Salazar Leon[1,2,3] and Roy V. Sillitoe[1,2,3,4,5]*

[1]Department of Neuroscience, Baylor College of Medicine, Houston, TX, United States, [2]Department of Pathology & Immunology, Baylor College of Medicine, Houston, TX, United States, [3]Jan and Dan Duncan Neurological Research Institute at Texas Children's Hospital, Houston, TX, United States, [4]Department of Pediatrics, Baylor College of Medicine, Houston, TX, United States, [5]Development, Disease Models & Therapeutics Graduate Program, Baylor College of Medicine, Houston, TX, United States

Although dystonia is the third most common movement disorder, patients often also experience debilitating nonmotor defects including impaired sleep. The cerebellum is a central component of a "dystonia network" that plays various roles in sleep regulation. Importantly, the primary driver of sleep impairments in dystonia remains poorly understood. The cerebellum, along with other nodes in the motor circuit, could disrupt sleep. However, it is unclear how the cerebellum might alter sleep and mobility. To disentangle the impact of cerebellar dysfunction on motion and sleep, we generated two mouse genetic models of dystonia that have overlapping cerebellar circuit miswiring but show differing motor phenotype severity: *Ptf1a*^{Cre};*Vglut2*$^{fx/fx}$ and *Pdx1*^{Cre};*Vglut2*$^{fx/fx}$ mice. In both models, excitatory climbing fiber to Purkinje cell neurotransmission is blocked, but only the *Ptf1a*^{Cre};*Vglut2*$^{fx/fx}$ mice have severe twisting. Using *in vivo* ECoG and EMG recordings we found that both mutants spend greater time awake and in NREM sleep at the expense of REM sleep. The increase in awake time is driven by longer awake bouts rather than an increase in bout number. We also found a longer latency to reach REM in both mutants, which is similar to what is reported in human dystonia. We uncovered independent but parallel roles for cerebellar circuit dysfunction and motor defects in promoting sleep quality versus posture impairments in dystonia.

KEYWORDS

dystonia, sleep, circadian rhythms, Purkinje cells, cerebellar nuclei

Introduction

Dystonia presents with phenotypic and etiologic heterogeneity. Considered the third most common movement disorder, "dystonia" does not comprise a single disease or symptom, but rather describes an array of disorders sharing overlapping behavioral outcomes. While different forms of dystonia express unique etiologies, substantial evidence implicates the cerebellum as a major node in the underlying network disruptions [1–4]. Dysfunction of Purkinje cells and the cerebellar nuclei, the primary outputs of the cerebellar cortex and cerebellum, respectively, are implicated in both

hereditary and idiopathic forms of dystonia [4–7]. Importantly, while cerebellar dysfunction is sufficient to induce dystonia in animal models, therapies addressing cerebellar dysfunction can modulate dystonia and reduce motor symptom severity. One such therapy, cerebellar deep brain stimulation (DBS), has been used to effectively reduce motor symptom severity in both mouse models [4] and human patients [8, 9], further suggesting a critical cerebellar involvement in the etiology of dystonia. However, nonmotor behaviors are also relevant to the cerebellum and to dystonia.

Along with its known role in regulating motor function, increasing evidence shows that the cerebellum also serves as a key brain region in the control of a variety of nonmotor behaviors such as cognitive and emotional processing [10], associative learning [11], and reward expectation [11, 12]. Recent work also suggests that the cerebellum may play a role in sleep-related behaviors. Purkinje cells and cerebellar nuclei neurons have been found to display sleep-dependent activity, increasing their firing during NREM (non-rapid eye movement) sleep [13–16]. In addition, lesioning of the cerebellar vermis has been shown to impair sleep, suggesting that normal cerebellar circuitry and activity are important for maintaining sleep rhythms [17, 18]. Numerous studies have shown that cerebellar disruptions form the basis for the many comorbidities of motor disorders [19–22]. However, the role of the cerebellum and its circuit components in sleep regulation have not been studied thoroughly in dystonia. It is known that dystonic patients demonstrate increased sleep latency and REM (rapid eye movement) latency, and in some cases, persistent involuntary muscle contractions during sleep [23–25]. It is also noted that therapeutics which successfully alleviate the motor symptoms of dystonia appear to have little to no effect on the sleep disruptions [26]. The importance of addressing sleep dysfunction is becoming increasingly apparent in society, as sleep disruptions can significantly impact quality of life, driving many subsequent comorbidities [27, 28]. Disrupted sleep is also associated with impaired motor learning/function [29–31], as synaptic activity is normalized during sleep [32]. Together, the mounting evidence inspires a compelling model in which sleep and motor dysfunction in dystonia comprise two halves of a self-propelling cycle. It is possible that cerebellar dysfunction drives both the more commonly appreciated motor abnormalities and the nonmotor sleep disruptions, although how they emerge needs to be systematically resolved.

It remains unclear whether dystonic motor dysfunctions persist during all stages of sleep, and consistently across different manifestations of the disease; recent evidence from a survey of cervical dystonia patients suggests that, in cases of idiopathic cervical dystonia, it does [24]. The lack of clarity on which factors (motor dysfunction and/or cerebellar dysfunction) drive sleep dysfunction in dystonia highlights the significance of this knowledge gap. To investigate the relationship between cerebellar dysfunction, motor dysfunction, and sleep, here we used a constitutively active Cre/*lox*-p system to drive the deletion of the *Vglut2* gene in afferent neurons that project excitatory fibers that ultimately communicate with the Purkinje cells. *Vglut2* was deleted using the *Ptf1a* and *Pdx1* gene regulatory elements to spatially drive Cre expression: the resulting mice had the genotypes $Ptf1a^{Cre};Vglut2^{fx/fx}$ and $Pdx1^{Cre};Vglut2^{fx/fx}$. The *Ptf1a* and *Pdx1* genes are expressed in the excitatory neurons of the inferior olive, a region of the brainstem, which projects afferent fibers to the cerebellar cortex and terminate as excitatory climbing fibers [4, 33]. However, *Ptf1a* expression occurs in a wider distribution across the inferior olive relative to *Pdx1*, and *Pdx1* is also expressed in mossy fiber afferent neurons (Lackey et al., 2023 *in preparation*). Therefore, the silencing of excitatory climbing fiber synapses occurs with differential coverage in mice with *Ptf1a*- versus *Pdx1*-driven Cre expression. Only $Ptf1a^{Cre};Vglut2^{fx/fx}$ mice present with severe motor dysfunction involving twisting of the torso and hyperextensions of the back and limbs [4], while $Pdx1^{Cre};Vglut2^{fx/fx}$ adult mice show only subtle dystonic behaviors [34]. Thus, the use of both mouse models allows us to deliberately silence excitatory olivocerebellar synapses while also providing us with an opportunity to query varying severities of cerebellar dysfunction.

In this work, we report that, despite their different dystonia-related motor severities, $Pdx1^{Cre};Vglut2^{fx/fx}$ and $Ptf1a^{Cre};Vglut2^{fx/fx}$ mice display similarly impaired sleep physiology and circadian rhythms. Both mutants display highly disrupted sleep, spending greater time awake and in NREM sleep at the expense of REM sleep. Furthermore, we found that both the $Pdx1^{Cre};Vglut2^{fx/fx}$ and $Ptf1a^{Cre};Vglut2^{fx/fx}$ mutant mice display increased latency to reach REM, which is similar to what is observed in human patients with dystonia [23]. Intriguingly, only mice with overt dystonic motor behaviors ($Ptf1a^{Cre};Vglut2^{fx/fx}$) show differences in ECoG spectral power frequency, particularly in the latter half of the time spent asleep. We also found that circadian activity rhythms remain unchanged across all groups of mice, and that the circadian "master clock" remains ostensibly unaffected by our circuit manipulation. Our work demonstrates that aberrant cerebellar activity dually disrupts motor function and sleep, paving the way for improved future therapeutics that may be able to simultaneously address both motor and sleep dysfunction in the context of motor disease.

Methods

Animals

All mice used in this study were housed in a Level 3, AALAS-certified facility. All experiments and studies that involved mice were reviewed and approved by the Institutional Animal Care and Use Committee of Baylor College of Medicine (BCM AN-5996). Dr Chris Wright (Vanderbilt University School of Medicine) kindly provided the $Ptf1a^{Cre}$ mice. We purchased

the *Pdx1*^{Cre} (Pdx-Cre, #014647) and *Vglut2*^{floxed} (*Vglut2*^{fx}, #012898) mice from The Jackson Laboratory (Bar Harbor, ME, USA) and then maintained them in our colony using a standard breeding scheme. The conditional knock-out mice that resulted in dystonia were generated by crossing *Ptf1a*^{Cre};*Vglut2*$^{fx/fx}$ heterozygote mice or *Pdx1*^{Cre};*Vglut2*$^{fx/fx}$ heterozygote mice with homozygote *Vglut2*$^{fx/fx}$ mice. *Pdx1*^{Cre};*Vglut2*$^{fx/fx}$ and *Ptf1a*^{Cre};*Vglut2*$^{fx/fx}$ mice were considered experimental animals. A full description of the genotyping details (e.g., primer sequences and the use of a standard polymerase chain reaction) and phenotype for the *Ptf1a*^{Cre};*Vglut2*$^{fx/fx}$ mouse was provided in White and Sillitoe, 2017 [4]. A full description of the genotype and the initial observations of the phenotype of the *Pdx1*^{Cre};*Vglut2*$^{fx/fx}$ mouse was provided in Lackey, 2022 [34]. All littermates lacking Cre upon genotyping were considered control mice. Ear punches were collected before weaning and used for genotyping and identification of the different alleles. For all experiments, we bred mice using standard timed pregnancies, noon on the day a vaginal plug was detected was considered embryonic day (E)0.5 and postnatal day (P)0 was defined as the day of birth. Mice of both sexes were used in all experiments.

Immunohistochemistry

Perfusion and tissue fixation were performed as previously described [35]. Briefly, mice were anesthetized by intraperitoneal injection with Avertin (2, 2, 2-Tribromoethanol, Sigma-Aldrich, St. Louis, MO, USA; catalog #T4). Cardiac perfusion was performed with 0.1 M phosphate-buffered saline (PBS; pH 7.4), then by 4% paraformaldehyde (4% PFA) diluted in PBS. For cryoembedding, brains were post-fixed at 4°C for 24–48 h in 4% PFA and then cryoprotected stepwise in sucrose solutions (15% and 30% diluted in PBS) and embedded in Tissue-Tek O.C.T. compound (Sakura Finetek, Torrance, CA, USA; catalog #4583). Tissue sections were cut on a cryostat at a thickness of 40 µm and individual free-floating sections were collected sequentially and immediately placed into PBS. Our procedures for immunohistochemistry on free-floating frozen cut tissue sections have been described extensively in previous work [36, 37]. After completing the staining steps, the tissue sections were placed on electrostatically coated glass slides and allowed to dry.

Rabbit polyclonal anti-CA VIII (CAR8, 1:500, Proteintech # 12391-1-AP) and rabbit polyclonal anti-IP3R1 (1:500, Invitrogen # PA1-901) were used to label Purkinje cells. Guinea pig polyclonal anti-VGLUT2 (1:500, Synaptic systems # 135 404) was used to label olivocerebellar climbing fibers and their terminals. We visualized immunoreactive complexes using anti-rabbit or anti-guinea pig secondary antibodies conjugated to Alexa-488 and -647 fluorophores (1:1000 for both, Invitrogen, Waltham, MA, USA).

Tissue preparation and processing for *in situ* hybridization

Mice were anaesthetized with isoflurane and brains were removed from the skull and immersed in OCT (optimal cutting temperature). Immersed brains were flash frozen by placing tissue molds onto dry ice. Sagittal sections (25 µm) were cut through the cerebellum and the slices placed onto electrostatically coated glass slides (Probe On Plus Fisher Brand; Fisher Scientific). The tissue was probed with *Vglut2* (*SLC17A6*) or *Vgat* (*SLC32A1*) digoxigenin-labelled mRNA probes using an automated *in situ* hybridization procedure (Genepaint). All reagent incubations, washes and stains were automated and performed by the *in situ* hybridization robot. The signal was detected by colorimetric detection using BCPI/NBT reagents. After processing was completed, the slides were removed from the machine and then cover-slipped with permanent mounting medium (Entellan mounting media, Electron Microscopy Sciences, Hatfield, PA, USA) and left to dry before imaging.

Wheel-running behavior

Recordings were maintained in a ventilated, temperature-controlled, and light-tight room under either a 12:12 LD cycle or DD conditions. Mice were singly housed in wheel-running cages and allowed to entrain to the LD cycle for 2 weeks, before being released into DD conditions for 21 days, to assess endogenous circadian timekeeping ability. We assessed period length, activity onset, and average number of wheel revolutions per 5 min using ClockLab Analysis (Actimetrics).

ECoG/EMG sleep recordings

Mice were anesthetized with isoflurane and placed into a stereotaxic device, which continued to deliver isoflurane throughout surgery. Each mouse with implanted with a prefabricated ECoG/EMG headmount (Pinnacle Technology, Lawrence KS, #8201) with 0.10" EEG screws to secure headmounts to the skull (Pinnacle Technology, Lawrence KS, #8209). A midline incision was made, and the skull was exposed. The headmount was affixed to the skull using cyanoacrylate glue to hold in place while pilot holes for screws were made and screws were inserted. Screws were placed bilaterally over parietal cortex and frontal cortex. A small amount of silver epoxy (Pinnacle Technology, Lawrence KS, #8226) was applied to the screw-headmount connection. Platinum-iridium EMG wires on the prefabricated headmount were placed under the skin of the neck, resting directly on the trapezius muscles. The headmount was permanently affixed to the skull using "Cold-Cure" dental cement (A-M systems, #525000 and #526000). Mice were

allowed to recover for 3–4 days before being fitted with a preamplifier (#8202) and tethered to the recording device (#8204 and #8206-HR). ECoG and EMG signals were sampled at 400 Hz with 0.5 Hz and 10 Hz high-pass filters respectively.

Mice were recorded in light and temperature-controlled rooms, for 8 h, at the same time of day for every mouse. The first hour of recording was considered the acclimation period and was therefore excluded from final analysis. Food and water were available *ad libitum* throughout the recording day.

Sleep scoring and analysis of sleep data

Sleep was automatically scored offline via SPINDLE [38]. For spectral frequency analysis of ECoG and EMG activity, raw files were also pre-processed in MATLAB (MathWorks) using the free toolkit EEGLAB (UC San Diego). Scored files were downloaded from SPINDLE as a.csv and statistical analysis was performed in R v4.1.2. Only ECoG spectral power from frontal cortex is discussed in depth, as the spectral power from parietal cortex was the same between all groups for all frequency bands: Delta: one-way ANOVA, $F = 0.031$, $p = 0.97$, Theta: one-way ANOVA, $F = 0.663$, $p = 0.524$, Alpha: one-way ANOVA, $F = 0.327$, $p = 0.724$, Beta: one-way ANOVA, $F = 0.079$, $p = 0.924$, Gamma: one-way ANOVA, $F = 0.483$, $p = 0.622$.

Data analysis and statistics

Data are presented as mean ± SEM and analyzed as a one-way ANOVA followed by Tukey's Honest Significant Difference test for post-hoc comparisons or a repeated measures two-way ANOVA with Bonferroni correction for multiple comparisons. $p < 0.05$ was considered as statistically significant. All statistical analyses were performed using R v4.1.2.

Results

Ptf1a^{Cre};*Vglut2*$^{fx/fx}$ and *Pdx1*^{Cre};*Vglut2*$^{fx/fx}$ mice display overlapping cerebellar circuit deficits, but only the *Ptf1a*^{Cre};*Vglut2*$^{fx/fx}$ mice show overt dystonic symptoms

We have previously demonstrated that silencing glutamatergic olivocerebellar synapses can induce severe dystonic motor phenotypes [4]. To elucidate the relative contributions of cerebellar versus motor dysfunction on sleep impairments, we additionally leveraged a previously generated mouse model of cerebellar dysfunction lacking overt motor dysfunction: the *Pdx1*^{Cre};*Vglut2*$^{fx/fx}$ mouse [34] (Supplementary Video S1). Both the *Ptf1a*^{Cre};*Vglut2*$^{fx/fx}$ and *Pdx1*^{Cre};*Vglut2*$^{fx/fx}$ mouse models utilize the Cre/*lox*-p system to drive the deletion of *Vglut2*, but under different promoters (Figure 1A). A detailed characterization of the *Ptf1a*^{Cre};*Vglut2*$^{fx/fx}$ mice and their resulting dystonia were previously described [4], whereas the behavior and circuit basis of the *Pdx1*^{Cre};*Vglut2*$^{fx/fx}$ mice will be described extensively in an independent study (Lackey et al., 2023 *in preparation*). While both models result in the loss of VGLUT2 protein after genetically targeting glutamatergic olivocerebellar synapses in Purkinje cells (Figures 1B, C), the differential expression patterns of *Ptf1a* (in climbing fiber neurons) and *Pdx1* (in climbing fiber and mossy fiber neurons) yield differential synapse silencing resulting in different motor phenotypes (Figure 1D; Supplementary Figure S1). Compared to wildtype littermate controls (Figure 1E), the *Ptf1a*^{Cre};*Vglut2*$^{fx/fx}$ mice display overt dystonic motor phenotypes and dystonic behaviors (Figure 1F), while the *Pdx1*^{Cre};*Vglut2*$^{fx/fx}$ mice do not display overt dystonic motor phenotypes such as spontaneous twisting postures and hyperextension of the back, limbs, or digits (Figure 1G). To better understand the alterations in motor phenotypes in both mouse models, we implanted mice with cortical (ECoG) and muscular (EMG) electrodes for *in vivo* monitoring. We calculated the overall EMG power in the 0–30 Hz frequency range, which has been previously used to quantitatively diagnose dystonia in human patients [39] (representative EMG traces per genotype; Figure 1H). As predicted, the overall EMG power was significantly elevated in the *Ptf1a*^{Cre};*Vglut2*$^{fx/fx}$ mice as compared to the control and *Pdx1*^{Cre};*Vglut2*$^{fx/fx}$ mice (Figures 1H, I). The EMG activity reflects prolonged over-contractions, which is a key phenotype observed in human patients with generalized and focal dystonia. Additionally, we found that this elevation of cervical EMG activity was maintained during all states, including both REM and NREM sleep (Supplementary Figures S2B–E). These findings support the idea that *Ptf1a*^{Cre};*Vglut2*$^{fx/fx}$ mice display elevated muscle activity due to cerebellar dysfunction, while *Pdx1*^{Cre};*Vglut2*$^{fx/fx}$ mice do not. These results further suggest that cerebellar circuit manipulations can occur without causing overt and severe motor dysfunctions and furthermore establishes the two mouse models for use in subsequent experiments in this study.

Circadian activity is unchanged in *Ptf1a*^{Cre};*Vglut2*$^{fx/fx}$ and *Pdx1*^{Cre};*Vglut2*$^{fx/fx}$ mutant mice

Wheel-running activity is commonly used in rodents as a proxy for measuring daily activity patterns [40]. Previous work has used wheel-running to understand circadian activity in other mouse models of movement disorders (for example, mild ataxia) [41]. Therefore, we sought to determine the extent of circadian activity disruption in *Ptf1a*^{Cre};*Vglut2*$^{fx/fx}$ and *Pdx1*^{Cre};*Vglut2*$^{fx/fx}$ mutant mice. Mice were singly housed with *ad libitum* access to food, water, and a running wheel in their home cage (Figure 2A). Wheel revolutions were automatically monitored throughout the recording period that lasted 35 days (14 days baseline (LD; light-dark),

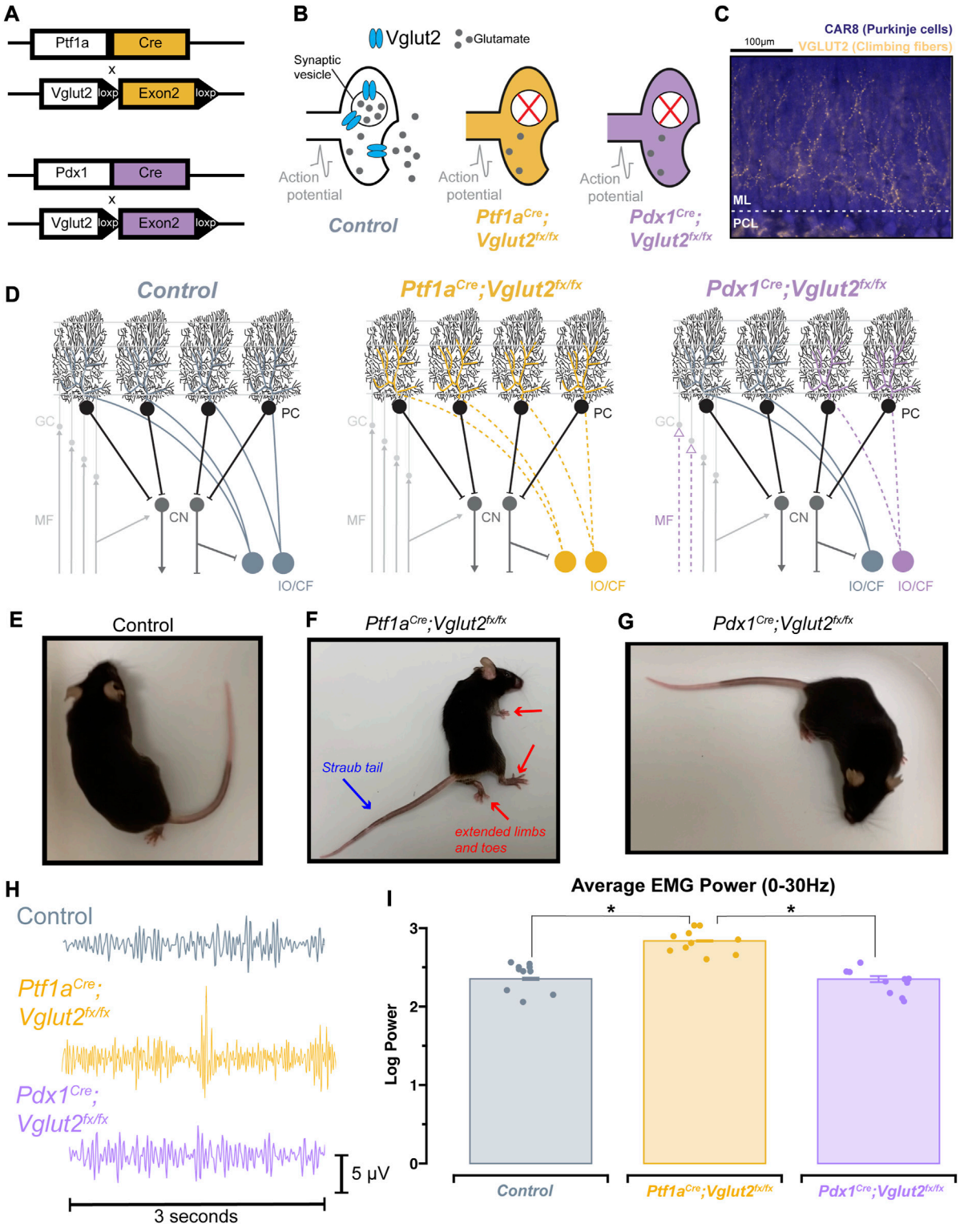

FIGURE 1
Ptf1a^{Cre};*Vglut2*$^{fx/fx}$ and *Pdx1*^{Cre};*Vglut2*$^{fx/fx}$ mice display differential dystonic motor phenotypes. **(A)** Using either the *Ptf1a*^{Cre} or *Pdx1*^{Cre} genetic driver lines, exon 2 of *Vglut2* was selectively removed and as a result VGLUT2 expression was deleted with spatial specificity. **(B)** Schematic illustration demonstrating the result of the *Vglut2* deletion and the subsequent synaptic silencing in the affected cells. **(C)** Immunohistochemical staining of the cerebellar cortex, showing Purkinje cells (blue) and VGLUT2-positive climbing fibers from the inferior olive (gold). Abbreviations: ML, molecular

(*Continued*)

FIGURE 1 (Continued)
layer; PCL, Purkinje cell layer. **(D)** Schematic demonstrating the end-result of the *Vglut2* deletion in the *Ptf1a*^{Cre};*Vglut2*$^{fx/fx}$ and *Pdx1*^{Cre};*Vglut2*$^{fx/fx}$ mice. *Ptf1a*^{Cre};*Vglut2*$^{fx/fx}$ mice have widespread silencing of olivocerebellar glutamatergic synapses, while *Pdx1*^{Cre};*Vglut2*$^{fx/fx}$ mice have comparatively more restricted silencing of a subset of olivocerebellar synapses. Abbreviations: GC, granule cell; MF, mossy fiber; PC, Purkinje cell, CF, climbing fiber; CN, cerebellar nuclei; IO, inferior olive. **(E)** Video still from a control mouse with no atypical function. **(F)** Video still demonstrating dystonic postures in a *Ptf1a*^{Cre};*Vglut2*$^{fx/fx}$ mouse, specifically showing the hindlimb hyperextension and Straub tail (noted by red and blue arrows). **(G)** Video still from a *Pdx1*^{Cre};*Vglut2*$^{fx/fx}$ mouse demonstrating the absence of overt dystonic motor dysfunction. **(H)** Raw EMG waveforms of trapezius muscle activity for a 3 s period. Control (grey), *Ptf1a*^{Cre};*Vglut2*$^{fx/fx}$ (gold), and *Pdx1*^{Cre};*Vglut2*$^{fx/fx}$ (purple) mice. **(I)** Quantification of the overall EMG activity (0–30 Hz) for all mice used in the study. Points on **I** represent individual mice, $n = 10$ per group. Source data and specific p-values for **I** are available in Supplementary Table S1.

21 days constant condition (DD; dark-dark periods; Figure 2B)). The collected data were analyzed and plotted as actograms for ease of viewing; each row represents a day and black tick marks represent revolutions of the running wheel, indicative of locomotor activity. Data is double plotted (as convention), such that 48 h of activity are plotted on the same line, to better visualize changes in activity patterns [40]. We predicted that differences in circadian activity patterns in our mutant mice would arise either from motor dysfunction or our cerebellar circuit manipulation. Given that *Pdx1*^{Cre};*Vglut2*$^{fx/fx}$ mice do not display severe dystonic motor behaviors, and the extent of their olivocerebellar manipulation is restricted relative to *Ptf1a*^{Cre};*Vglut2*$^{fx/fx}$ mice, we predicted that their circadian activity profiles would remain unchanged relative to littermate controls. As expected, we observed normal wheel-running behavior in *Pdx1*^{Cre};*Vglut2*$^{fx/fx}$ mice relative to littermate controls (Figures 2C, E). We also found that despite their overt motor dysfunction, *Ptf1a*^{Cre};*Vglut2*$^{fx/fx}$ mice did voluntarily run on the wheel and maintain rhythmic behavior, though after a longer (8-days) acclimation period (Figure 2D). We observed significantly lower average activity counts for *Ptf1a*^{Cre};*Vglut2*$^{fx/fx}$ mice with overt motor dysfunction during both LD and DD paradigms (Figures 2F, G). Nevertheless, both *Pdx1*^{Cre};*Vglut2*$^{fx/fx}$ and *Ptf1a*^{Cre};*Vglut2*$^{fx/fx}$ mice displayed characteristic nocturnal behavior even during the DD phase, similar to controls (Figures 2C–E). We also assessed endogenous circadian period length (tau), a measure of the period of a circadian rhythm. The tau length refers to the length of time it takes for the rhythm to complete one cycle [40]. At the end of the DD paradigm, all mice displayed an average tau of ~23.7 h (Figure 2H). This slight deviation from 24 h is expected, as endogenous tau length in mice is slightly less than 24 h [40]. In addition, we also found that the "siesta" period—a brief bout of sleep during the active period [42] — in *Ptf1a*^{Cre};*Vglut2*$^{fx/fx}$ mice is significantly longer by 7–10 min (Figure 2I). However, this increase may be a result of the low background activity for *Ptf1a*^{Cre};*Vglut2*$^{fx/fx}$ mice. To validate that our genetic manipulation of *Vglut2* did not significantly alter the major sleep center of the brain, we assessed *Vglut2* mRNA expression in control *Ptf1a*^{Cre} and *Pdx1*^{Cre} mice (without *floxed* alleles of *Vglut2*) using *in situ* hybridization. We found a lack of *Vglut2* expression in the suprachiasmatic nucleus (SCN) "master clock." This was anticipated since the SCN is a heavily GABAergic region [43] (*Vgat*-expressing, Supplementary Figure S3). These results suggest that in the *Pdx1*^{Cre};*Vglut2*$^{fx/fx}$ and *Ptf1a*^{Cre};*Vglut2*$^{fx/fx}$ mice, circadian rhythms remain largely unchanged despite cerebellar and motor dysfunction.

Cerebellar dysfunction disrupts sleep stages independently of the dystonic phenotype

The relationship between sleep and motor function is particularly relevant in dystonia, as reports suggest that motor symptoms are easier to manage after a good night's sleep, and earlier in the morning, shortly after waking up [44]. Therefore, a major goal was to determine the overall sleep quality in *Ptf1a*^{Cre};*Vglut2*$^{fx/fx}$ and *Pdx1*^{Cre};*Vglut2*$^{fx/fx}$ mice. We implanted *Ptf1a*^{Cre};*Vglut2*$^{fx/fx}$ and *Pdx1*^{Cre};*Vglut2*$^{fx/fx}$ mice with ECoG/EMG electrodes that were made out of silver wire and recorded signals continuously for 8 h during the light phase (Figures 3A–C). Raw ECoG/EMG waveforms show that both *Ptf1a*^{Cre};*Vglut2*$^{fx/fx}$ and *Pdx1*^{Cre};*Vglut2*$^{fx/fx}$ mice display characteristic spectral activity which defines wake, NREM, and REM sleep (Figure 3D). We also note that high-amplitude spikes in the EMG activity were observed in *Ptf1a*^{Cre};*Vglut2*$^{fx/fx}$ mice during brief periods of wake, indicative of motor dysfunction, while no such phenomenon was observed in the *Pdx1*^{Cre};*Vglut2*$^{fx/fx}$ mice (Figure 3D). We then assessed the total time spent awake, in NREM sleep, and in REM sleep. While sleep cycles in mice are shorter than in humans, they do follow the similar pattern of wake, followed by NREM, and then REM sleep (Figure 3E). Representative hypnograms of 1 h of total recording time showed that both the *Ptf1a*^{Cre};*Vglut2*$^{fx/fx}$ and *Pdx1*^{Cre};*Vglut2*$^{fx/fx}$ mice displayed disrupted sleep. The periods of wake were more frequent and last longer compared to the littermate controls (Figure 3F). We found that both *Pdx1*^{Cre};*Vglut2*$^{fx/fx}$ and *Ptf1a*^{Cre};*Vglut2*$^{fx/fx}$ mice spent more time awake and in NREM at the expense of decreased REM sleep (Figures 3G–I). These results suggest that, although motor dysfunction may occur in brief periods of spontaneous wakefulness (*Ptf1a*^{Cre};*Vglut2*$^{fx/fx}$),

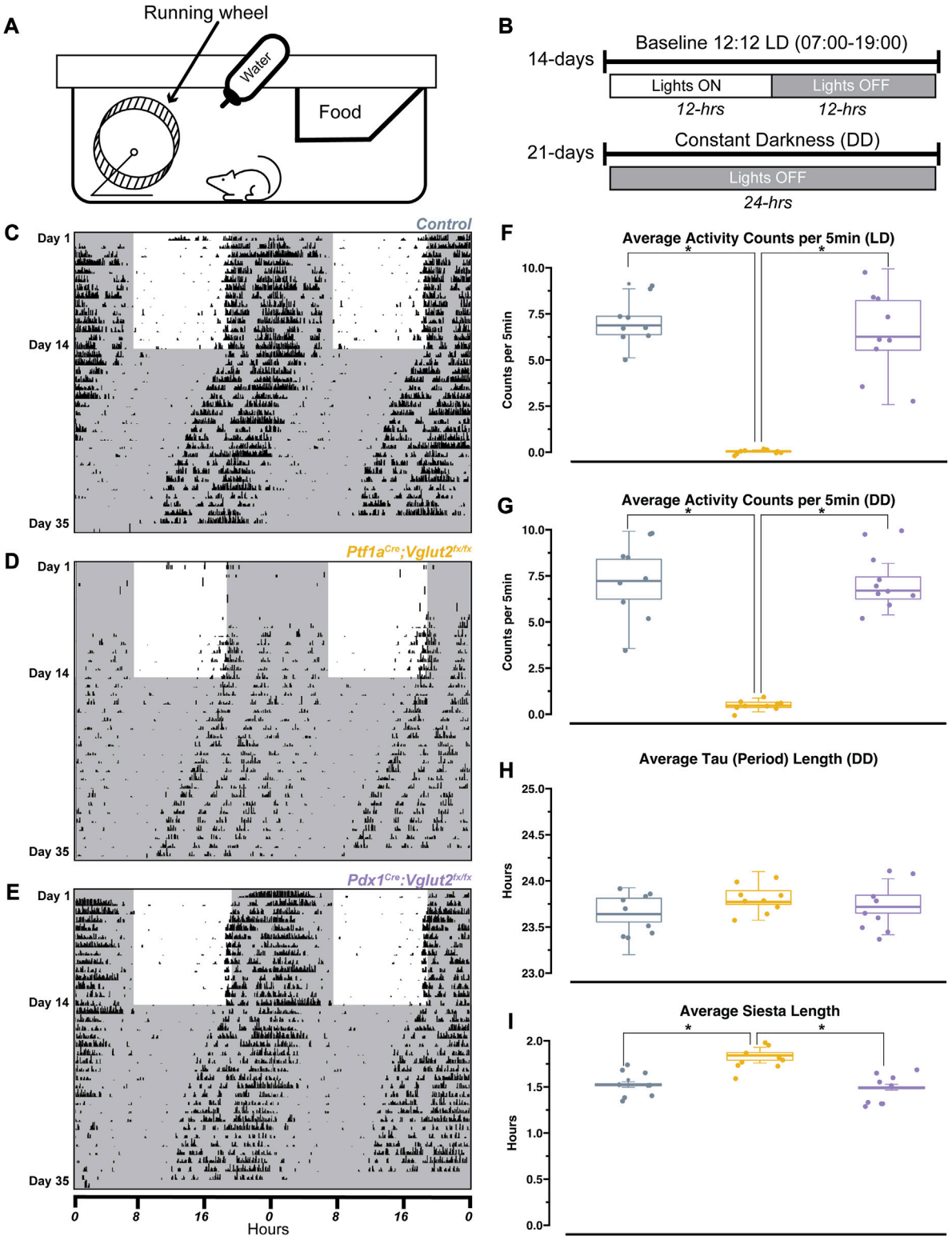

FIGURE 2
Ptf1a^{Cre};*Vglut2*$^{fx/fx}$ and *Pdx1*^{Cre};*Vglut2*$^{fx/fx}$ mice display normal circadian rhythmicity. **(A)** Schematic illustration of the wheel-running setup. **(B)** Timeline of wheel-running experiment. **(C)** Representative double-plotted actogram for a control mouse. Each row represents a day, black tick marks represent wheel-running activity (measured as revolutions of the running wheel). Black shaded regions represent "lights OFF," unshaded regions represent "lights ON". **(D)** Same as **(C)** but for a *Pdx1*^{Cre};*Vglut2*$^{fx/fx}$ mouse. **(E)** Same as **(C)** but for a *Ptf1a*^{Cre};*Vglut2*$^{fx/fx}$ mouse. **(F)**
(*Continued*)

FIGURE 2 (Continued)
Quantification of average activity counts per 5min for all mice, only during the LD paradigm. **(G)** Same as **(F)** but only quantifying activity during the DD paradigm. **(H)** Quantification of circadian period (tau) for all mice, during the DD paradigm. **(I)** Quantification of "siesta" bout length for all mice throughout the 35 days recording period. Points on **F–I** represent individual mice, n = 9 mice per group. The source data and specific p-values for **F–I** are available in Supplementary Table S2.

cerebellar dysfunction alone may be sufficient to alter sleep activity independent from gross motor dysfunction (*Pdx1*^{Cre};*Vglut2*$^{fx/fx}$).

Disrupted sleep patterns occur independent of overt dystonic motor dysfunction when comparing *Ptf1a*^{Cre};*Vglut2*$^{fx/fx}$ and *Pdx1*^{Cre};*Vglut2*$^{fx/fx}$ models of dystonia

We observed that cerebellar dysfunction was sufficient to disrupt sleep stages in *Ptf1a*^{Cre};*Vglut2*$^{fx/fx}$ and *Pdx1*^{Cre};*Vglut2*$^{fx/fx}$ mice, mouse models with and without overt dystonic motor phenotypes, respectively. However, the fluctuations in the frequency of sleep stages or length of sleep states, both of which could be driving the observed differences in sleep versus awake time, remained unclear (Figure 4A). Therefore, to further understand the fragility of sleep stages, and the disruption of each stage, we calculated both the total number of sleep-stage bouts along with the average length of bouts for wake, NREM, and REM. We note that these calculations were performed after the onset of sleep, which was determined using a similar approach to previous work [45] (Figure 4B). We found that the total number of wake bouts was not different between *Ptf1a*^{Cre};*Vglut2*$^{fx/fx}$, *Pdx1*^{Cre};*Vglut2*$^{fx/fx}$, and the littermate controls (Figure 4C). However, for both *Pdx1*^{Cre};*Vglut2*$^{fx/fx}$ and *Ptf1a*^{Cre};*Vglut2*$^{fx/fx}$ mutant mice, the awake bouts were significantly longer than in controls, by an average of ~67 min (Figure 4D). To examine the disruptions in sleep stages after sleep onset, we calculated the total number of REM and NREM bouts. We found that both the *Pdx1*^{Cre};*Vglut2*$^{fx/fx}$ and *Ptf1a*^{Cre};*Vglut2*$^{fx/fx}$ mice displayed an increase in the overall number of NREM bouts coupled with fewer REM bouts (Figures 4E, G), while the average length of both REM and NREM bouts remained the same between all groups (Figures 4F, H). Previous work in human patients with cervical dystonia suggests that dystonic patients display an increased latency to sleep, with a particular effect on the REM stage of sleep [23]. We hypothesized that these phenotypes may be recapitulated in the *Pdx1*^{Cre};*Vglut2*$^{fx/fx}$ and *Ptf1a*^{Cre};*Vglut2*$^{fx/fx}$ mice. Therefore, we calculated the latency to reach REM and NREM sleep, as this could further indicate whether sleep dysfunction is primarily related to falling asleep versus staying asleep (or both). While both groups of mutant mice displayed a normal latency to reach NREM sleep (Figure 4J), latency to reach REM sleep was significantly elevated in both groups by an average of 47 min (Figure 4I). Together, these experiments highlight the specific deficits of sleep architecture that have been disordered in the *Pdx1*^{Cre};*Vglut2*$^{fx/fx}$ and *Ptf1a*^{Cre};*Vglut2*$^{fx/fx}$ mutant mice, and that the same deficits occur in both groups independently of how severe and constant the motor phenotype may be.

Changes in delta, beta, and gamma spectral power may underlie sleep state impairments in *Ptf1a*^{Cre};*Vglut2*$^{fx/fx}$ but not *Pdx1*^{Cre};*Vglut2*$^{fx/fx}$ mice

Arousal states are defined, in part, by spectral frequency oscillations that occur across specific frequency bands, ranging from 0.5 to >100 Hz (Figure 5A). Accordingly, changes in sleep stages are marked by changes in delta (0.5Hz–4 Hz in mice) or theta (5Hz–8 Hz in mice) power, indicating both an increase or a decrease in sleep quality [46, 47]. Therefore, changes in spectral power can give some insight as to how sleep/wake dynamics are being interrupted at the neuronal level. As dystonia is a heterogenous motor disorder [1], and our two mouse models show differing severity in dystonic motor symptoms overall, we predicted that between the models we would see specific differences in ECoG spectral activity in sleep-dependent frequency bands. Such analysis may also provide insight into the potential mechanisms of sleep dysfunction, given that different frequency bands can be used to report on changes in overall brain connectivity [48]. We therefore sought to determine whether the *Pdx1*^{Cre};*Vglut2*$^{fx/fx}$ and the *Ptf1a*^{Cre};*Vglut2*$^{fx/fx}$ mice displayed measurable differences in spectral power across frequency bands of interest (Figure 5B), relative to controls. We implanted mice with two cortical (ECoG) electrodes to detect changes in oscillation power spectral frequency at various sleep stages. We calculated overall average spectral power frequency from two independent ECoG electrodes placed over the parietal cortex and the frontal cortex, to measure delta (0.5–4 Hz), theta (5–8 Hz), alpha (8–13 Hz), beta (13–30 Hz), and gamma (35–44 Hz) frequency bands. *Ptf1a*^{Cre};*Vglut2*$^{fx/fx}$, but not the *Pdx1*^{Cre};*Vglut2*$^{fx/fx}$ mice, displayed differential spectral power frequencies in the frontal cortex for delta and beta frequency bands (Figures 5C, I). Specifically, delta power was significantly increased relative to the controls, while beta power was decreased. As delta power can be an effective indicator of NREM sleep, this observed increase may reflect the overall increased time spent in NREM sleep that

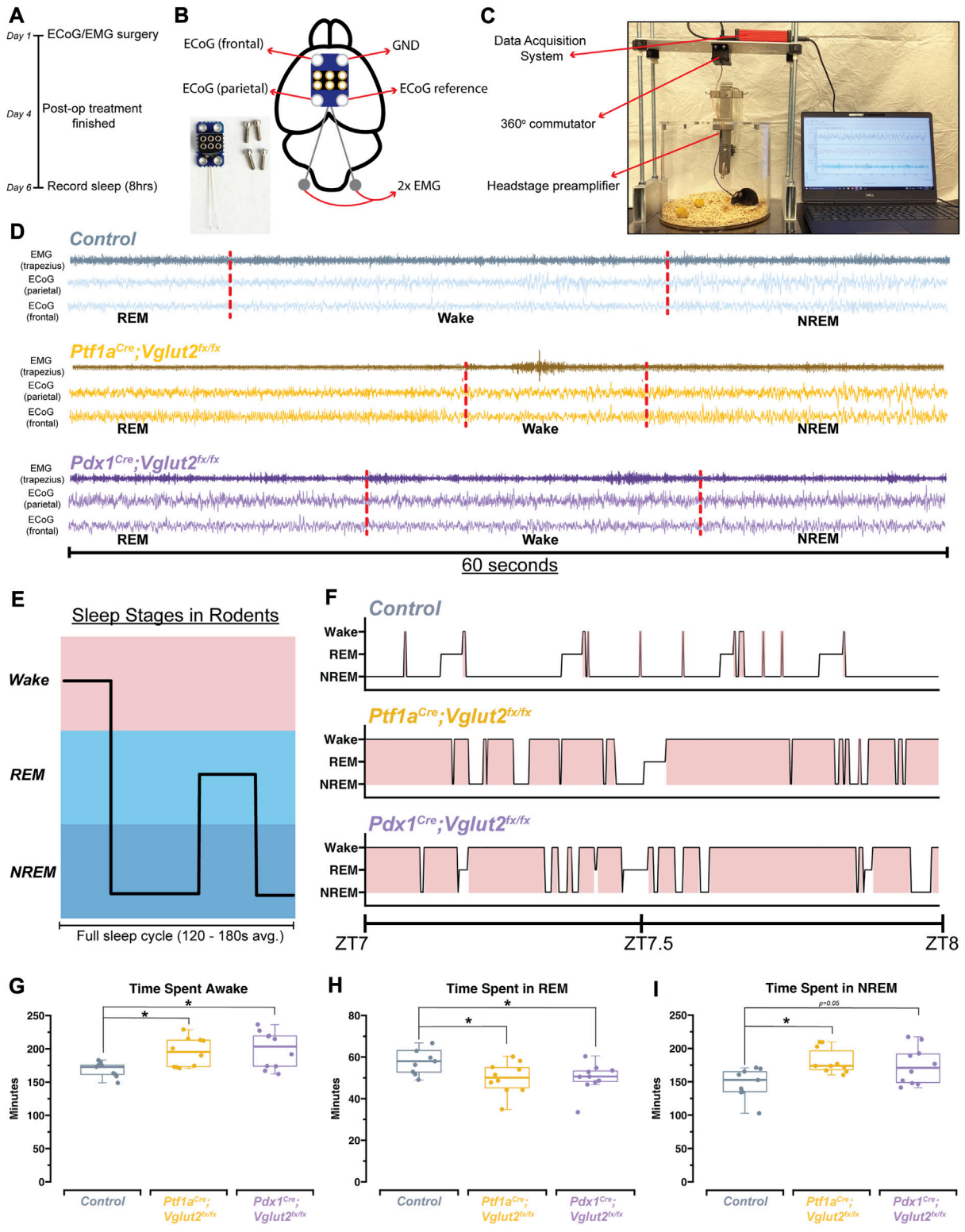

FIGURE 3
Ptf1a^{Cre};*Vglut2*$^{fx/fx}$ and *Pdx1*^{Cre};*Vglut2*$^{fx/fx}$ mice display disrupted sleep patterns. **(A)** Schematic illustration of the experimental timeline. **(B)** Schematic illustration of a mouse brain showing the placement of the ECoG/EMG headmount. An image of the headmount and mounting screws is also shown in the bottom left. **(C)** Video still from a sample sleep recording showing the experimental setup while a mouse is being recorded. **(D)** Raw waveforms of EMG activity (top trace for each sample) and ECoG activity (bottom two traces for each sample) for representative mice from each

(*Continued*)

FIGURE 3 (Continued)
group. Each example is 60-seconds in length. Sleep stage, as determined by SPINDLE (see Methods), is noted under each example. Dotted red lines are added to help distinguish each sleep/wake state. **(E)** Schematic showing sleep stages and their organization for a mouse. **(F)** Hypnograms for a single representative mouse from each group, for the same 1 h period, ZT7-ZT8, where ZT0 = lights ON, ZT1 = 1 h after lights ON, etc. Periods of wake are highlighted in red. **(G)** Quantification of total time spent awake for all mice in each group. **(H)** Quantification of the total time spent in REM for all mice in each group. **(I)** Quantification of the total time spent in NREM for all mice in each group. Points on **G–I** represent individual mice, n = 10 mice per group. The source data and specific p-values for **G–I** are shown in Supplementary Table S3.

the *Ptf1a*^{Cre};*Vglut2*$^{fx/fx}$ mice display. We also note that although gamma power was decreased in *Ptf1a*^{Cre};*Vglut2*$^{fx/fx}$ mice, the change did not meet the threshold for significance (Figure 5K). Overall, theta and alpha power were unchanged from controls for *Ptf1a*^{Cre};*Vglut2*$^{fx/fx}$ and *Pdx1*^{Cre};*Vglut2*$^{fx/fx}$ mice (Figures 5E, G).

Sleep, and by extension the spectral oscillations defining sleep, are known to possess some intrinsic rhythmicity. Therefore, we also sought to determine whether the observed changes in spectral frequency power displayed temporal properties. To do this, we divided each animal's sleep recording into 3 distinct periods. After performing spectral frequency analysis, we found that *Ptf1a*^{Cre};*Vglut2*$^{fx/fx}$ mice continue to display increased delta and decreased beta power (Figures 5D, J). Interestingly, for both frequency bands, spectral power was only different during mid (ZT6-8) and late (ZT8-10) recording periods. For Gamma power, a significant decrease was only observed during the mid-recording period for both *Pdx1*^{Cre};*Vglut2*$^{fx/fx}$ and *Ptf1a*^{Cre};*Vglut2*$^{fx/fx}$ mice (Figure 5L). As we observed with overall power, neither theta nor alpha showed differences when we calculated changing power over time (Figures 5F, H). These data demonstrate that measurable spectral frequency changes accompany sleep impairments in dystonia, but predominantly in *Ptf1a*^{Cre};*Vglut2*$^{fx/fx}$ mice that experience overt motor dysfunction. The data indicate the possibility that while sleep impairments arise from cerebellar dysfunction in dystonia, the overt motor defects, which can arise in parallel, can also influence specific aspects of sleep physiology in the disease.

Discussion

We genetically dissected the interaction between sleep impairments and cerebellar-initiated motor impairments in two mouse models of dystonia. Altogether, the results from this work provide insight into the unique sleep, ECoG, and EMG disturbances observed in our mouse models of cerebellar circuit dysfunction (Figure 6A). We found that sleep impairments, a common nonmotor symptom in human dystonia, occur in *Ptf1a*^{Cre};*Vglut2*$^{fx/fx}$ and *Pdx1*^{Cre};*Vglut2*$^{fx/fx}$ mouse models of cerebellar miswiring, with and without severe dystonia-related motor dysfunctions. We show that both groups of mutant mice display an increase in the length of wake bouts, increased NREM and more frequent NREM bouts, and decreased REM and less frequent REM bouts (Figure 6A). While existing studies on sleep quality in dystonia patients is limited, our results are striking in that they reflect patterns of sleep deficits observed in dystonia patients [23–25]. We also highlight our finding that motor activity in *Ptf1a*^{Cre};*Vglut2*$^{fx/fx}$ mice remains elevated in all stages of sleep, even during REM. This result is particularly intriguing. Existing studies are split, some suggesting that abnormal muscle activity in dystonic patients disappears during sleep [23] while other indicate that it might persist during sleep [24]. On the one hand, it is possible that our results indicate that dysfunction of the mechanisms involved in synaptic renormalization are affected in dystonia, which are believed to occur during sleep and mediate muscle recovery and atonia during sleep [32, 49, 50]. On the other hand, as a reconciling interpretation, the work we presented here could also suggest that cerebellar dysfunction, in the presence or absence of dystonic motor dysfunction, is sufficient to drive nonmotor impairments in sleep in mouse models of dystonia (Figure 6B). Existing knowledge suggests that the cerebellum and its circuit components (namely, the Purkinje cells and cerebellar nuclei neurons) are a key node in dystonia [4, 51]. Therefore, our results may point to the cerebellum as a central dystonia locus, which could help to anchor future studies on the development of therapies that can address motor and nonmotor (sleep) dysfunction in dystonia.

Evidence from case-control studies in patients with cervical dystonia suggests that human patients with dystonia exhibit distinct abnormalities in their circadian rhythms, including fatigue and excessive daytime sleepiness [25, 26, 52]. We sought to understand if the clinical symptoms of dystonia that are relevant to sleep were observed in our two mouse models that exhibit cerebellar dysfunction, with and without motor deficits. Our results show that both *Pdx1*^{Cre};*Vglut2*$^{fx/fx}$ and *Ptf1a*^{Cre};*Vglut2*$^{fx/fx}$ mice display normal circadian timing of behavior (Figures 2C–E,H), suggesting that cerebellar dysfunction and motor deficits do not impact overall circadian behavior. Although these data are intriguing, given the substantial sleep impairments experienced by these mice, this finding is in line with work in mice with cerebellar ataxia, which also show normal circadian wheel-running behavior [41]. To make sure that our genetic manipulation in each model did not disrupt activity in the SCN master clock, we verified in our mice existing work, which states that the SCN is 95% GABAergic in its neuronal identity [43]. In accordance with our *in situ* hybridization results (Supplementary Figure S3), this may indicate that while the

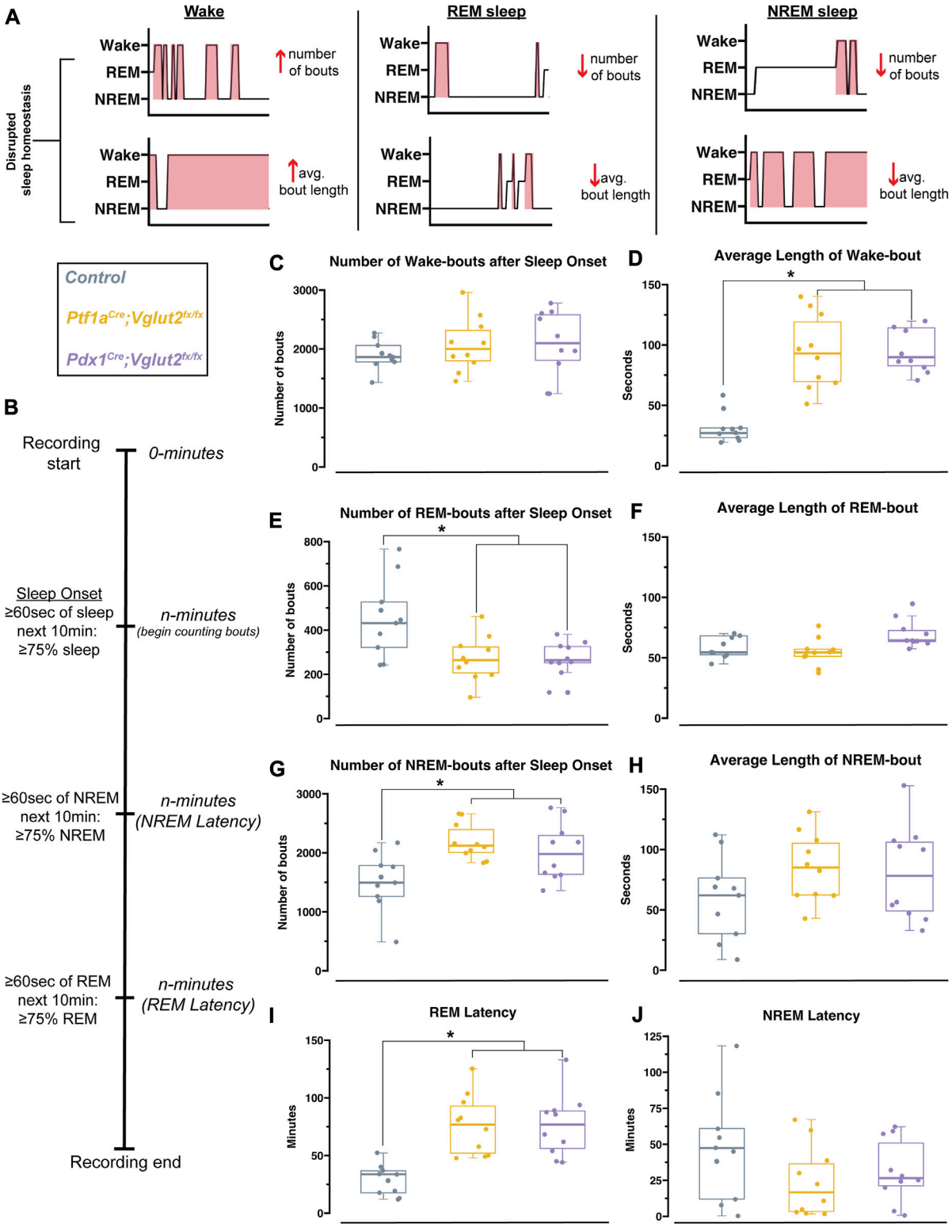

FIGURE 4
Pdx1^{Cre};*Vglut2*$^{fx/fx}$ and *Ptf1a*^{Cre};*Vglut2*$^{fx/fx}$ mutant mice display equivalent impairments in sleep. **(A)** Schematic with hypnogram examples of how possible forms of sleep disruption may appear. **(B)** Schematic showing sleep recording timeline and how sleep onset, NREM latency, and REM latency were defined and calculated, similar to Hunsley & Palmiter, 2004 [45]. **(C)** Quantification of the total number of wake bouts. **(D)** Quantification of the average length of wake bouts. **(E)** Quantification for the number of REM bouts after sleep onset. **(F)** Quantification for the average length of REM

(*Continued*)

FIGURE 4 (Continued)
bouts. **(G)** Quantification for the number of NREM bouts after sleep onset. **(H)** Quantification of the average length of NREM bouts. **(I)** Quantification of the latency to REM sleep. **(J)** Quantification of the latency to NREM sleep. Points on **C–J** represent individual mice, $n = 10$ mice per group. The source data and specific p-values for **C–J** are available in Supplementary Table S4.

cerebellum is involved in the regulation of sleep, its role in circadian timekeeping is limited, at least in the current context. Indeed, while numerous projections exist between the cerebellum and the major circadian centers of the brain, including the hypothalamus, locus coeruleus, and pedunculopontine nucleus, direct projections between the cerebellum and the SCN master clock are lacking [53, 54]. It is possible then that cerebellar access to circadian processes is tightly regulated and restricted to sleep rather than overall activity rhythms. In this case, the fatigue and excessive daytime sleepiness experienced by patients with dystonia may be attributed to lack of sleep rather than aberrant circadian timekeeping.

While dystonia is commonly considered a network disorder in humans [1], our genetic manipulation attempts to recreate the circuit-wide defects through a mechanism that initiates the dystonia by precisely blocking glutamatergic signaling in the cerebellum. Although both *Pdx1* and *Ptf1a* are expressed in several brain regions, including in the hypothalamus, neither *Pdx1* nor *Ptf1a* is expressed in the SCN, the circadian master clock of the brain [33, 55]. Furthermore, as discussed before, over 95% of the cells in the suprachiasmatic nucleus are GABAergic [43], which further suggests that our genetic manipulation does not extend to directly affect the master clock. Indeed, our analysis of *Vglut2* mRNA expression showed that *Vglut2* expression in the suprachiasmatic nucleus is sparse (Supplementary Figure S3). As suggested by existing work, these regions instead heavily express *Vgat,* indicative of using primarily GABAergic signaling. Therefore, it is possible that human dystonia patients do experience malfunctioning circadian rhythmicity, but our model is unable to capture this specific aspect of heterogeneity in dystonia network dysfunction.

While overall circadian rhythm patterns remained unchanged in our mutant mice, we did observe a difference in siesta time for $Ptf1a^{Cre};Vglut2^{fx/fx}$ mice. The siesta period is a brief bout of sleep during the active period [42]; it represents an important output of the circadian systems' sleep regulation process [42, 56]. Thus, it serves as an additional marker of typical circadian rhythmicity. We note that the siesta period in the $Ptf1a^{Cre};Vglut2^{fx/fx}$ mice does appear more pronounced and is significantly longer by 7–9 min (Figure 2I). However, given the low overall activity profile of the $Ptf1a^{Cre};Vglut2^{fx/fx}$ mice, it is difficult to determine whether this increase in siesta time is circadian in origin, or if it arises as a result of the decreased overall activity, making the accurate calculation of siesta onset/offset difficult. Recent work does suggest that daily timing of the siesta is under control of the SCN [57], which we have determined to be spared from our genetic manipulation. Together, these data further support the finding that circadian rhythmicity is largely unaffected in $Ptf1a^{Cre};Vglut2^{fx/fx}$ mice and also in the $Pdx1^{Cre};Vglut2^{fx/fx}$ model of dystonia.

Human studies suggest that alterations in sleep efficiency and sleep latency are prevalent in dystonia patients [19, 23, 24, 26, 52, 53]. We found that changes in sleep/wake dynamics are of particular interest, as they begin to explain the specific ways in which sleep deficits arise in the disease. Our results further suggest that REM disruption may be one of the primary sleep deficits encountered by our mouse models. We found not only that our mutants spend less time in REM, but that this impairment is complemented by an increase in both wake and NREM sleep (Figures 3G–I). Though mice sleep in bouts of 120–180 s per full sleep cycle [58] and not in long consolidated bouts like humans, they do follow similar sleep stage patterns (Figure 3E). Despite REM representing the lightest sleep stage, it is typically preceded by NREM sleep [59]. Therefore, the increase in NREM sleep combined with decrease in REM sleep suggests that the sleep deficits in our mice specifically result from involuntary waking during NREM sleep. This is further evidenced by our EMG results for the $Ptf1a^{Cre};Vglut2^{fx/fx}$ mice, which display elevated cervical EMG power in all sleep states (Supplementary Figure S1). As mice must pass through NREM again before entering REM as they start a new sleep cycle, this prolongs the time spent in NREM while decreasing the time spent in REM. Further work needs to be conducted in order to connect our findings in mice to human patients with dystonia, as an equivalent result in humans could potentially explain the reported symptoms of daytime fatigue. Even if the total sleep time is similar between dystonic and non-dystonic patients, the quality of sleep is still being affected, as proportions of NREM versus REM during the sleeping phase are equally as important as overall time spent asleep versus awake [59].

Given the cerebellums' known projections to/from a variety of cortical regions involved not only in sleep regulation, but also regulation of specific sleep stages (NREM and REM) [53, 54, 60], it was not unsurprising to find that sleep-stage specific deficits exist in both $Pdx1^{Cre};Vglut2^{fx/fx}$ and $Ptf1a^{Cre};Vglut2^{fx/fx}$ mice. Other groups have found that dystonia patients [23, 26] and mouse models of motor dysfunction [61] present with sleep-stage specific deficits. Our findings of increased average wake bout length (Figure 4D), increased number of NREM bouts (Figure 4G) and decreased number of REM bouts (Figure 4E) specifically highlight and further reinforce our main findings of

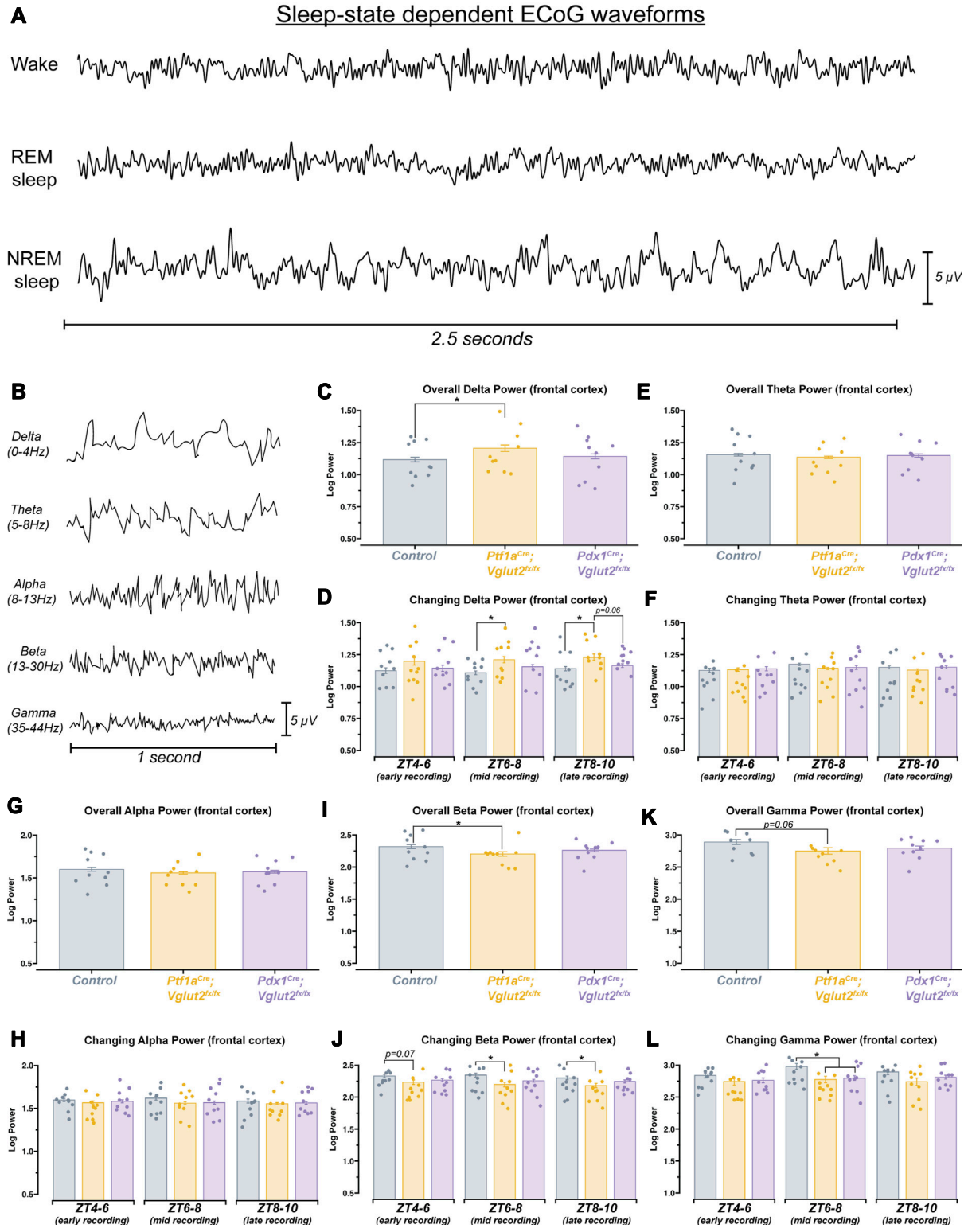

FIGURE 5
Ptf1a^{Cre};*Vglut2*$^{fx/fx}$ mice show differences in spectral frequency oscillations that define arousal states. **(A)** 2.5 s samples of raw ECoG waveforms for awake, REM, and NREM from a control mouse. **(B)** 1 s samples of raw ECoG waveforms for frequency bands of interest, from a control mouse. **(C)** Quantification of delta power (0–4 Hz). Average power across the entire recording period. **(D)** Quantification of the changing delta power across the recording period. **(E)** Quantification of theta power (5–8 Hz). Average power across the entire recording period. **(F)** Quantification of the changing theta power across the recording period. **(G)** Quantification of alpha power (8–13 Hz). Average power across the entire recording period. **(H)**
(*Continued*)

FIGURE 5 (Continued)
Quantification of the changing alpha power across the recording period. **(I)** Quantification of beta power (13–30 Hz). Average power across the entire recording period. **(J)** Quantification of the changing beta power across the recording period. **(K)** Quantification of gamma power (35–44 Hz). Average power across the entire recording period. **(L)** Quantification of the changing gamma power across the recording period. Points on **C–L** represent individual mice, n = 10 mice per group. The source data and specific p-values for **C–L** are available in Supplementary Table S5.

impairments in overall sleep stage timing. These results highlight the existence of significant REM-related sleep deficits. This is further reflected in our results of increased latency to reach REM for both *Pdx1*^{Cre};*Vglut2*$^{fx/fx}$ and *Ptf1a*^{Cre};*Vglut2*$^{fx/fx}$ mice (Figure 4I). For *Ptf1a*^{Cre};*Vglut2*$^{fx/fx}$ mice, the motor dysfunction may partially explain this result. REM-related sleep impairments are typically accompanied by some form of motor dysfunction [24, 26, 61], as the canonical mechanisms of muscle atonia during REM are disrupted [62]. However, since our *Pdx1*^{Cre};*Vglut2*$^{fx/fx}$ mouse model does not display overt motor dysfunction, but still displays the same wake, NREM, and particularly REM-related deficits, motor dysfunction may not be the sole culprit for impaired sleep. In this case, cerebellar dysfunction may also be to blame. Indeed, the cerebellum itself and many regions receiving direct cerebellar innervation are known to be involved in sleep regulation or control sleep-dependent behaviors, particularly REM regulation [53]. The locus coeruleus regulates NREM/REM intensity [63] while sending and receiving dense projections to cerebellar Purkinje cells and the cerebellar nuclei [64–66]. The pedunculopontine nucleus is a known regulator of REM sleep [67] and also sends/receives inputs between cerebellum and the basal ganglia [68]. Therefore, it is possible that the cerebellar malfunctions in the *Pdx1*^{Cre};*Vglut2*$^{fx/fx}$ and *Ptf1a*^{Cre};*Vglut2*$^{fx/fx}$ mice directly and indirectly influence REM latency through intermediary regions such as the pedunculopontine nucleus or the locus coeruleus, or even other regions, all of which play a role in the regulation of REM sleep and receive/send direct innervation from the cerebellum [54, 60, 63]. The circuit pathways mediating the direct versus indirect effects on sleep were not resolved in the current work. Ultimately, the impaired sleep dynamics further reinforces our results, which suggest that *Pdx1*^{Cre};*Vglut2*$^{fx/fx}$ and *Ptf1a*^{Cre};*Vglut2*$^{fx/fx}$ mice experience interrupted sleep cycles, cutting REM sleep short or missing it entirely and re-starting subsequent sleep cycles from NREM sleep.

Our ECoG spectral activity results are of particular interest from a mechanistic view, as they may not only explain the factors underlying sleep deficits in *Pdx1*^{Cre};*Vglut2*$^{fx/fx}$ and *Ptf1a*^{Cre};*Vglut2*$^{fx/fx}$ mice but may also serve as additional "biomarkers" that differentiate each group based on their degree of cerebellar dysfunction. For instance, we observed an increase in delta power for *Ptf1a*^{Cre};*Vglut2*$^{fx/fx}$ but not *Pdx1*^{Cre};*Vglut2*$^{fx/fx}$ mice, which occurs predominantly in the latter stages of recording (Figures 5C, D). The increase for *Ptf1a*^{Cre};*Vglut2*$^{fx/fx}$ is in agreement with recent work suggesting that higher delta power is associated with arousal and sleep impairment, particularly in the context of obstructive sleep apnea which involves both motor dysfunction and cerebellar dysfunction [69]. However, as delta power in *Pdx1*^{Cre};*Vglut2*$^{fx/fx}$ is also elevated relative to control mice and is not significantly different from *Ptf1a*^{Cre};*Vglut2*$^{fx/fx}$, there stands the possibility that the lack of significance stems from the "intermediate" phenotype of *Pdx1*^{Cre};*Vglut2*$^{fx/fx}$ mice. We have shown that *Pdx1*^{Cre};*Vglut2*$^{fx/fx}$ mice lack overt motor dysfunction (Figures 1H, I; Supplementary Figure S2, Supplementary Video S1), and that the extent of *Vglut2* deletion in the cerebellar cortex, at least with respect to the climbing fibers, is less extensive relative to the *Ptf1a*^{Cre};*Vglut2*$^{fx/fx}$ mice (Supplementary Figure S1). Therefore, if we consider each mutant group as a model for different cerebellar/motor disorders of varying intensity, we expect to see such differences in spectral power despite similar sleep deficits. In this case, spectral differences may represent "biomarkers" of disease severity. It is known that changes in delta power can differ across individuals with different diseases even if all individuals display poor sleep [47]; it is possible then that *Pdx1*^{Cre};*Vglut2*$^{fx/fx}$ and *Ptf1a*^{Cre};*Vglut2*$^{fx/fx}$ mice, even with an overlap in the genetic manipulations, indeed represent different manifestations of dystonic motor disease. Ultimately, this is evident with the difference in observed dystonic motor phenotypes between the two groups. It should be noted though, the measurement of sleep-related spectral difference between the *Pdx1*^{Cre};*Vglut2*$^{fx/fx}$ and *Ptf1a*^{Cre};*Vglut2*$^{fx/fx}$ mice could still intersect with the induced alterations in the motor program, as movement patterns are known to impact ECoG spectral activity [70].

Additional patterns of significantly different spectral power for *Ptf1a*^{Cre};*Vglut2*$^{fx/fx}$ but not *Pdx1*^{Cre};*Vglut2*$^{fx/fx}$ mice are seen for beta power, indicative of alert wakefulness (Figures 5I, J). While beta power is typically increased in patients with primary insomnia, previous work has shown that decreased beta activity is also associated with poor sleep quality, particularly in patients with obstructive sleep apneas [69]. The relationship between the cerebellum and breathing is well-established and may provide a fruitful avenue for further research in the context of dystonia. The cerebellum is known to be involved in both the rhythmicity of breathing and in regulating air hunger [71]; both mechanisms are known to play a role in obstructive sleep apneas [19, 72]. It is possible that *Ptf1a*^{Cre};*Vglut2*$^{fx/fx}$ mice, with overt motor dysfunction, have some degree of sleep apnea behavior, which could contribute to their observed sleep impairment. Interestingly, cortical gamma power was only significantly

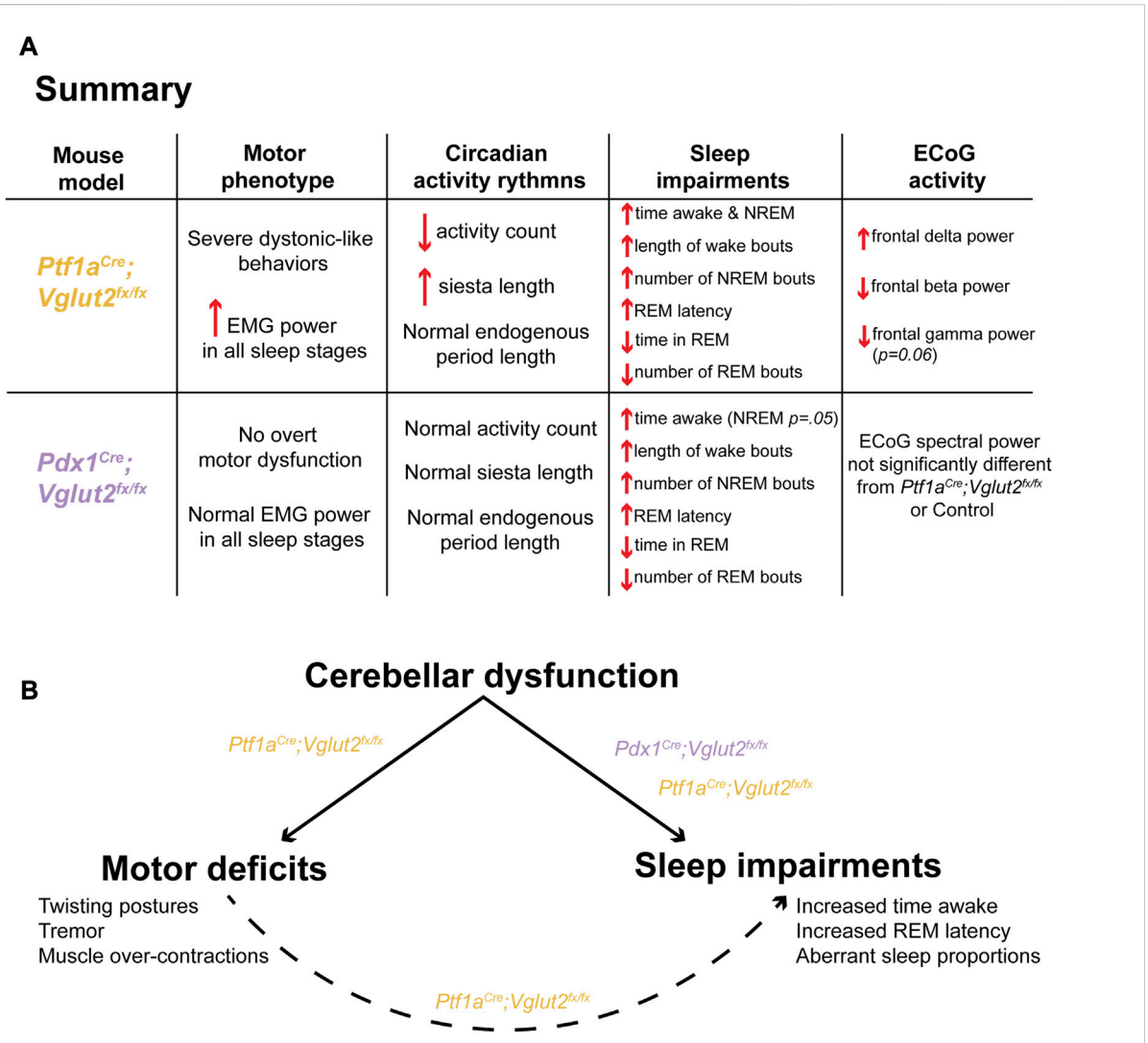

FIGURE 6
A model in which cerebellar dysfunction independently drives dystonic motor behavior and sleep impairments in *Ptf1a*^{Cre};*Vglut2*$^{fx/fx}$ and *Pdx1*^{Cre};*Vglut2*$^{fx/fx}$ mice. **(A)** A summary of the main findings of this study, stratified for each mouse model. **(B)** A proposed model of the main finding of this study.

changed during the middle of the recording period, for both the *Pdx1*^{Cre};*Vglut2*$^{fx/fx}$ and the *Ptf1a*^{Cre};*Vglut2*$^{fx/fx}$ mutant mice (Figure 5L). While gamma oscillations are typically associated with working memory and attention, human and mouse EEG/ECoG studies have found that gamma oscillations occur spontaneously during REM and NREM sleep [73, 74]. This may explain why the overall gamma power is not significantly lower for either the *Pdx1*^{Cre};*Vglut2*$^{fx/fx}$ or *Ptf1a*^{Cre};*Vglut2*$^{fx/fx}$ mice, yet it does reach the threshold for significance during "mid-recording". *Ptf1a*^{Cre};*Vglut2*$^{fx/fx}$ and *Pdx1*^{Cre};*Vglut2*$^{fx/fx}$ mice exhibit an increase in NREM and a decrease in REM sleep, and gamma oscillations spontaneously occur during both stages; changes in gamma activity may be effectively "canceled out" due to the opposing NREM and REM dynamics. While these observed changes in spectral frequency oscillations uncover some of the potential mechanisms driving the observed changes in sleep in our *Ptf1a*^{Cre};*Vglut2*$^{fx/fx}$ and *Pdx1*^{Cre};*Vglut2*$^{fx/fx}$ mice, we note that attributing sleep disruption to specific directional changes in any one frequency band is difficult. Both positive and negative changes in average power, in any frequency band, can be associated with various disease states, and notably with disordered sleep [46, 47]. Therefore, here, we highlight the presence of a change in spectral frequency power as an indicator of fractured sleep homeostasis in our mouse circuit models of dystonia, without differentiating the specific directionality of the change in spectral frequency power.

Our findings build upon existing evidence from both human patients and mouse models of motor disease demonstrating that sleep impairments are a common nonmotor symptom in dystonia. Previous work has been unable to distinguish

between dystonia-dependent versus independent sleep dysfunction, particularly in the context of dystonic motor dysfunction. Importantly, our results suggest a model in which cerebellar dysfunction alone (Figure 6B), without overt dystonic motor phenotypes, can drive sleep deficits. This may be an indication of a broader set of network dysfunctions in dystonia, with the cerebellum located at the center of multiple disease symptoms.

Data availability statement

All data generated or analyzed in this study are included in the article and Supplementary Material.

Ethics statement

Animal experimentation: All animals were housed in an AALAS-certified facility that operates on a 14 h light cycle. Husbandry, housing, euthanasia, and experimental guidelines were reviewed and approved by the Institutional Animal Care and Use Committee (IACUC) of Baylor College of Medicine (protocol number: AN-5996).

Author contributions

Technical and conceptual ideas in this work were conceived by LS and RS. LS performed the experiments and LS and RS performed data analysis and data interpretation. LS and RS wrote and edited the manuscript. All authors contributed to the article and approved the submitted version.

Funding

This work was supported by Baylor College of Medicine (BCM), Texas Children's Hospital, The Hamill Foundation, and the National Institutes of Neurological Disorders and Stroke (NINDS) R01NS100874, R01NS119301, and R01NS127435 to RS. Research reported in this publication was supported by the Eunice Kennedy Shriver National Institute of Child Health & Human Development of the National Institutes of Health under Award Number P50HD103555 for use of the Animal Behavior Core and the Cell and Tissue Pathogenesis Core (BCM IDDRC). Support was also provided by a Dystonia Medical Research Foundation (DMRF) grant to RS. Research reported in this publication was supported in part by the RNA *In Situ* Hybridization Core facility at Baylor College of Medicine, which is supported by a Shared Instrumentation grant from the NIH (S10OD016167) and the NIH IDDRC grant U54HD083092 from the Eunice Kennedy Shriver National Institute of Child Health & Human Development.

Conflict of Interest

The authors declare that the research was conducted in the absence of any commercial or financial relationships that could be construed as a potential conflict of interest.

Author disclaimer

The content is solely the responsibility of the authors and does not necessarily represent the official views of the Eunice Kennedy Shriver National Institute of Child Health & Human Development or the National Institutes of Health.

Supplementary material

The Supplementary Material for this article can be found online at: https://www.frontierspartnerships.org/articles/10.3389/dyst.2023.11487/full#supplementary-material

SUPPLEMENTARY FIGURE S1
Deletion of VGLUT2 in the cerebellum is more widespread in the climbing fibers of the *Ptf1a*^{Cre};*Vglut2*$^{fx/fx}$ mice than in the *Pdx1*^{Cre};*Vglut2*$^{fx/fx}$ mice. **(A)** Quantification of relative fluorescence units (normalized per area) for each group. **(B)** Fluorescence immunohistochemical stain of the cerebellar cortex for a control mouse. Purkinje cell bodies and axons are shown in blue (labeled with CAR8/IP3R1). Climbing fibers express VGLUT2 and are labeled in gold. Scale bars are 20um and indicated with white bars. The molecular layer (ML) and Purkinje cell layer (PCL) are labeled for orientation. **(C)** Same as **(B)** but for a *Ptf1a*^{Cre};*Vglut2*$^{fx/fx}$ mouse. **(D)** Same as **(B)** but for a *Pdx1*^{Cre};*Vglut2*$^{fx/fx}$ mouse. Points on **A** represent individual sections (n = 4) from 3 mice per group. The source data and specific p-values for **A** are available in Supplementary Table S6.

SUPPLEMENTARY FIGURE S2
Cervical EMG activity in *Ptf1a*^{Cre};*Vglut2*$^{fx/fx}$ mice remains elevated in all states. **(A)** Schematic illustration of a mouse showing the musculature and relative placement of the EMG electrodes. **(B)** Raw EMG waveforms of trapezius activity (3-seconds) for REM and NREM sleep for mice of each group. **(C)** Quantification of changing EMG power for control mice. ZT0 = lights ON, ZT4 = 4-hr after lights on. . . etc. **(D)** Same as **(C)** but for *Ptf1a*^{Cre};*Vglut2*$^{fx/fx}$ mice. **(E)** Same as **(C)** but for *Pdx1*^{Cre};*Vglut2*$^{fx/fx}$ mice. Points on **C–E** represent individual mice, n = 10 mice per group. The source data and specific p-values for **C–E** are available in Supplementary Table S7.

SUPPLEMENTARY FIGURE S3
The major circadian centers of the hypothalamus are comprised primarily of GABAergic inhibitory neurons. **(A)** Schematic illustration of a sagittal mouse brain highlighting several brain regions of interest that are related to circadian behavior. The hypothalamus is shown in blue, the suprachiasmatic nucleus (SCN) is in green, and the intermediate regions located between the SCN-cerebellum are shown in orange. **(B)** Images processed using *in situ* hybridization revealing *Vglut2* mRNA expression on sagittal sections cut through the adult mouse brain. The regions of interest are outlined in white. **(C)** Same as **(B)** but for *Vgat* mRNA expression.

SUPPLEMENTARY VIDEO S1
Differential motor phenotypes in *Pdx1*^{Cre};*Vglut2*$^{fx/fx}$ and *Ptf1a*^{Cre};*Vglut2*$^{fx/fx}$ mice. A single video of the mutant mice showing the absence (*Pdx1*^{Cre};*Vglut2*$^{fx/fx}$) and presence (*Ptf1a*^{Cre};*Vglut2*$^{fx/fx}$) of dystonic motor behaviors.

SUPPLEMENTARY TABLE S1
Source data and statistics for Figure 1.

SUPPLEMENTARY TABLE S2
Source data and statistics for Figure 2.

SUPPLEMENTARY TABLE S3
Source data and statistics for Figure 3.

SUPPLEMENTARY TABLE S4
Source data and statistics for Figure 4.

SUPPLEMENTARY TABLE S5
Source data and statistics for Figure 5.

SUPPLEMENTARY TABLE S6
Source data and statistics for Supplementary Figure S1.

SUPPLEMENTARY TABLE S7
Source data and statistics for Supplementary Figure S2.

References

1. Corp DT, Joutsa J, Darby RR, Delnooz CCS, van de Warrenburg BPC, Cooke D, et al. Network localization of cervical dystonia based on causal brain lesions. *Brain* (2019) 142:1660–74. doi:10.1093/brain/awz112

2. Fremont R, Tewari A, Angueyra C, Khodakhah K. A role for cerebellum in the hereditary dystonia DYT1. *eLife* (2017) 6:e22775. doi:10.7554/eLife.22775

3. Campbell DB, North JB, Hess EJ. Tottering mouse motor dysfunction is abolished on the purkinje cell degeneration (pcd) mutant background. *Exp Neurol* (1999) 160:268–78. doi:10.1006/exnr.1999.7171

4. White JJ, Sillitoe RV. Genetic silencing of olivocerebellar synapses causes dystonia-like behaviour in mice. *Nat Commun* (2017) 8:14912. doi:10.1038/ncomms14912

5. van der Heijden ME, Kizek DJ, Perez R, Ruff EK, Ehrlich ME, Sillitoe RV. Abnormal cerebellar function and tremor in a mouse model for non-manifesting partially penetrant dystonia type 6. *J Physiol* (2021) 599:2037–54. doi:10.1113/JP280978

6. Fremont R, Tewari A, Khodakhah K. Aberrant Purkinje cell activity is the cause of dystonia in a shRNA-based mouse model of rapid onset dystonia-parkinsonism. *Neurobiol Dis* (2015) 82:200–12. doi:10.1016/j.nbd.2015.06.004

7. Washburn S, Fremont R, Moreno-Escobar MC, Angueyra C, Khodakhah K. Acute cerebellar knockdown of Sgce reproduces salient features of myoclonus-dystonia (DYT11) in mice. *eLife* (2019) 8:e52101. doi:10.7554/eLife.52101

8. Brown EG, Bledsoe IO, Luthra NS, Miocinovic S, Starr PA, Ostrem JL. Cerebellar deep brain stimulation for acquired hemidystonia. *Mov Disord Clin Pract* (2020) 7:188–93. doi:10.1002/mdc3.12876

9. Horisawa S, Kohara K, Nonaka T, Mochizuki T, Kawamata T, Taira T. Case report: deep cerebellar stimulation for tremor and dystonia. *Front Neurol* (2021) 12:642904. doi:10.3389/fneur.2021.642904

10. Popa LS, Hewitt AL, Ebner TJ. The cerebellum for jocks and nerds alike. *Front Syst Neurosci* (2014) 8:113. doi:10.3389/fnsys.2014.00113

11. Larry N, Yarkoni M, Lixenberg A, Joshua M. Cerebellar climbing fibers encode expected reward size. *eLife* (2019) 8:e46870. doi:10.7554/eLife.46870

12. Carta I, Chen CH, Schott AL, Dorizan S, Khodakhah K. Cerebellar modulation of the reward circuitry and social behavior. *Science* (2019) 363:eaav0581. doi:10.1126/science.aav0581

13. Zhang LB, Zhang J, Sun MJ, Chen H, Yan J, Luo FL, et al. Neuronal activity in the cerebellum during the sleep-wakefulness transition in mice. *Neurosci Bull* (2020) 36:919–31. doi:10.1007/s12264-020-00511-9

14. Mano N. Changes of simple and complex spike activity of cerebellar purkinje cells with sleep and waking. *Science* (1970) 170:1325–7. doi:10.1126/science.170.3964.1325

15. McCarley RW, Hobson JA. Simple spike firing patterns of cat cerebellar purkinje cells in sleep and waking. *Electroencephalogr Clin Neurophysiol* (1972) 33:471–83. doi:10.1016/0013-4694(72)90211-8

16. Dang-Vu TT, Schabus M, Desseilles M, Albouy G, Boly M, Darsaud A, et al. Spontaneous neural activity during human slow wave sleep. *Proc Natl Acad Sci* (2008) 105:15160–5. doi:10.1073/pnas.0801819105

17. Cunchillos JD, De Andrés I. Participation of the cerebellum in the regulation of the sleep-wakefulness cycle. Results in cerebellectomized cats. *Electroencephalogr Clin Neurophysiol* (1982) 53:549–58. doi:10.1016/0013-4694(82)90067-0

18. De Andrés I, Garzón M, Reinoso-Suárez F. Functional anatomy of non-REM sleep. *Front Neurol* (2011) 2:70. doi:10.3389/fneur.2011.00070

19. Song B, Zhu JC. A narrative review of cerebellar malfunctions and sleep disturbances. *Front Neurosci* (2021) 15:590619. doi:10.3389/fnins.2021.590619

20. Bradnam LV, Meiring RM, Boyce M, McCambridge A. Neurorehabilitation in dystonia: a holistic perspective. *J Neural Transm* (2021) 128:549–58. doi:10.1007/s00702-020-02265-0

21. Yang J, Shao N, Song W, Wei Q, Ou R, Wu Y, et al. Nonmotor symptoms in primary adult-onset cervical dystonia and blepharospasm. *Brain Behav* (2016) 7:e00592. doi:10.1002/brb3.592

22. Duane DD, Bakken EC. Additional clinical observations on psychiatric disorders in adult-onset focal dystonia: a case control study. *Mov Disord* (2011) 26:1572. author reply 1573. doi:10.1002/mds.23493

23. Antelmi E, Ferri R, Provini F, Scaglione CML, Mignani F, Rundo F, et al. Modulation of the muscle activity during sleep in cervical dystonia. *Sleep* (2017) 40:zsx088. doi:10.1093/sleep/zsx088

24. Smith B. *Lived experience with dystonia* (2021). p. 633. Available from: https://dystoniasurveys.files.wordpress.com/2021/08/lived-experience-dystonia-patient-surveys-2020-2021.pdf (Accessed January 13, 2023).

25. Silvestri R, De Domenico P, Di Rosa AE, Bramanti P, Serra S, Di Perri R. The effect of nocturnal physiological sleep on various movement disorders. *Mov Disord* (1990) 5:8–14. doi:10.1002/mds.870050104

26. Eichenseer SR, Stebbins GT, Comella CL. Beyond a motor disorder: a prospective evaluation of sleep quality in cervical dystonia. *Parkinsonism Relat Disord* (2014) 20:405–8. doi:10.1016/j.parkreldis.2014.01.004

27. Boudreau P, Dumont GA, Boivin DB. Circadian adaptation to night shift work influences sleep, performance, mood and the autonomic modulation of the heart. *PloS One* (2013) 8:e70813. doi:10.1371/journal.pone.0070813

28. Pimenta AM, Kac G, Souza RRCE, Ferreira LM, Silqueira SMF. Night-shift work and cardiovascular risk among employees of a public university. *Rev Assoc Med Bras.* (2012) 58:168–77. doi:10.1016/s2255-4823(12)70177-7

29. Al-Sharman A, Siengsukon CF. Sleep enhances learning of a functional motor task in young adults. *Phys Ther* (2013) 93:1625–35. doi:10.2522/ptj.20120502

30. Walker MP, Brakefield T, Seidman J, Morgan A, Hobson JA, Stickgold R. Sleep and the time course of motor skill learning. *Learn Mem* (2003) 10:275–84. doi:10.1101/lm.58503

31. De Zeeuw CI, Canto CB. Sleep deprivation directly following eyeblink-conditioning impairs memory consolidation. *Neurobiol Learn Mem* (2020) 170:107165. doi:10.1016/j.nlm.2020.107165

32. Tononi G, Cirelli C. Sleep and the price of plasticity: from synaptic and cellular homeostasis to memory consolidation and integration. *Neuron* (2014) 81:12–34. doi:10.1016/j.neuron.2013.12.025

33. Song J, Xu Y, Hu X, Choi B, Tong Q. Brain expression of Cre recombinase driven by pancreas-specific promoters. *Genes.* (2010) 48:628–34. doi:10.1002/dvg.20672

34. Lackey E. *Neural function of Cerebellar inputs in Dystonia-like behavior*. Doctoral. Baylor College of Medicine (2022).

35. Zhou J, Brown AM, Lackey EP, Arancillo M, Lin T, Sillitoe RV. Purkinje cell neurotransmission patterns cerebellar basket cells into zonal modules defined by distinct pinceau sizes. *eLife* (2020) 9:e55569. doi:10.7554/eLife.55569

36. Sillitoe RV, Künzle H, Hawkes R. Zebrin II compartmentation of the cerebellum in a basal insectivore, the madagascan hedgehog tenrec echinops telfairi. *J Anat* (2003) 203:283–96. doi:10.1046/j.1469-7580.2003.00216.x

37. White JJ, Sillitoe RV. Postnatal development of cerebellar zones revealed by neurofilament heavy chain protein expression. *Front Neuroanat* (2013) 7:9. doi:10.3389/fnana.2013.00009

38. Miladinović Đ, Muheim C, Bauer S, Spinnler A, Noain D, Bandarabadi M, et al. Spindle: end-to-end learning from EEG/EMG to extrapolate animal sleep scoring across experimental settings, labs and species. *PLOS Comput Biol* (2019) 15:e1006968. doi:10.1371/journal.pcbi.1006968

39. Go SA, Coleman-Wood K, Kaufman KR. Frequency analysis of lower extremity electromyography signals for the quantitative diagnosis of dystonia. *J Electromyogr Kinesiol* (2014) 24:31–6. doi:10.1016/j.jelekin.2013.11.002

40. Eckel-Mahan K, Sassone-CorsiPhenotyping P. Phenotyping circadian rhythms in mice. *Curr Protoc Mouse Biol* (2015) 5:271–81. doi:10.1002/9780470942390.mo140229

41. Mendoza J, Pévet P, Felder-Schmittbuhl MP, Bailly Y, Challet E. The cerebellum harbors a circadian oscillator involved in food anticipation. *J Neurosci* (2010) 30:1894–904. doi:10.1523/JNEUROSCI.5855-09.2010

42. Stowie AC, Glass JD. Longitudinal study of changes in daily activity rhythms over the lifespan in individual male and female C57bl/6J mice. *J Biol Rhythms* (2015) 30:563–8. doi:10.1177/0748730415598023

43. Abrahamson EE, Moore RY. Suprachiasmatic nucleus in the mouse: retinal innervation, intrinsic organization and efferent projections. *Brain Res* (2001) 916:172–91. doi:10.1016/s0006-8993(01)02890-6

44. Caverzasio S, Amato N, Manconi M, Prosperetti C, Kaelin-Lang A, Hutchison WD, et al. Brain plasticity and sleep: implication for movement disorders. *Neurosci Biobehav Rev* (2018) 86:21–35. doi:10.1016/j.neubiorev.2017.12.009

45. Hunsley MS, Palmiter RD. Altered sleep latency and arousal regulation in mice lacking norepinephrine. *Pharmacol Biochem Behav* (2004) 78:765–73. doi:10.1016/j.pbb.2004.05.008

46. Bjorness TE, Booth V, Poe GR. Hippocampal theta power pressure builds over non-REM sleep and dissipates within REM sleep episodes. *Arch Ital Biol* (2018) 156:112–26. doi:10.12871/00039829201833

47. Long S, Ding R, Wang J, Yu Y, Lu J, Yao D. Sleep quality and electroencephalogram delta power. *Front Neurosci* (2021) 15:803507. doi:10.3389/fnins.2021.803507

48. Torres-Herraez A, Watson T, Rondi-Reig L. Delta oscillations coordinate intra-cerebellar and cerebello-hippocampal network dynamics during sleep. *J Neurosci* (2022) 42:2268–81. doi:10.1523/JNEUROSCI.1479-21.2021

49. Frank MG. Sleep and synaptic plasticity in the developing and adult brain. *Curr Top Behav Neurosci* (2015) 25:123–49. doi:10.1007/7854_2014_305

50. Loschky SS, Spano GM, Marshall W, Schroeder A, Nemec KM, Schiereck SS, et al. Ultrastructural effects of sleep and wake on the parallel fiber synapses of the cerebellum. *eLife* (2022) 11:e84199. doi:10.7554/eLife.84199

51. Kim JE, Chae S, Kim S, Jung YJ, Kang MG, Heo WD, et al. Cerebellar 5HT-2A receptor mediates stress-induced onset of dystonia. *Sci Adv* (2021) 7:eabb5735. doi:10.1126/sciadv.abb5735

52. Smit M, Kamphuis ASJ, Bartels AL, Han V, Stewart RE, Zijdewind I, et al. Fatigue, sleep disturbances, and their influence on quality of life in cervical dystonia patients. *Mov Disord Clin Pract* (2017) 4:517–23. doi:10.1002/mdc3.12459

53. Salazar Leon LE, Sillitoe RV. Potential interactions between cerebellar dysfunction and sleep disturbances in dystonia. *Dystonia* (2022) 1:10691. doi:10.3389/dyst.2022.10691

54. Van Dort CJ, Zachs DP, Kenny JD, Zheng S, Goldblum RR, Gelwan NA, et al. Optogenetic activation of cholinergic neurons in the PPT or LDT induces REM sleep. *Proc Natl Acad Sci U S A* (2015) 112:584–9. doi:10.1073/pnas.1423136112

55. Fujiyama T, Miyashita S, Tsuneoka Y, Kanemaru K, Kakizaki M, Kanno S, et al. Forebrain Ptf1a is required for sexual differentiation of the brain. *Cell Rep* (2018) 24:79–94. doi:10.1016/j.celrep.2018.06.010

56. Whitney MS, Shemery AM, Yaw AM, Donovan LJ, Glass JD, Deneris ES. Adult brain serotonin deficiency causes hyperactivity, circadian disruption, and elimination of siestas. *J Neurosci* (2016) 36:9828–42. doi:10.1523/JNEUROSCI.1469-16.2016

57. Collins B, Pierre-Ferrer S, Muheim C, Lukacsovich D, Cai Y, Spinnler A, et al. Circadian VIPergic neurons of the suprachiasmatic nuclei sculpt the sleep-wake cycle. *Neuron* (2020) 108:486–99. doi:10.1016/j.neuron.2020.08.001

58. Adamantidis AR, Zhang F, Aravanis AM, Deisseroth K, de Lecea L. Neural substrates of awakening probed with optogenetic control of hypocretin neurons. *Nature* (2007) 450:420–4. doi:10.1038/nature06310

59. Patel AK, Reddy V, Shumway KR, Araujo JF. Physiology, sleep stages. In: *StatPearls*. Treasure Island, FL: StatPearls Publishing (2022).

60. Eban-Rothschild A, Rothschild G, Giardino WJ, Jones JR, de Lecea L. VTA dopaminergic neurons regulate ethologically relevant sleep–wake behaviors. *Nat Neurosci* (2016) 19:1356–66. doi:10.1038/nn.4377

61. Medeiros DC, Lopes Aguiar C, Moraes MFD, Fisone G. Sleep disorders in rodent models of Parkinson's disease. *Front Pharmacol* (2019) 10:1414. doi:10.3389/fphar.2019.01414

62. Lydic R. The motor atonia of REM sleep: A critical topics forum. Introduction. *Sleep* (2008) 31:1471–2. doi:10.1093/sleep/31.11.1471

63. Swift KM, Gross BA, Frazer MA, Bauer DS, Clark KJD, Vazey EM, et al. Abnormal locus coeruleus sleep activity alters sleep signatures of memory consolidation and impairs place cell stability and spatial memory. *Curr Biol* (2018) 28:3599–609. doi:10.1016/j.cub.2018.09.054

64. Hoffer BJ, Siggins GR, Oliver AP, Bloom FE. Activation of the pathway from locus coeruleus to rat cerebellar purkinje neurons: pharmacological evidence of noradrenergic central inhibition. *J Pharmacol Exp Ther* (1973) 184:553–69.

65. Moises HC, Waterhouse BD, Woodward DJ. Locus coeruleus stimulation potentiates purkinje cell responses to afferent input: the climbing fiber system. *Brain Res* (1981) 222:43–64. doi:10.1016/0006-8993(81)90939-2

66. Schwarz LA, Miyamichi K, Gao XJ, Beier KT, Weissbourd B, DeLoach KE, et al. Viral-genetic tracing of the input-output organization of a central noradrenaline circuit. *Nature* (2015) 524:88–92. doi:10.1038/nature14600

67. Romigi A, Placidi F, Peppe A, Pierantozzi M, Izzi F, Brusa L, et al. Pedunculopontine nucleus stimulation influences REM sleep in Parkinson's disease. *Eur J Neurol* (2008) 15:e64–5. doi:10.1111/j.1468-1331.2008.02167.x

68. French IT, Muthusamy KA. A review of the pedunculopontine nucleus in Parkinson's disease. *Front Aging Neurosci* (2018) 10:99. doi:10.3389/fnagi.2018.00099

69. Liu S, Shen J, Li Y, Wang J, Wang J, Xu J, et al. EEG power spectral analysis of abnormal cortical activations during REM/NREM sleep in obstructive sleep apnea. *Front Neurol* (2021) 12:643855. doi:10.3389/fneur.2021.643855

70. Mihajlovic V, Patki S, Grundlehner B. The impact of head movements on EEG and contact impedance: an adaptive filtering solution for motion artifact reduction. In: 2014 36th annual international conference of the IEEE engineering in medicine and biology society; 26-30 August 2014; Chicago, IL, USA (2014). p. 5064–7.

71. Liu Y, Qi S, Thomas F, Correia BL, Taylor AP, Sillitoe RV, et al. Loss of cerebellar function selectively affects intrinsic rhythmicity of eupneic breathing. *Biol Open* (2020) 9:bio048785. doi:10.1242/bio.048785

72. Canto CB, Onuki Y, Bruinsma B, van der Werf YD, Zeeuw CID. The sleeping cerebellum. *Trends Neurosci* (2017) 40:309–23. doi:10.1016/j.tins.2017.03.001

73. Brankack J, Kukushka VI, Vyssotski AL, Draguhn A. EEG gamma frequency and sleep-wake scoring in mice: comparing two types of supervised classifiers. *Brain Res* (2010) 1322:59–71. doi:10.1016/j.brainres.2010.01.069

74. Valderrama M, Crépon B, Botella-Soler V, Martinerie J, Hasboun D, Alvarado-Rojas C, et al. Human gamma oscillations during slow wave sleep. *PloS One* (2012) 7:e33477. doi:10.1371/journal.pone.0033477

DYSTONIA

Dystonia is the official journal of
the Dystonia Medical Research Foundation

The mission of the DMRF is to advance research for more treatments and ultimately a cure, to promote awareness and education, and to support the needs and well being of affected individuals and families.

Discover more of our Special Issues

See more →

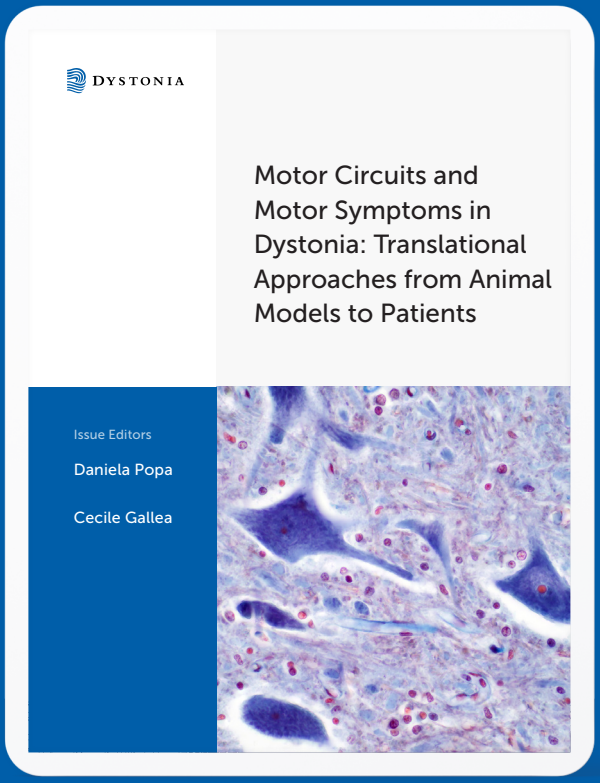

fro.ntiers.in/special-issue
frontierspartnerships.org

Contact
+41 (0) 21 510 17 40
dystonia@frontierspartnerships.org